

12-2002

Modeling Boundaries of Influence among Positional Uncertainty Fields

Joshua P. King

Follow this and additional works at: <http://digitalcommons.library.umaine.edu/etd>

 Part of the [Databases and Information Systems Commons](#), and the [Geographic Information Sciences Commons](#)

Recommended Citation

King, Joshua P., "Modeling Boundaries of Influence among Positional Uncertainty Fields" (2002). *Electronic Theses and Dissertations*. 583.
<http://digitalcommons.library.umaine.edu/etd/583>

This Open-Access Thesis is brought to you for free and open access by DigitalCommons@UMaine. It has been accepted for inclusion in Electronic Theses and Dissertations by an authorized administrator of DigitalCommons@UMaine.

**MODELING BOUNDARIES OF INFLUENCE AMONG
POSITIONAL UNCERTAINTY FIELDS**

By

Joshua P. King

B.S. University of Maine, 2000

A THESIS

Submitted in Partial Fulfillment of the

Requirements for the Degree of

Master of Science

(in Spatial Information Science and Engineering)

The Graduate School

The University of Maine

December, 2002

Advisory Committee:

Anthony Stefanidis, Assistant Professor of Spatial Information Science and
Engineering, Advisor

Peggy Agouris, Associate Professor of Spatial Information Science and Engineering

Mary Kate Beard-Tisdale, Professor of Spatial Information Science and Engineering

MODELING BOUNDARIES OF INFLUENCE AMONG POSITIONAL UNCERTAINTY FIELDS

By Joshua P. King

Thesis Advisor: Dr. Anthony Stefanidis

An Abstract of the Thesis Presented
in Partial Fulfillment of the Requirements for the
Degree of Master of Science
(in Spatial Information Science and Engineering)
December, 2002

Within a GIS environment, the proper use of information requires the identification of the uncertainty associated with it. As such, there has been a substantial amount of research dedicated to describing and quantifying spatial data uncertainty.

Recent advances in sensor technology and image analysis techniques are making image-derived geospatial data increasingly popular. Along with development in sensor and image analysis technologies have come departures from conventional point-by-point measurements. Current advancements support the transition from traditional point measures to novel techniques that allow the extraction of complex objects as single entities (e.g., road outlines, buildings). As the methods of data extraction advance, so too must the methods of estimating the uncertainty associated with the data. Not only will object uncertainties be modeled, but the connections between these uncertainties will also be estimated.

The current methods for determining spatial accuracy for lines and areas typically involve defining a zone of uncertainty around the measured line, within which the "actual" line exists with some probability. Yet within the research community, the proper shape of this 'uncertainty

band' is a topic with much dissent. Less contemplated is the manner in which such areas of uncertainty interact and influence one another. The development of positional error models, from the epsilon band and error band to the rigorous G-band, has focused on statistical models for estimating independent line features. Yet these models are not suited to model the interactions between uncertainty fields of adjacent features. At some point, these distributed areas of uncertainty around the features will intersect and overlap one another. In such instances, a feature's uncertainty zone is defined not only by its measurement, but also by the uncertainty associated with neighboring features. It is therefore useful to understand and model the interactions between adjacent uncertainty fields.

This thesis presents an analysis of estimation and modeling techniques of spatial uncertainty, focusing on the interactions among fields of positional uncertainty for image-derived linear features. Such interactions are assumed to occur between linear features derived from varying methods and sources, allowing the application of an independent error model. A synthetic uncertainty map is derived for a set of linear and aerial features, containing distributed fields of uncertainty for individual features. These uncertainty fields are shown to be advantageous for communication and user understanding, as well as being conducive to a variety of image processing techniques. Such image techniques can combine overlapping uncertainty fields to model the interaction between them. Deformable contour models are used to extract sets of continuous uncertainty boundaries for linear features, and are subsequently applied to extract a boundary of influence shared by two uncertainty fields. These methods are then applied to a complex scene of uncertainties, modeling the interactions of multiple objects within the scene.

The resulting boundary uncertainty representations are unique from the previous independent error models which do not take neighboring influences into account. By modeling the boundary

of interaction among the uncertainties of neighboring features, a more integrated approach to error modeling and analysis can be developed for complex spatial scenes and datasets.

ACKNOWLEDGEMENTS

I would like to thank my advisor, Dr. Anthony Stefanidis, for his extensive knowledge and guidance. I would also like to thank the members of my committee, Drs. Peggy Agouris and Mary Kate Beard-Tisdale, for their support and feedback. The help of my fellow Spatial Information Science and Engineering graduate students was also greatly appreciated, specifically: Kristin Eickhorst, Georgios Mountrakis, Panayotis Partsinevelos, and especially Sotirios Gyftakis for his help with research issues and data sets.

Finally, I would like to praise God and thank my family and friends for the love and support that every student needs.

This work was supported by the National Science Foundation under NSF grant numbers IIS-9702233 and IIS-0121269.

This support is gratefully acknowledged.

TABLE OF CONTENTS

ACKNOWLEDGEMENTS.....	ii
LIST OF TABLES.....	vi
LIST OF FIGURES.....	vii
1. INTRODUCTION.....	1
1.1 Geospatial Uncertainty.....	1
1.2 Objective.....	4
1.3 Intended Audience.....	5
1.4 Thesis Structure.....	5
2. LITERATURE REVIEW.....	7
2.1 Concepts and Definitions.....	7
2.1.1 Overview of Spatial Uncertainty.....	7
2.1.2 Measurements of Spatial Information.....	10
2.1.3 Statistical Measures of Accuracy.....	12
2.1.4 Data Quality.....	16
2.1.5 Uncertainty in Image Applications.....	17
2.2 Estimation and Modeling Techniques for Spatial Uncertainty.....	22
2.2.1 Statistical Probability Methods.....	23
2.2.2 Fuzzy Set Theory.....	27
2.2.3 Bayesian Statistics.....	29
2.2.4 Dempster-Shafer Belief Theory.....	30
2.3 Image-based Positional Measurements.....	33
2.3.1 Film-based Photogrammetry.....	33

2.3.2	Digitizing.....	36
2.3.3	Digital Remote Sensing and Image Processing.....	38
2.3.4	Deformable Contour Models.....	41
3.	ESTIMATING POSITIONAL UNCERTAINTY OF A LINE	
	SEGMENT IN GIS.....	46
3.1	Rigorous Error Models.....	48
3.2	Improving Communication and Estimation of Positional Uncertainty Models.....	59
4.	MODELING UNCERTAINTY FIELD INTERACTIONS AMONG ADJACENT FEATURES.....	73
4.1	Extracting Continuous Uncertainty Boundaries Using Snakes.....	74
4.2	Modeling and Estimating Interactions Between Uncertainty Fields.....	84
4.3	Modeling Interactions of Uncertainty Boundaries Within Complex Scenes.....	94
5.	CONCLUDING REMARKS.....	99
5.1	Summary.....	99
5.2	Future Research Issues.....	100
	REFERENCES	101
	APPENDICES	107
	Appendix A. Models for Estimating and Assessing Positional Uncertainty.....	108
	Appendix B. Methods for Deriving Positional Uncertainty of Digital Spatial Features.....	110
B.1	Chrisman (1982) and Perkal's Epsilon Band.....	112
B.2	Dutton's Error Band Simulations.....	113
B.3	Caspary and Scheuring's Error-Band.....	116

B.4 Shi and Tempfli's Error Model.....	119
B.5 Shi and Liu's G-Band Model.....	121
BIOGRAPHY OF THE AUTHOR.....	129

LIST OF TABLES

Table 1.	Rules of thumb for errors of definition with stereoplotter.....	36
Table 2.	Advantages and disadvantages of uncertainty field representations and intensity stretches.....	70

LIST OF FIGURES

Figure 1.	Conceptual model of uncertainty.....	8
Figure 2.	Illustration of accuracy versus precision using shots at a target.....	15
Figure 3.	An extension of the conceptual model of uncertainty for image applications.....	22
Figure 4.	Normal (Gaussian) distribution curve.....	24
Figure 5.	Error ellipse and its components.....	26
Figure 6.	Fuzzy membership function with interval [0,1].....	28
Figure 7.	Dempster-Shafer belief functions.....	31
Figure 8.	Geometric relationships between focal plane, camera lens, and ground.....	34
Figure 9.	Chrisman's ϵ - band.....	48
Figure 10.	Dutton's experiment simulating line segments.....	50
Figure 11.	Approximation of the error-band.....	52
Figure 12.	Cell array and random lines simulation.....	52
Figure 13.	The probability density function (bivariate) of the point (x,y).....	54
Figure 14.	The probability density function of a line.....	56
Figure 15.	G-bands under varied conditions: (a) equal, uncorrelated errors; (b) unequal, correlated errors.....	57
Figure 16.	Location of minimum error circle: (a) $\sigma_0 < \sigma_1$, $t < 1/2$; (b) $\sigma_0 > \sigma_1$, $t > 1/2$;.....	58
Figure 17.	Visualization of G-band as composite of error ellipses (circles).....	58
Figure 18.	G-band of a line segment with unequal endpoint errors following a circular normal distribution.....	61

Figure 19.	Uncertainty field of a line segment, with contours at $\sigma \cdot n$, where $n = 0.25, 0.5, 0.75, 1.0$	62
Figure 20.	Smoothed uncertainty field of a line segment, for $\sigma \cdot n$, $n \in [0,1]$	63
Figure 21.	Uncertainty field of a line segment, for $\sigma \cdot n$, $n \in [0, 3.2]$	63
Figure 22.	Uncertainty field of a line segment emphasizing 1σ while displaying field up to 2.5σ	64
Figure 23.	Stretching of uncertainty shading values over range $[0,10]$ as a function of distance from measured line segment. Note the valley shaped stretch of intensity values.....	65
Figure 24.	Some examples of “staircase” and “peak-valley” intensity stretching.....	67
Figure 25.	More examples of “peak-valley” intensity stretching.....	68
Figure 26.	Some examples of “plateau” intensity stretching; note that d) is essentially a basic uncertainty field stretch over $[0-10]$	69
Figure 27.	Overlaid G-bands (including error ellipses) of two adjacent line segments.....	73
Figure 28.	G-band overlays of five connected line segments.....	75
Figure 29.	Uncertainty map overlay, consisting of five connected line segments’ individual uncertainty fields.....	76
Figure 30.	Uncertainty maps; a) staircase representation, b) peak-valley representation.....	76
Figure 31.	Example gradient images; a) basic uncertainty field, b) staircase field, c) plateau stretch, d) peak-valley stretch.....	78
Figure 32.	Sample point approximations for figure 33.....	79
Figure 33.	Snakes extraction using only endpoint approximations, as seen in figure 32; high weight on gradient, minimal weight on continuity.....	80

Figure 34.	Many G-band approximation points used, minimal weighting.....	80
Figure 35.	Sample overlaid uncertainty fields, staircase representation.....	82
Figure 36.	Segment endpoint and midpoint G-Band approximations used, snake interpolates points based on weighted continuity, medium gradient and curvature.....	82
Figure 37.	Many G-band approximation points used, heavy weighting on continuity, minimal weighting on curvature and gradient.....	82
Figure 38.	Uncertainty fields of (a) an individual line segment and (b) a composite line feature	85
Figure 39.	Sample geometry of two adjacent line features.....	85
Figure 40.	Intersection of uncertainty distributions for neighboring features.....	86
Figure 41.	Overlapping uncertainty bands of neighboring line features.....	87
Figure 42.	Result of minimum operation between two uncertainty field images.....	88
Figure 43.	Result of maximum operation between two uncertainty field images.....	89
Figure 44.	Overlaying the result of the maximum operation (figure 41) on the two uncertainty fields...note the dark boundary produced within the area of intersection.....	91
Figure 45.	Snake extraction of original line feature.....	91
Figure 46.	Enhancement of area of intersection.....	92
Figure 47.	Snake extraction of the boundary of influence between two uncertainty fields.....	93
Figure 48.	Uncertainty field of a line feature.....	95
Figure 49.	Uncertainty fields of 3 adjacent building outlines.....	95
Figure 50.	Result of minimum operation showing extent of interactions between uncertainty fields.....	96

Figure 51.	Following maximum operation, complex scene of uncertainty combining building uncertainty boundaries with that of the line feature's.....	96
Figure 52.	Snake extraction of boundary of influence of original line feature's uncertainty field within complex scene.....	97
Figure B.1.	Error ellipse and its components.....	111
Figure B.2.	Chrisman's ϵ - band.....	113
Figure B.3.	Dutton's experiment simulating line segments.....	115
Figure B.4.	Approximation of the error-band.....	117
Figure B.5.	Cell array and random lines (schematic).....	118
Figure B.6.	The probability density function (bivariate) of the point (x,y).....	120
Figure B.7.	The probability density function of a line.....	121
Figure B.8.	The probability density function of a line [enlarged].....	125
Figure B.9.	G-bands under varied conditions: (a) equal, uncorrelated errors; (b) unequal, correlated errors.....	126
Figure B.10.	Location of minimum error circle: (a) $\sigma_0 < \sigma_1$, $t < 1/2$; (b) $\sigma_0 > \sigma_1$, $t > 1/2$	127
Figure B.11.	Visualization of G-band as composite of error ellipses (circles).....	128

1. INTRODUCTION

1.1 Geospatial Uncertainty

Attempting to describe and quantify uncertainty as it relates to spatial data has become a developing interest in the past decade. The wide array of topics currently being studied extends from error modeling and communication to the use of risk management procedures to help deal with spatial data uncertainty in decision-making. While there exists a sizeable amount of research dedicated to the sources, effects, and solutions of spatial uncertainty, much of the academic research has yet to be applied in the form of usable tools that can be used in everyday practice (Hunter, 1999). The reason for this is the rather complex mathematical and statistical concepts involved in spatial uncertainty estimation, and the poor communication potential of these concepts.

A geographical information system (GIS) is a computer-based system capable of assembling, storing, manipulating, and displaying geographically referenced information. The term GIS typically encompasses not only the computer-based system, but also the collection of data and operating procedures that are applied within the system. GISs are commonly utilized as a medium to store and display spatial objects and their associated attributes. Thus, a GIS database is a digital representation of the spatial organization of objects and phenomena in the real world.

GISs are characterized by the multitude of data, sources, and methodologies employed in data production and manipulation. Data in a GIS are often stored in the form of data layers or coverages. Multiple data types can be overlaid to present the user with a wealth of information in a single view. Roads, rivers, contours, political boundaries, and building layers are just a few common examples of data layers employed in a GIS. GIS data are often treated as precisely located, or *deterministic* values, rather than probabilistic, *stochastic* values. Yet measurement procedures, imperfect by nature, produce spatial data with limited accuracy, leading to uncertain

description of spatial objects. Spatial objects are typically represented in a GIS with definite boundaries, while in reality they have indeterminate boundaries and fuzzy spatial extent. Using GIS data in a deterministic sense tends to ignore the many kinds of uncertainty associated with the data. Space, attribute, time, inconsistency, and incompleteness are characteristics of spatial data that contribute uncertainty (Guptill and Morrison, 1995); positional and attribute error models are considered the most important for a GIS. Thus, uncertainties exist within and despite the crisp object description of geographical entities (Cheng, 2002).

Spatial data layers may originate from a variety of sources: digitized maps, points acquired through global positioning devices, and surveyed attributes entered into a software package are examples. Layers may also consist of objects extracted from remotely-sensed imagery (e.g. road networks, forest coverage). Recent advances in sensor technology and image analysis techniques are making image-derived geospatial data increasingly popular. While the spatial data community is eager to apply the products of these new technologies, the data is often used without regard to the uncertainty of the data production process. Within a GIS environment, the proper use of information requires the identification of the uncertainty estimates associated with it. Currently, a major dilemma in evaluating the positional accuracy of a GIS dataset lies in determining the uncertainty of different objects within the set. Positional accuracy assessments typically examine error by attempting to predict its propagation from points to lines and objects within a GIS. Yet, along with development in sensor and image analysis technologies have come departures from conventional point-by-point measurements. Current advancements support the transition from traditional point measures to novel techniques that allow the extraction of complex objects as single entities (e.g., road outlines, buildings). The current methods for determining spatial accuracy for lines and areas typically involve defining a zone of uncertainty around the measured line, within which the "actual" line exists with some probability. Yet within the research community, the proper shape of this 'uncertainty zone' is a topic with much dissent

(Veregin, 1998). Less contemplated is the manner in which such areas of uncertainty interact and influence one another. Distributed areas of uncertainty around linear features will intersect and overlap one another at a given juncture. In such instances, a feature's uncertainty is defined not only by its measurement, but by the uncertainty associated with neighboring features. It is therefore useful to understand and model the interactions between adjacent uncertainty fields. In the context of this thesis, such uncertainty interactions are assumed to occur among features derived from differing sources and derivation methods.

The most fundamental geometric elements are points and lines, and an analysis of positional accuracy would logically begin with these simple objects. The fields of geodesy, surveying, and cartography have long studied the uncertainty associated with points. Knowing the error of each point, the error along a line can be determined and an arbitrary point on the line can have an accuracy index associated with it. Error models for points and the lines segments that connect them have been developed, such as the epsilon-band, confidence region, and G-Band models (Shi and Liu 2000). These models are based on an assumed statistical distribution of the error associated with each point, typically a Gaussian (Normal) distribution. However, these error models have typically been restricted to individual line segments, i.e., they are unable to take into account outside influences or dependencies affecting a feature's uncertainty.

Within our discussion, the terms 'error' and 'uncertainty' will be used almost interchangeably. The spatial data community, while recognizing the inherent differences between the terms, is often at odds when trying to define or separate them. This confusion is due, in part, to the similar concepts the terms are meant to convey. Error analysis is used to determine the discrepancy between the true and measured values of an object or location. However, a true value or location is a luxury not often available in spatial data. For example, determining a 'true' location for a wetlands boundary, or 'true' location of objects extracted from coarse imagery. In the absence of

a true value, uncertainty is substituted for error. In order to achieve the goals of this paper, we must analyze and apply previous research on positional error and uncertainty. Any investigation of uncertainty measurement methods reveals extensive use of error analysis techniques. For the sake of simplicity we will assume that the terms ‘uncertainty’, and ‘error’ both indicate a deviation from an expected value. In addition, the term accuracy can be considered the complement to the two terms, i.e., the “closeness” to the true value.

In this thesis we are addressing uncertainty boundary estimation, with an emphasis on linear segments. The process applied herein approaches maps and other GIS layers as composites of data produced from different sources and techniques. We will therefore be examining the case where such segments are derived through differing extraction methods. In one method of feature extraction, deformable contour models, line segments are linked in a continuous manner based on an energy minimization function. Just as these contour models can extract a feature’s outline, they can also extract an uncertainty boundary. It is then worthwhile to examine how uncertainty associated with neighboring line segments contributes to uncertainty of the featured object. By modeling the boundary of interaction between the uncertainties of two features, we investigate how this information can be merged together for spatial scenes containing a composite of datasets.

1.2 Objective

The objective of this thesis is to analyze estimation and modeling techniques of spatial uncertainty. More specifically, we are interested in examining interactions among fields of positional uncertainty for image-derived linear features. By investigating current positional error models, we hope to offer improvements in communication, understanding, and uncertainty estimation. We derive a synthetic uncertainty map for a set of linear features to model a distributed field of uncertainty for a feature, which offers advantages for communication and user

understanding. We apply digital image processing techniques to communicate and estimate the uncertainty associated with these features, extracting a set of continuous uncertainty boundaries. Adjacent uncertainty fields are combined to model the interactions between them, and a deformable contour model will be applied to extract the boundary of influence shared by two uncertainty fields. These methods are then applied to a complex scene of uncertainties, modeling the interactions of multiple objects within the scene. The resulting boundary representations are unique from the previous independent error models which do not take neighboring influences into account.

1.3 Intended Audience

The intended audience of this thesis are those professionals, researchers, and participants in the fields of GIS, remote sensing, photogrammetry, surveying, and computer programming. The research and results apply to a broad range of fields due to the examination of spatial data and the uncertainty associated with it. Programmers manipulating boundary representation objects may be interested in the interaction between boundaries of distributed features. The fields of surveying, remote sensing, and photogrammetry will be able to apply the concepts to any and all collected spatial data in order to improve its accuracy and objectivity.

1.4 Thesis Structure

Section 1 provides an overview of the scope and intent of this thesis. Section 2.1 discusses topics and definitions relevant to spatial uncertainty. Estimation and modeling techniques for spatial uncertainty are examined in Section 2.2, including statistical methods, fuzzy set theory, Bayesian statistics, and Dempster-Shafer theory. Section 2.3 touches upon image-based positional measurements, including photogrammetry, remote sensing, and digital image processing. In Section 3, positional uncertainty of a line segment is studied, including some rigorous error models that have advanced the field. Section 3.2 offers possible improvements for

communicating and estimating positional uncertainty of a line segment via an uncertainty field. Section 4 concentrates on the modeling of interactions among adjacent uncertainty fields. Digital image processing techniques are used in conjunction with uncertainty fields to estimate positional uncertainty of continuous line segments in Section 4.1. Interactions between uncertainty fields are modeled in Section 4.2, and a boundary of interaction is extracted using deformable contour models. Section 4.3 examines this same uncertainty field interaction and boundary extraction within a complex scene. Section 5 brings the thesis to a close with a summary and outlets for future research.

2. LITERATURE REVIEW

2.1 Concepts and Definitions

This purpose of this section is to detail fundamental notions and concepts within the realm of spatial uncertainty. An overview of spatial uncertainty begins by exploring accuracy and quality of spatial information while examining sources and causes of uncertainty. In addition, spatial uncertainty estimation and modeling techniques are reviewed. Section 2 closes with a summary of remote sensing as well as digital image processing techniques to be applied towards uncertainty estimation.

2.1.1 Overview of Spatial Uncertainty

The definition of uncertainty as it relates to spatial information systems is a much debated and often cloudy issue. A variety of terms have been used, almost interchangeably, to communicate spatial uncertainty, including: *error*, *accuracy*, *precision*, *vagueness*, *ambiguity*, and *reliability*. Uncertainty is broader than any of these terms and includes these more restrictive concepts (Gottsegen, Montello, and Goodchild, 1999).

Klir and Yuan (1995) define uncertainty issues as either products of fuzziness or products of ambiguity. Fisher (1999) takes the work a step further, defining uncertainty as dependent upon how well objects or classes are defined. Figure 1 illustrates Fisher's different types of uncertainty within spatial information and the methods that deal with them.

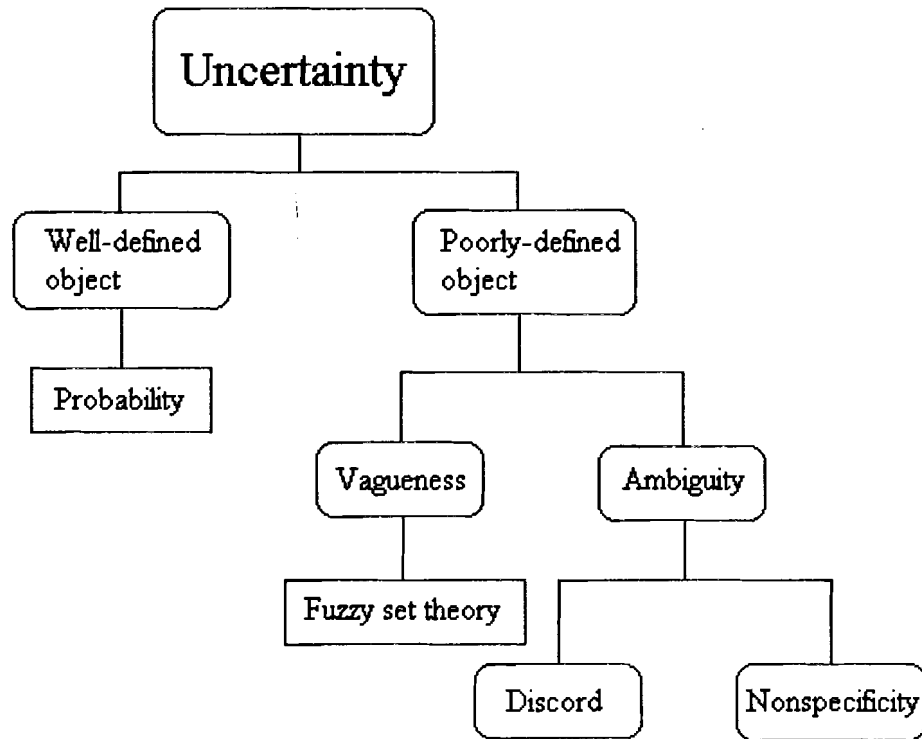


Figure 1. Conceptual model of uncertainty (adapted from Fisher, 1999, and Klir and Yuan, 1995)

In order to determine which elements of uncertainty affect a specific spatial object, it is necessary to determine whether the class of objects is well defined or poorly defined. If the object is well defined, (e.g., land ownership boundaries), then the uncertainty is caused by errors and is probabilistic in nature. If the object is poorly defined, such as vegetation or soil boundaries, then specific types of uncertainty, vagueness or ambiguity, can be acknowledged. Here Fisher replaces Klir and Yuan's fuzziness with vagueness. Vagueness is associated with poor definition of the class in which the object belongs. For example, using the class definitions of "dry", "medium", and "wet" to label regions by average rainfall would be an example of vague class definition. There is no distinct boundary between the classes, resulting in uncertainty in the

classification process. Similarly, classifying a person as “tall” or “bald” are vague concepts that give rise to uncertainty.

Ambiguity is associated with instances when there exists doubt as to how an object should be classified because of differing perceptions of it. Ambiguity can be further broken down into discord (disagreement over which class an object belongs to) and non-specificity (object belonging to no class). Discord occurs when an object is clearly defined, yet differing perceptions of the classification scheme allow the object to be classified in more than one class. As an example of discord, Fisher cites dispute over territorial claims of land. Both India and Pakistan have border conflicts and disagreements over the Kashmir area. Both countries claim Kashmir as part of their territory, resulting in discord over the political classification of the geographic area. Differing classification schemes regarding wetlands can result in discord between organizations in their classifications of marsh areas.

Non-specificity occurs when features have no appropriate class to be assigned to. Consider a census charting the ethnic diversity of a region. If the census provides Caucasian and African American as the only two ethnic choices, it is non-specific to a variety of other alternatives, such as Hispanic or Native American. When studying vagueness and ambiguity, it is apparent that uncertainty arising from poorly defined objects is mainly a problem of labeling. This point will be discussed in more detail in Section 2.1.5.

It is important to note that the conceptual model provided is not an exhaustive representation of the possibilities within uncertainty. It is better used as a general framework to provide insight to the sources and types of uncertainty in spatial data. It is a model of reality that varies with scale, processing, and application; different models, definitions, and interpretations can be adapted from

it. For instance, an increase in scale will often amplify both the variety of features discernible as well as the complexity of classes needed to categorize these features.

Most research on expressing uncertainty within spatial databases has concentrated on two main methods: fuzzy set theory to represent vagueness, and probability theory to characterize error (Fisher, 1999). Linear features are well-defined objects and our measurement of them is a measurement of space. We are concerned not necessarily with measurements of attributes such as position or length, but rather of extractions of the objects themselves. Our work with spatial uncertainty focuses on well-defined elongated objects observed in digital images. In Section 2.1.5 we therefore provide an adapted model of uncertainty to apply to image-based applications.

2.1.2 Measurements of Spatial Information

Uncertainty arises from imperfect measurement of spatial information. Spatial information exists in three components:

- Time
- Space
- Attribute

Measurements of time, or the temporal aspect of data, act as an important reference to characterize data. Time can be treated as an absolute series with a desired origin and unit of measurement, such as 1918 A.D. or 2:42 PM. Time can also be treated as cyclical, such as days of the week or seasons of the year. The assignment of temporal values to data is referred to as dating. Another consideration is the temporal validity of spatial data. It is useful to know whether spatial data is valid to make decisions based on its time frame. A study of income distribution throughout Europe during World War I would have little meaning using today's salary figures. Temporal validity can depend on an absolute date or can be conditional on a

period of time (e.g., 10 days). The temporal aspect of data, while often not emphasized, plays an important role in spatial analysis.

Measurements of space are taken to define the geographic location and extent of objects or phenomena. Spatial measurements can be carried out over varying dimensions (1-D, 2-D, 3-D), units (feet, meters, degrees, etc.), and reference systems (Cartesian, latitude-longitude, etc.). Furthermore, spatial measurement can be placed in a relative or absolute context. A relative measurement locates a feature with respect to its surrounding environment, such as the location of a library within a university campus. Absolute measurements locate objects on a universal scale, linking any two positions using a common origin and measurement system. Typical absolute spatial measurements assume a 2-D representation of the earth's surface and exist as (X,Y) coordinate pairs or latitude-longitude pairs. However, the varying third dimension of the Earth's surface (height) plays an important role in spatial measurement.

Spatial measurements are not solely declarations of the positions of geographic features. Spatial measurements are also used to derive representations of objects. Examples include road edges, the outline of a house, or the extent of a forest. Road centerlines often indicate the average position of a linear road feature, but do not provide information as to the extent or width of the feature. An accurate representation of the road encompasses these spatial characteristics, often in the form of an outline. A house can be represented by a single position, perhaps the center of a land area. Yet the house is better characterized by an outline of its edges, often in the form of a four-cornered polygon. Consider a forest, where a single average position within the forest would be of little use to a data user. Representing the forest as an area with extent in multiple directions, rather than as a simple coordinate pair, is a far more appropriate approximation.

Attribute measurements are those that deal with the nonspatial elements of data. An attribute value represents specific characteristics of spatial features. Attribute values can be anything from average age of a town, length or elevation of a feature, or spectral reflectance of a pixel. Accordingly, attribute values can take any units necessary (or no units at all) to adequately describe the characteristics of geographic features.

2.1.3 Statistical Measures of Accuracy

No measurement, spatial or otherwise, is ever perfect or exact. Every measurement contains *error*, and different measurements have different degrees of error. Two common indicators to the degree of error are *accuracy* and *precision*. An analysis of uncertainty within information of any type would be incomplete without addressing these fundamental terms.

All observations and measured values contain errors. An error is a discrepancy between the measured and actual value of a particular attribute for a given entity (Veregin, 1998). When dealing with observations and measurements, the three sources of error are:

- Instrumental Those caused by imperfections in instrument functionality
- Natural Errors caused by changing conditions in the environment
- Personal Those errors created by limitations in the human senses

Examples of instrumental errors could be uncalibrated parts or lenses in an imaging device, or non-uniform spacing between divisions on a theodolite or total station instrument. Natural errors may include variations in temperature, wind, atmospheric pressure, gravitational fields, and magnetic fields. Personal errors arise from one's inability to perfectly see, perceive, or interpolate observations. Examples include errors from actions such as digitizing a point, centering a level bubble, or reading angles from a theodolite (Wolf and Ghilani, 1997).

While errors can be categorized by their sources, these sources can produce three distinct types of errors: blunders, systematic errors, and random errors. Blunders are errors (usually large) that result from the carelessness of the observer, such as mistakes in reading or writing observations values or using the wrong datum. Systematic errors are those that follow some physical law and hence can be predicted. Often systematic errors are removed by deriving corrections based on the physical conditions that created them (e.g., atmospheric interference, solar radiation). Random errors are errors inherent in the nature of measurement, those errors that exist after all blunders and systematic errors have been removed. Random errors can arise from human and instrument imperfection, as well as imperfect corrections. Random errors are impossible to avoid and do not follow any physical laws. Therefore they must be handled according to the mathematical laws of probability and corrected by a series of adjustments (Leick, 1995; Wolf and Ghilani, 1997).

When analyzing uncertainty within remote sensing and GIS, a common assumption is that all blunders and systematic errors have been accounted for, either through elimination or by having some correction applied. The result is an uncertainty analysis that focuses on assessing and predicting the random errors within the system or model. This assumption is useful for assessing positional uncertainty of spatial features and serves as the basis of the many probability-based methods examining spatial uncertainty. Unfortunately, the random error assumption proves too limiting when taking thematic uncertainty into account. The biases inherent in a classification scheme require a more complex method to assess thematic uncertainty.

Some common statistical indicators of error within a set of measurements are standard deviation, variance, covariance, and correlation. Error is the difference between a measurement and its true value. Often the true value is unknown and can be replaced by an expected value, such as an

average. A sample variance can give an estimate of the spread of a set of measurements. The equation for the sample variance (σ^2) is:

$$\sigma^2 = \frac{\sum_{i=1}^n (x_i - \bar{x})^2}{n-1}$$

where n is the number of measurements and \bar{x} is the sample mean. The standard deviation (σ) for a set of measurements is the square root of the variance:

$$\sigma = \sqrt{\sigma^2}$$

and is an estimate of how tightly measurements are clustered about the mean. Covariance is a measurement of the relationships that exist between two variables; in other words, how the variables tend to vary together. The equation for the covariance between two variables is:

$$\text{cov}(x, y) = \frac{\sum_{i=1}^n [(x_i - \bar{x})(y_i - \bar{y})]}{n-1}$$

While the variance is the average of the squared deviation of a feature from its mean, the covariance is the average of the products of the deviations of feature values from their means (Duda 1997). Covariance can be used to calculate correlation between measurements, which expresses the degree that measurements interact together. A correlation coefficient of +1 means the measurements are highly correlated, while a correlation coefficient of -1 indicates the measurements are inversely related. The correlation coefficient can be calculated as:

$$\text{cor}(x, y) = \frac{\text{cov}(x, y)}{\sigma_x \sigma_y}$$

Two measures of quality regarding spatial measurements are *accuracy* and *precision*. These terms are often used together, without an adequate understanding of the differences. Accuracy is

how close a set of observations are to the true value. It is a relative measure, since accuracy is always measured relative to the specification. Precision is a measure of the consistency of repeated observations; variance can be an estimate of precision. Consider the targets in Figure 2 to help illustrate the concepts of accuracy and precision. Since accuracy is a measure of closeness to a “true” value (the target center), the shots in figure 2(a) are inaccurate. In addition, the randomlike pattern of shots indicates imprecision due to lack of repeatability. The shots in 2(b) are precise because they are clustered together, but inaccurate because they failed to hit the intended target. In figure 2(c), the shots are accurate because their average position is the target center; however, the shots are imprecise because they are not clustered. Figure 2(d) demonstrates both high accuracy and precision: the shots are clustered around the intended target.

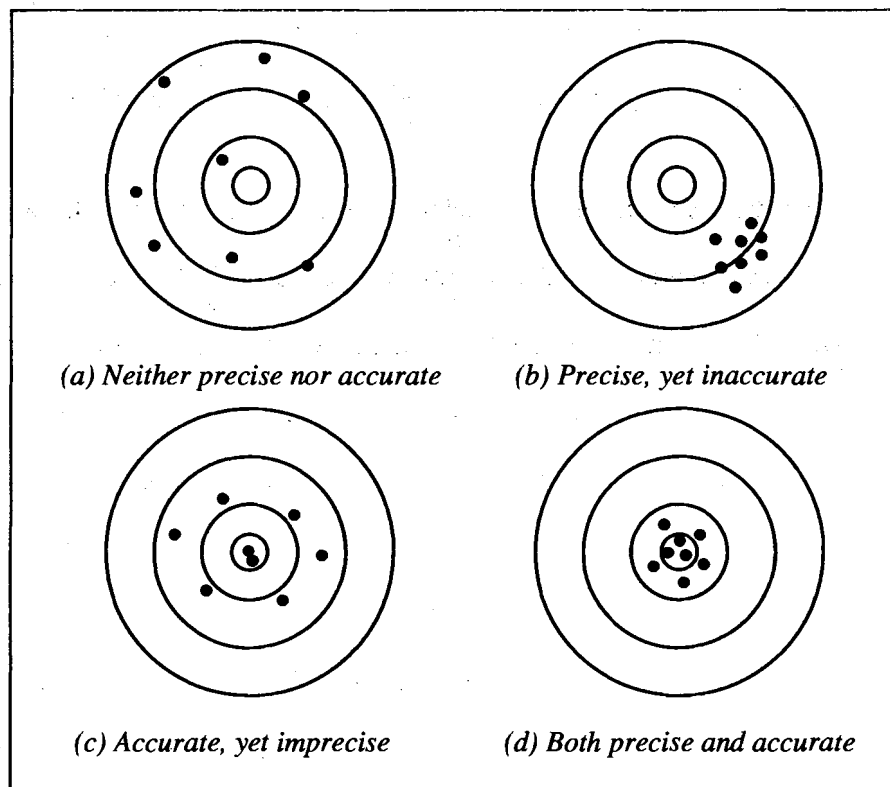


Figure 2. Illustration of accuracy versus precision using shots at a target

2.1.4 Data Quality

Uncertainty has emerged as the preferred term to describe the difference between what a database indicates and what exists in reality (Goodchild, 1998). However, another oft-used term to describe how well data represents objects or phenomenon in the real world is data quality. Data quality is a term used by various spatial data standards in their attempts to categorize components of uncertainty. It is therefore significant to address data quality in a study of uncertainty.

Data quality is itself a difficult term to categorize. The term *data quality* is broader than the *accuracy* of the data. Accuracy plays a large part in evaluating quality, but there are related issues that must also be considered. There are many varying classification schemes developed by research organizations to describe data quality. The objective of the different categorizations is to separate data suitability into distinct components. For instance, the U.S. Spatial Data Transfer Standard breaks data quality down into five divisions (US National Institute of Standards and Technology 1992):

- Lineage – Sources of data, operations and transformations applied
- Positional Accuracy – Spatial and geometric accuracy of data
- Attribute Accuracy – Accuracy of values and classification of nonspatial elements in data
- Logical Consistency – Truthfulness of relationships; internal consistency of data
- Logical Completeness – How completely data represents world; commission and omission

Meanwhile, the International Organization for Standardization (Technical Committee 211) data quality categorization is slightly different:

- Temporal Accuracy – Includes accuracy, consistency, validity of temporal context
- Positional Accuracy

- Thematic Accuracy – See: Attribute Accuracy above
- Logical Consistency
- Completeness – See: Logical Completeness above

While these are just two examples of differing perceptions of data quality, they demonstrate that there is no universally accepted definition of the concept. The difficulty in defining and distinguishing between terms such as uncertainty, quality, and accuracy is not simply a semantic problem confined to the realm of research. It directly affects the ease with which metadata, descriptive information about the data, is defined and produced. Metadata allows details of the data, including important temporal, thematic, and positional uncertainty estimates, to be provided to the user. In this way the user can gain an understanding of the level of uncertainty present. The data quality categorizations and their parameters are defined and determined by the data producers (Bonin, 1998). However, producers' differing classifications and content of metadata inhibit the usefulness and analysis of spatial data. Without a universal structure and content of metadata, users are unable to confidently interchange data from various sources. Lack of a common metadata format or derivation of accuracy estimates is a hindrance to uncertainty analysis. Often uncertainty in the data is ignored and data is taken at "face-value"; linear features extracted from an image are represented as crisp lines, despite uncertainty associated with them. The lack of well-accepted definitions of uncertainty or quality within the world of spatial data is an obstacle in estimating these concepts. The problem filters from producers to users and ultimately to subjective interpretations of data.

2.1.5 Uncertainty in Image Applications

As previously stated in Section 2.1.1, poorly defined objects are typically products of classification or some labeling process. We now present a more general framework for uncertainty than that presented by Fisher (1999) and Klir and Yuan (1995). We are interested in

uncertainty as it relates to features within spatial imagery. While Fisher's model is object-based, our model is directed towards use with spatial imagery and finds its foundation in the three components of spatial measurement discussed in Section 2.1.2. The model's applications to spatial imagery include images themselves, as well as features and objects within the images.

No measurement is without error; the presence of error introduces uncertainty. The three types of measurement of spatial information are temporal, spatial, and attribute-based. An image-driven model of spatial uncertainty should therefore have time, space, and attribute at its foundation. Temporal uncertainty arises from assigning values of time to information, and determining the validity of data to relevant situations. Both spatial and attribute values are dependent on the temporal measurement of data, and therefore the flow of uncertainty begins with the temporal aspect.

The positioning of an image, feature, or object possesses uncertainty that is neither vague nor ambiguous; there is one position and extent in space. However, the measurement of position is an imperfect process and therefore subject to error. The concept of spatial positioning can be expanded into two components, position and extent. Position is the location in space of an object or feature, whether absolute or relative. Every point in an image, feature, object, etc. has a position. Extent is the area or coverage in space that an object or feature occupies, often represented as an outline. Extent refers to the measurable geometric qualities of a feature, whereas position is used to place the extent in a spatial reference system. For an image, the extent is the physical ground coverage recorded in the image. The image has position as well, such as the absolute GPS position of the image's center. On the other hand, the extent of an object can be an outline of a house or the edges of a road. Object extent is defined by points connected by lines, planes, and polygons. The objects have position in space as well, whether the area's center or nodal positions.

Determining position and extent are imperfect procedures affected by random error and are therefore inherently uncertain. The process of assessing and estimating positional uncertainty can be generalized according to our conceptual model of uncertainty, which will be seen in figure 3. Positioning (spatial measurement) of features is a process free from vagueness and ambiguity, yet subject to error. Although vagueness and ambiguity may arise in determining where features begin and end, this is a problem of labeling and will be discussed shortly. However, once the feature boundaries are defined, the measurement of these boundaries is subject only to error. We are assuming that blunders and systematic errors have been removed, leaving random errors to be assessed. Random errors are probabilistic in nature, and are best handled using spatial statistics and probability theory.

Labeling spatial features is the process of determining characteristics to record and then assigning values to those characteristics. The uncertainties associated with labeling are:

- Vagueness (associated with object or class *description*)
- Ambiguity (associated with attribute value or object *assignment*)

Vagueness occurs when there is poor definition of class or individual object; it is a result of attempts to *describe* objects or classes. Vagueness indicates the presence of borderline cases for a term, concept, or classification. For instance, when classifying road condition as “straight” or “curvy” where does the border exist between the two? If a road with no curves is straight, how does one classify a road with one curve? Or a road with a few minor curves? In this manner, borderline cases can arise, where the classifier is uncertain as to the extent of class boundaries. Terms such as “wet”, “dry”, “smooth”, “bumpy”, “long”, etc. are vague terms with no concrete definition.

In addition, vagueness has an implication that is synonymous with generality. It is often claimed that vagueness exists because “broad categories ease the task of classification” (Sorensen, 2002). Vagueness is present in the process of describing entities, and is inherent in class definitions. No feature or object can be completely described, no matter how many attributes are detailed. The process of choosing which attributes are significant enough to describe a feature is subjective, and the resulting representation will be vague to some degree. For instance, a road can be described as a feature made up of asphalt. This definition is vague in that it fails to distinguish the road from a parking lot or some rooftops, which are made of the same material. If the road class definition is expanded to be an elongated object made up of asphalt, this is a less vague description. Including a smoothness attribute for curves and angles is an even less vague description. Attempting to describe images, features, or objects by attributes is a vague notion that is subjective to views of what is significant and important to record.

We have shown that vagueness arises from the description of classes and attributes. Alternatively, the process of *assigning* values to attributes or objects to classes can lead to ambiguity. Ambiguity occurs when there is doubt as to how an object should be labeled, resulting in assignment to more than one class (discord) or no classes (non-specificity). If a process is unable to distinguish between two different classes or types of objects, the result is ambiguous.

Ambiguity can occur in the absence of vagueness, meaning that even though classes are well-defined, the process of assigning objects or values is unable to sufficiently distinguish between these classes. Ambiguity is a result of confusion over the definition of sets, typically due to differing classification schemes. It arises “when there is doubt as to how a phenomenon should be classified” (Fisher, 1999). Ambiguity is therefore process-dependent; i.e., the means used to assign objects or features determines whether the results are ambiguous. Consider a well-defined

road classification scheme based on spectral signatures from digital imagery. An unsupervised classification may still incorrectly classify as roads those areas far removed from roads. The inability to distinguish between roads and non-roads is a problem of ambiguity. In addition, differing classification schemes can produce different results. A supervised classification may detect different road instances than an unsupervised classification; classifying a feature as a road with one process and a non-road with another process is a result of ambiguity. The differing perceptions of roads and their identification is ambiguous. Fisher (1999) provides examples of differing classification schemes, including the Indian-Pakistani dispute over Kashmir, and differing views of wetlands. For example, if a classification process intended to assign lakes to countries, would the Great Lakes belong to the United States or Canada? Depending on the complexity of the process (whether it allows for lakes to exist in multiple countries) the results could be ambiguous. Estimating uncertainty arising from labeling requires robust methods that utilize logic, rule-based sets, and decision-making. Among the robust methods for modeling thematic uncertainty are fuzzy set theory, Bayesian statistics, and Dempster-Shafer Belief theory.

Figure 3 outlines an extended framework for uncertainty in image applications. Uncertainty originates in the three basic measurements of spatial information: time, space, and attribute. Temporal uncertainty is found in the dating of information and the validity of the data for its use. Spatial uncertainty originates from the error inherent in the position and extent of spatial objects and phenomena. Attribute uncertainty arises from the labeling of spatial features; the imperfect description of features yields vagueness, while the process of assigning values and objects to classes produces ambiguity.

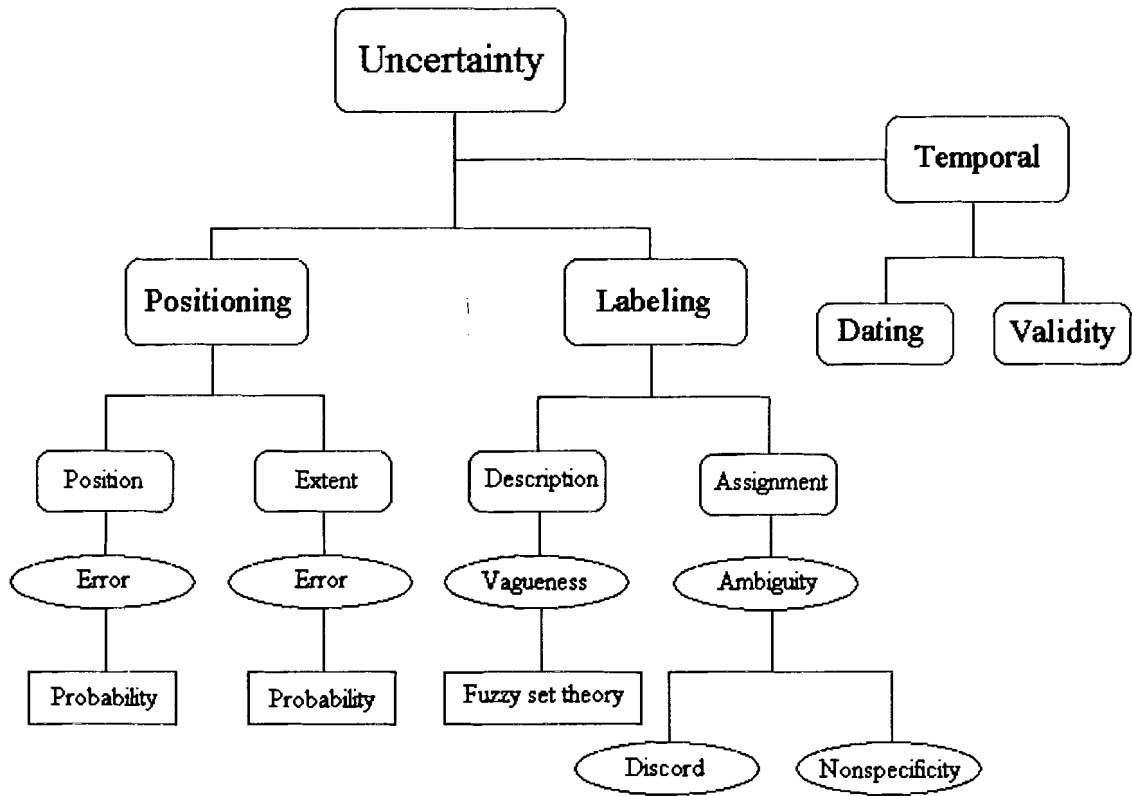


Figure 3. An extension of the conceptual model of uncertainty for image applications

2.2 Estimation and Modeling Techniques for Spatial Uncertainty

This section introduces some definitions of statistical probability methods and indicates why they are useful for modeling positional uncertainty. The majority of spatial uncertainty analysis is accomplished via statistics, probability theory, and adjustments, well-known mathematical techniques. However, these are not the sole methods for uncertainty assessment. Certain types of uncertainties (vagueness, ambiguity, imprecision) require more robust means of uncertainty determination. Methods such as fuzzy set theory, Bayesian statistics, and Dempster-Shafer theory are often more suitable for uncertainty within poorly defined data (Carosio and Kutterer, 2001).

2.2.1 Statistical Probability Methods

For any measurement of a parameter, there is a probability that it is correctly measured. Methods for determining uncertainty using probability are based on assumptions of standard error theory. While errors occur both systematically and randomly, most methods assume systematic error has been corrected for (e.g., via calibration). As a result, uncertainty related to the observation or measurement of values is considered to be random. When many independent random factors act in an additive manner to create variability, data (or errors) will follow a bell-shaped distribution called the normal, or Gaussian, distribution. The normal distribution has some distinct mathematical properties that form the basis of many statistical tests. It is characterized by a symmetric, bell-shaped density curve. The normal distribution is symmetric about a central value, the mean of the random variable, at which point the peak density occurs. The distribution is therefore described by its mean and standard deviation, indicating the spread of the curve. The total area under the normal curve is equal to 1, and any area under the normal curve corresponds to a specific probability. The equation for a normal distribution's probability density function is:

$$f(x) = \frac{1}{\sigma\sqrt{2\pi}} e^{-\frac{(x-\mu)^2}{2\sigma^2}}, \quad -\infty < x < \infty$$

All normal curves exhibit an important property related to the area under the curve and the standard deviation from the mean. Considering a normal distribution of measurements, approximately 68% of all observations (x) fall within one standard deviation (σ) of the mean (μ), in the interval $(\mu - \sigma, \mu + \sigma)$. Thus, 68% of observations fall within $\mu - \sigma < x < \mu + \sigma$. In addition, 95% of all data will fall within two standard deviations (2σ) from the mean, and 99.7% of the data will fall within three standard deviations (3σ) from the mean. Thus, for a normal distribution, practically all data lie within three standard deviations from the mean

(Narasimhan, 1996). Figure 4 illustrates the graphical representation of a normal curve centered on mean (μ) with 68% of its data falling within the range: $-\sigma < x < \sigma$.

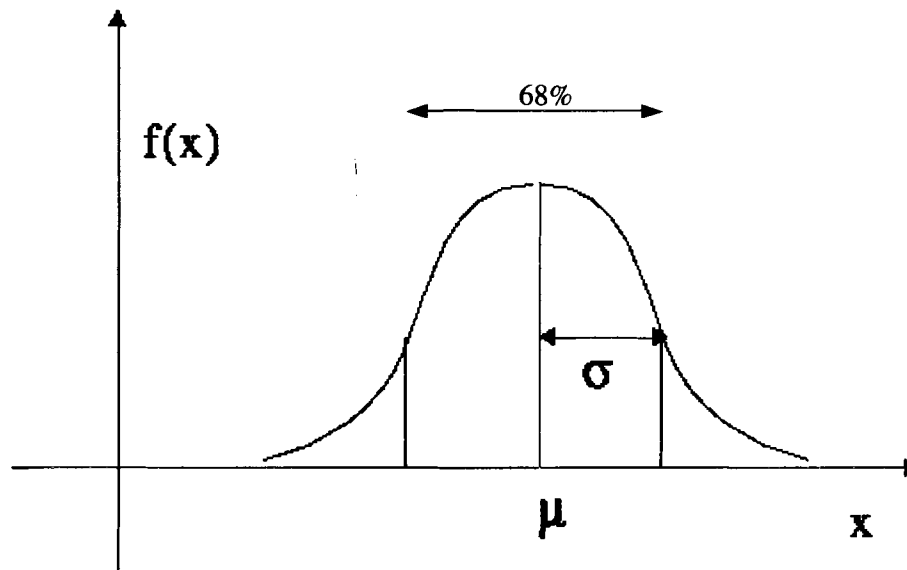


Figure 4. Normal (Gaussian) distribution curve
(Figure from Computational Science Education Project, 1996)

The normal distribution plays a central role in statistics because of a mathematical relationship known as the Central Limit Theorem. The central limit theorem states that if randomly selected samples are large enough, the distribution of sample means will follow a normal distribution even if the population is not normal. Since most statistical tests are concerned only with differences between means, the central limit theorem lets these tests work well even when the populations are not normal. For this to be valid, the samples have to be reasonably large, depending on how far the population distribution differs from a normal distribution (Motulsky, 1999).

Random errors vary in such a way that individual errors of an observation cannot be predetermined. A statistical approach can model these errors, and an estimated “correct” value can be calculated in this manner. Generally there is a probability distribution function that can be applied to the behavior of random errors. While most data capturing is not done in a statistical

manner, the observations are often assumed to be like random variables whose errors follow a normal distribution. These assumptions and their models allow the uncertainty of observations to be estimated (Azouzi, 1999).

Indeed, the U.S. Federal Geographic Data Committee (US FGDC) has adopted a standard for reporting positional accuracy of points that relies on the assumption of normally distributed positional errors (US FGDC, 1998). Goodchild and Hunter argue that while this distribution may apply to positional uncertainty in points, no comparable theory exists for complex features. In the absence of evidence supporting a normal distribution of complex feature separations, the authors propose a method that is non-parametric (1997). In fact, there are numerous methods and models for determining the positional uncertainty of spatial features, be they points, lines, or polygons. Estimating positional uncertainty will be examined more closely in Section 3 and Appendix A.

Positional uncertainty of digital spatial databases is typically expressed through point error measurements. Point errors can be quantified using standard deviations of points in the x, y, and z directions. Due to the two-dimensional nature of maps and imagery, error is typically quantified as either a single directionally independent measure (σ), or as a standard deviation in two directions (σ_x, σ_y). One important measure of error that utilizes standard deviations is the root-mean-square positional error, or RMSP. The RMSP for a point can be calculated accordingly:

$$RMSP = \sqrt{\sigma_x^2 + \sigma_y^2} \quad (\text{Caspary and Scheuring, 1992})$$

A visual indicator of error or uncertainty of points is an error ellipse. An error ellipse uses standard deviations in two directions (e.g., x and y) to define its semi-major and semi-minor axes and rotation. The ellipse's axes are defined in the following manner:

$$\text{Semi-major axis} = \frac{\sigma_x^2 \sigma_y^2}{2} + \sqrt{\frac{\sigma_x^2 \sigma_y^2}{4} + \sigma_{xy}^2}$$

$$\text{Semi-minor axis} = \frac{\sigma_x^2 \sigma_y^2}{2} - \sqrt{\frac{\sigma_x^2 \sigma_y^2}{4} + \sigma_{xy}^2}$$

Along with the rotation of the ellipse (angle t in figure 5), these axes provide useful visual information regarding a point's positional uncertainty. The semi-major axis defines the weakest direction in which a point's position is known (i.e., the direction of maximum uncertainty).

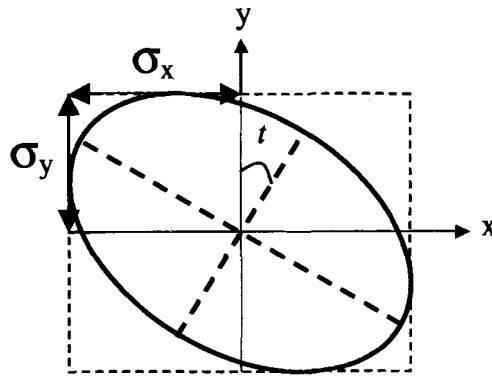


Figure 5. Error ellipse and its components

Consequently, the semi-minor axis defines the point's direction of least uncertainty, or the strongest direction in which the point's position is known (Wolf and Ghilani, 1997). If the uncertainties in both directions are equal (i.e., $\sigma_x = \sigma_y$) and independent, the ellipse's shape is an error circle. Yet another measure of positional uncertainty is Circular Error Probable (CEP). The CEP is defined to be $CEP = 0.589(\sigma_x \sigma_y)$, where the probability of the point's true position lying inside a circle with radius CEP is 50 percent. The RMSP, error ellipse, and CEP are common methods of quantifying point positional error. Appendix B offers a more comprehensive examination of statistical probability methods for positional uncertainty.

While point error models provide information regarding positional uncertainty, it is more useful to obtain uncertainty measures for lines and objects. Despite solid point modeling theory, lines and polygons have proven more problematic for visualizing and modeling their associated errors. The complexity arises from the need to take independent error models of individual points and combine them to form a more complex, dependent model. Just as a line is composed of two endpoints, the line's error is derived from the error of its endpoints. In like manner, a polygon's error can be derived from the error of its boundary line segments. By designing error models for spatial objects based on the error models of their more basic components, it is hoped that a building-block approach can be used to formulate uncertainty indices for complex objects.

2.2.2 Fuzzy Set Theory

Within a GIS, spatial phenomena often possess indeterminate boundaries yet are represented by sharply bounded objects. This data may be better characterized by a more vague or fuzzy description when class boundaries are unclear. Fuzzy set theory is one such approach which can manage vague objects and classes. It is a mathematical modeling environment that incorporates uncertainty, imprecision, and partial truths in its process.

Fuzzy set theory represents a method for assigning levels of membership to elements in a set. It is closely related to fuzzy logic, which allows the assignment of weights to propositions within a system and is useful for decision-making. Fuzzy set theory is well suited for handling vagueness (i.e., poor object or class definition). Fuzzy sets use membership functions to assign real numbers in the interval $[0,1]$ to elements. Membership in a fuzzy set is treated as a probability, which can be considered a degree of truthfulness for an assertion using fuzzy logic. The real number value indicates the element's grade of membership within the set, with 1 being complete membership and 0 being no membership. When fuzzy membership functions are used to classify spatial data, fuzzy objects with indeterminate boundaries result. Fuzzy set theory can enhance traditional

vector data models by incorporating existing uncertainty into the qualitative and visual representation of the data. Crisp boundaries are therefore replaced by fuzzy borders, yielding a less precise but more accurate spatial portrayal. Within raster data, fuzzy set theory can divide spatially continuous fields into fuzzy regions or classes. The typical approach in image analysis begins by segmenting the image into regions that are similar with regard to an attribute(s). However, it is often difficult to divide data into distinct classes, as is the case with remotely sensed forest and vegetation imagery. With the presence of vague class boundaries, fuzzy set theory can be very useful in handling complex class membership schemes.

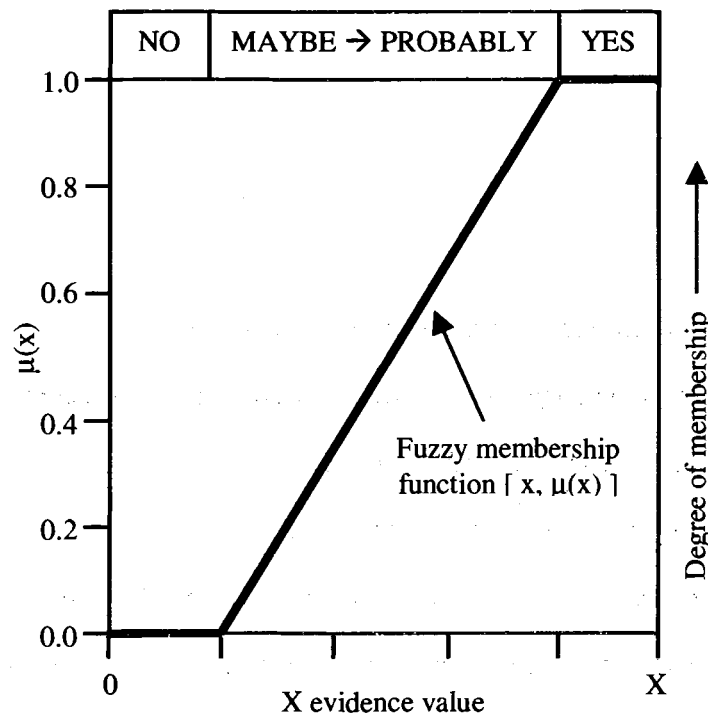


Figure 6. Fuzzy membership function with interval [0,1]
(Figure from Rogge and Halden, 2000)

Some other advantages of fuzzy set theory are its ability to use an infinite set of membership grades, and the ability to use functions and quantifiers that are inherently vague. However, drawbacks include the problems associated with changing class intervals, and when data has zero value or is missing, resulting in a skewed class distribution.

2.2.3 Bayesian Statistics

Bayesian statistics are used to combine information from different sources with varying degrees of reliability. Bayesian networks are a powerful tool that can define a complete probabilistic model based on local conditional probability distributions. These probabilistic models can then be applied to manage uncertainty in GIS applications.

While probability is at the foundation of Bayesian statistics, their significance stems from the additional use of prior knowledge concerning the variables or parameters of interest. Bayesian networks contain rule-based reasoning capability that can incorporate this prior knowledge (e.g., uncertainty estimates). Bayesian techniques can be applied to mathematical models, probability distributions, and thematic spatial data. Within spatial analysis, Bayesian statistics are useful for showing how an observed value of a variable is significantly different from the mean or expected value.

Bayesian networks are capable of representing a system's variables, relationships, and underlying probabilities. Variables are represented by nodes, with the relationships between the nodes expressed as conditional probabilities and represented by arcs. Prior knowledge can be input into each node (variable), and this information can be propagated through its dependent nodes in the system. Flow from one node to another may exist in only one direction, indicating that the source node is conditionally independent of the other.

Bayesian statistics provide a meaningful and straightforward interpretation of probabilistic inferences by incorporating prior knowledge. Such knowledge may come in the form of estimates for an underlying distribution, acquired via sampling and field data. Berztiss (2002) uses the example of estimating the number of left-handed people in your city. If at the time of the sampling you know a convention of left-handed people is being held, this prior knowledge can be

used to adjust the observed probability. Bayesian networks are essentially extended probabilistic models. By combining the model predictions with outside knowledge, the resulting estimates are able to provide a more accurate approximation than probability models alone.

2.2.4 Dempster-Shafer Belief Theory

Similar to Bayesian networks, Dempster-Shafer theory presents a useful tool for making decisions under uncertainty, combining information from different sources. The theory allows a method for pooling the total evidence available for a decision. Dempster-Shafer focuses on the combination of degrees of belief or support from distinct bodies of evidence. Uncertain belief for propositions based on evidence is represented by belief functions. Conventional probability theory (and Bayesian networks) use probabilities that are fixed and known in advance. Dempster-Shafer theory is a generalization of probability theory, in that only the upper and lower bounds on probabilities are available.

Dempster-Shafer theory attempts to fully describe the evidence concerning inferences or propositions. To accomplish this, Dempster-Shafer techniques quantify the degree of support for a proposition (*belief*), support for the negation of a proposition (*disbelief*), as well as the degree to which the negation of the proposition is not supported (*uncertainty* or *lack of belief*). In this manner there may be some belief that is uncommitted, and therefore a distinction between *disbelief* in a hypothesis and *lack of belief* in a hypothesis.

The portrayal of evidence for a hypothesis within Dempster-Shafer theory is based on two independent “belief functions”. The upper boundary function of uncertainty, plausibility, separates disbelief from uncertainty. The plausibility function represents an optimistic assessment that the evidence supports a proposition. The lower boundary function, belief, is the conservative assessment that the proposition is supported by the evidence. The belief function

separates uncertainty from belief. Uncertainty is considered the degree of confidence in the belief portrayal, and is represented by a confidence band bounded by the belief functions (Rogge and Halden, 2000). A real number between 0 and 1 indicates the degree of support a body of evidence provides for a proposition. In this manner:

$$\text{Belief} + \text{Disbelief} + \text{Uncertainty} = 1$$

This contrasts with Bayesian theory which assumes that the inference or proposition is Boolean; it either exists or does not exist. In the Bayesian case:

$$\text{Belief} + \text{Disbelief} = 1$$

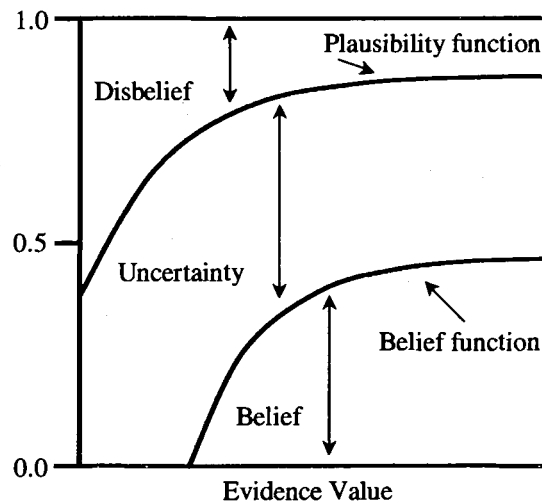


Figure 7. Dempster-Shafer belief functions (Figure from Rogge and Halden, 2000)

By integrating uncertainty with belief and disbelief, Dempster-Shafer theory allows a process that can adapt to accumulating evidence. Gordon and Shortliffe (1985) developed an algorithm which adjusts the belief functions based on new evidence, attempting to narrow uncertainty to either belief or disbelief.

There is limited research applying Dempster-Shafer to decision-making and GIS. Most GIS projects employing Dempster-Shafer theory have focused on the thematic aspect of spatial data. Such research typically derives evidence for class membership from various spatial data sources, including remotely sensed imagery and GIS field data. Further investigation could focus on incorporating Dempster-Shafer theory into criteria selection, uncertainty evaluation, and risk analysis in the GIS environment.

An insightful comparison of the Bayesian statistical model and the Dempster-Shafer belief theory is provided by Flack (1996), who claims the difference between the two measures is conceptual. The Bayesian model assumes that phenomena are Boolean, meaning they either exist or do not exist:

“The result of this assumption leads to the implication that commitment of belief to a hypothesis leads to the commitment of the remaining belief to its negation. If there is little belief for the existence of a phenomena this would imply, under Bayesian formulation, a large belief to its non-existence.” (Flack, 1996)

As we have shown, Dempster-Shafer theory assumes more complex, non-Boolean behavior, and therefore lack of belief in a proposition does not imply disbelief.

Flack additionally notes another distinction between Bayesian statistics and Dempster-Shafer theory, that of prior probabilities. Bayesian networks use probabilities that are fixed and known in advance; therefore each parameter within the Bayesian model must be assigned a prior probability. Within some applications, such as ground truthing within remote sensing, this can be a daunting task (Strahler, 1980). However, supporters of Bayesian theory claim that prior probabilities, representing a priori expectations that are refined as evidence is accumulated, are a

natural part of reasoning (Flack, 1996). Stassopoulou and Caelli (2000) provide a method of building detection using Bayesian networks, while (Stassopoulou et al, 1996) incorporate Bayesian and neural networks for geographic information processing.

Some advantages of Dempster-Shafer theory are its capability to handle missing or zero-value data, and its application to areas not well explored. However, critics cite the impracticality of trying to conceptualize belief and disbelief as a major drawback.

2.3 Image-based Positional Measurements

2.3.1 Film-based Photogrammetry

Remotely sensed imagery provides a fast and efficient means of collecting large volumes of information about the earth's surface. Remote sensing is the act of measuring electromagnetic energy from a region (visible light, radio waves, heat, etc.) at a distance. The measurement of electromagnetic energy can be performed either photographically or electronically, and the results are recorded and stored in the form of images. The art of measuring and interpreting remotely sensed images is termed photogrammetry. Photogrammetry allows measurements from photographs and digital images to be converted into X,Y,Z ground coordinates of individual points through the process of aerotriangulation.

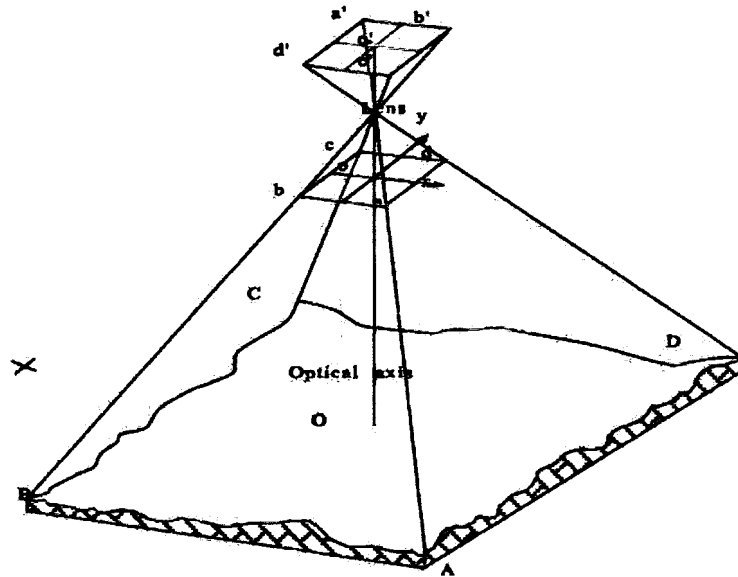


Figure 8. Geometric relationships between focal plane, camera lens, and ground (Fahsi, 1996)

Analytical photogrammetry deals mainly with film-based aerial photography, while digital photogrammetry makes use of digital imagery that has been either digitized or remotely sensed. Analytical photogrammetry is typically of higher precision due to manual input and measurement of reference points. Digital photogrammetry employs powerful automated detection and extraction procedures which allow large amounts of data to be processed quickly. Film-based photographs, their features, and measurements can be converted for use in digital databases through digitizing or digital image scanning.

Analytical photogrammetry is that realm of photogrammetry that deals with film-based remotely sensed imagery. Film-based imagery is often collected via aerial cameras, or sometimes high-altitude terrestrial cameras. Photogrammetric measurements such as length, angles, or coordinates are made with respect to the image negatives. Analytical measurements are made with various equipment, the most rigorous and complex of which is the stereoplotter. A stereoplotter is used to align two parallel aerial images in a way that three-dimensional ground

measurements can be derived from them. These ground measurements are determined through aerotriangulation, which utilizes the condition that an object point, its photo image, and the exposure station all lie along a straight line.

The accuracy of points or targets measured by stereoplotters is dependent on the flying height when the image was captured. A well-marked target in an image can be measured by a stereoplotter to $\sigma_{xy} = \pm 5\mu m$. The actual horizontal ground accuracy this represents depends on the scale of the image. The scale of an image (S_I) is related to the image flying height (Z) and the focal length of the camera (c).

$$S_I = Z/c$$

Vertical accuracy can be measured by a stereoplotter to approximately 0.006% of the flying height. For instance, at a flying height of 1,000m, a stereoplotter can measure with a vertical accuracy of ($\sigma_z = 6cm$).

When dealing with points that are not well marked, (i.e., natural points like corners of buildings or manholes) a manual operator will be subject to the stereoplotter's measuring limitations ($\pm 6\mu m$) as well as identification error. Identification error arises from imperfect definition of points or objects within an image. A human's ability to discern objects is limited and therefore affects the accuracy with which these objects are measured. A general formula for determining the accuracy of measuring natural points involves the stereoplotter's measuring accuracy (σ_m) as well as error of definition (σ_{def}).

$$\sigma = \sqrt{\sigma_m^2 + \sigma_{def}^2}$$

Table 1 outlines typical errors of definition when using a stereoplotter to measure various points. The table illustrates that errors of definition are larger than a stereoplotter's errors of measurement.

<i>Point</i>	Error of definition: $\sigma_{xy (def)}$	Error of definition: $\sigma_z (def)$
Corner of building	7 - 12cm	8 - 15cm
Manhole	4 - 6cm	1 - 3cm
Corner of field	20 - 100cm	10 - 20cm
Bushes, Trees	20 - 100cm	20 - 100cm

Table 1: Rules of thumb for errors of definition with stereoplotter

Manually measuring continuous lines with a stereoplotter is less accurate than point measurement. The horizontal accuracy of such lines typically ranges from 0.3 - 0.45 μ m. A coarse formula for the vertical accuracy of measuring lines is $\pm 0.025\%$ of the flying height. Photogrammetric plotters can also be used as a stereo (3D) digitizer, collecting planimetric and height data for digital maps. When used to measure heights within an image, the plotters surface measurements are interpolated between measurements to produce continuous digital elevation models (DEM).

2.3.2 Digitizing

Before geographic information systems can be designed, the data they consist of first has to exist in digital form. Paper maps and other physical representations are converted to digital form by the process of *digitizing*. Manual digitizing by an operator is used to record key features from a physical representation and convert them to vector data consisting of points, lines, and polygons. In addition, image scanners can be used to digitize whole maps or photographic images into

continuous raster data. Often the two methods are combined: physical images are often converted to raster data through digital scanning, and a human operator can then perform vector tracing of the new digital image. Similar to digitizing, vector tracing is the process of recording relevant features from a raster image to be stored in vector form. The accuracy of digitizing/vector tracing is dependent on both the resolution of the representation being traced and the accuracy of the human operator. A digitizing table will also have accuracy dependent on the resolution of the signal passed between the table and the digitizing pen. Typically a digitizing table's measurement accuracy is in the range of 0.075 mm to 0.5 mm, without taking into account human error (Jackson and Woodsford, 1991). Human error is almost impossible to model due to cognitive decision making far too complex for any mathematical model. The process of digitizing typically involves the extraction of continuous multi-nodal features, such as road networks or polygons. The continuity of the vector tracing of such features gives rise to continuity and dependency among their errors, which further complicates the error modeling process.

Digital scanners have varying accuracies depending on cost and intended use; today's simple office scanners typically have a scanning accuracy of 0.021 mm, which translates to 1200 dots per inch. High end scanners are capable of accuracies greater than 0.002 mm, or 12,500 dots per inch. Inaccuracies in digitized map features arise for a variety of reasons, such as the original article's resolution, circumstances of data capture, the manner in which features are represented in a database, and the ways which data are manipulated (Dutton, 1992). When determining accuracies of digitizing maps or images, standard deviations can be derived through differences of repeat digitizations (Caspary and Scheuring, 1992). These standard deviations can then be used as point error models for error adjustment and propagation of error through complex objects. Errors arising due to the digitization process are sometimes described using a *circular normal distribution*. A circular normal distribution involves two variables with no correlation to each

other and equal standard deviations. The lack of correlation indicates the variables are independent, and the equal standard deviations indicate uniform error in all directions. An error circle can be used to visualize this condition, as discussed in Appendix B.

2.3.3 Digital Remote Sensing and Image Processing

Film-based photography measures and records electromagnetic data on film. Digital photography is similar to film photography, but image data is recorded on arrays of charge-coupled devices (CCDs). These electronic sensors generate an electrical signal that corresponds to the energy variations in the original scene. The resulting digital image consists of pixels storing each sensor's signal as an integer (digital number). Digital remotely sensed data can be obtained through handheld digital cameras, digital aerial cameras, and space-borne satellites. Digital camera image formats range from 512 by 512 pixels to 2048 by 2048 pixels or higher, with a typical pixel size of 9 by 9 μm . The ground resolution of digital aerial cameras is dependent on flying height, but common results range from 0.5 to 4 meters per pixel (Lillesand and Kiefer, 1994). Satellite sensors are continuously measuring electromagnetic energy and streaming the data to earth in digital format. These satellites house diverse sensors that can detect multispectral bands of the electromagnetic spectrum. Remote sensing spacecraft such as Landsat, SPOT, and NOAA satellites can provide imagery with ground resolution between 1 and 30 meters.

Film-based photography offers a higher degree of spatial detail and geometric integrity than electronic sensing devices. However, electronic sensors can detect a broader range of the electromagnetic spectrum, results are achieved quickly and are stored in convenient digital form. Digital image data is extremely useful for geographic information systems for many reasons. It allows the storage and cataloging of numerous images, and most importantly, data analysis of the images can be automated. Broad spectral patterns can be quickly and fully examined using automated techniques, a process that would otherwise be tedious for a human operator. Since

digital images are simply sets of pixels with numerical values, computers can apply equations and algorithms on a pixel-by-pixel basis to manipulate and interpret them. Among the computer-assisted techniques are image rectification and restoration, enhancement, and image classification. Image rectification adjusts image distortion or degradation to “create a more faithful representation of the original scene” (ibid.). Image enhancement techniques adjust images to more effectively prepare images for analysis and interpretation. Examples include thresholding, contrast stretching, spatial filtering, edge enhancement, and Fourier analysis. Yet the most significant of automated processes of digital images are those involving image classification.

Classifying pixels in an image allows visual analysis to be replaced by automated quantitative techniques for identification of features in a scene. The goal of classification is to categorize an image’s pixels into various land cover classes or themes. Classification is based on both spectral pattern recognition (trends in the recorded spectral responses) and spatial pattern recognition (geometry of features in a scene). Spectral patterns are useful because different feature types exhibit different spectral reflectance properties across wavelength bands. Spatial pattern recognition categorizes image pixels based on their spatial relationships with neighboring pixels. Aspects of spatial patterns taken into account are texture, pixel nearness, shape, directionality, and repetition. Spatial pattern recognition attempts to mimic the cognitive spatial analysis performed by humans during visual interpretation of images. Consequently, such classification tends to be more complex and computationally intensive than spectral pattern recognition procedures (ibid.). Often the best classification result is obtained through a combination of both spectral and spatial pattern recognition. As a result, a variety of methods of pixel classification exist to transform imagery into simpler maps for such themes as land use or vegetation cover (Goodchild and Min-hua, 1989).

The spectral response recorded for each pixel in a digital image is an integral over the area of the pixel of a continuous, spatially autocorrelated variable. Consequently, it is common to think of response data as a random sampling of a continuous surface or field. Yet an image that has been classified can be conceptualized as an array of discrete values in which each pixel has been assigned to one of a number of classes (ibid.). As a result, there are no objects or features to be located; pixels are simply members of a group. Therefore, classification accuracy is a function of the errors in the assignment of classes to each pixel.

Another fundamental photogrammetric operation related to classification is automated feature extraction. It is a technology that can assist and facilitate image analysis and interpretation of remotely sensed data. By applying post-processing techniques to enhance and isolate feature definition within digital imagery, automated feature extraction can identify relevant features and their outlines. Such post-processing techniques include mathematically strengthening feature-to-background contrast, eliminating image “noise”, and pattern recognition (NCRST, 2001).

Feature extraction is typically semi-automated, requiring human input for some manual approximations which are then applied within automated algorithms. Which tools and approaches to use, as well as the quality of the results, depends upon the qualities and characteristics of the imagery and on the nature of the feature extraction problem. The complete process requires setting up a sequence of processing steps and defining the parameters and initialization criteria for each step.

Automated feature extraction can be applied to a broad range of imagery interpretation tasks, employing complex image processing algorithms to isolate desired features. Success in isolating specific features depends on establishing a set of conditions that uniquely mark that feature. The spectral signature of a given feature, as represented by digital numbers stored in pixels, typically clusters around some mean value. This knowledge can be used to exclude large portions of an

image from consideration in the extraction process. While spectral signature alone is normally not sufficient to allow feature recognition, it is an important part of defining the subset of an image. In panchromatic imagery, only one value is used to represent each pixel in the image. In multispectral imagery, more information is available from different spectral bands which can be used to refine exclusion criteria. Knowledge of range and contrast of the surrounding pixels, referred to as texture or segmentation analysis, is also useful in automated feature extraction. The spectral characteristics of image subsets provide information about the features and transitions from one area of the image to another. Patterns (and their distribution) within an image aid in the filtering process by offering indicators of the location and configuration of a feature. As a result, linear features such as roads, railroads, and pipelines are prime candidates for automated feature extraction (ibid.).

Such linear features may take approximations in the form of an initial point and approximate direction, or a set of points that approximate the feature from start to end. These approximations are then employed by automated algorithms that conduct profile matching, line detection, edge analysis, or combinations of the methods (Agouris et al., 2001). Automated methods such as dynamic programming and deformable contour models are examples of robust methods for extracting linear features. Full automation of the feature extraction process is being researched by automating the selection of initial approximations, such as node locations or road orientation (ibid.).

2.3.4 Deformable Contour Models

A tool commonly used to extract linear features from digital imagery is the deformable contour model. This tool, sometimes referred to as an *active* contour model or a “snake” (Kass, et al., 1987), is a computer-generated curve that moves within images to find object boundaries. Snakes are often used in digital image processing and image analysis to detect and locate objects, and to

describe their shape. Within this thesis, deformable contour models will be examined as a means to obtain continuous uncertainty boundaries of extracted linear features. Subsequently, snakes will be used to model the interactions between the uncertainty boundaries of neighboring objects. A post-processing step following the extraction of the linear feature, this will serve as the second stage in the information extraction process.

Deformable contour models represent image contours that are easily manipulated by higher-level processes. A snake is essentially a deformable curve that moves under a variety of image constraints (which tend to be local) and object-model constraints. The snake is controlled by a minimizing function which converts high-level information (e.g., curvature and discontinuities) and low-level image information (e.g., gray values, edge gradients and terminations) into energies.

Snakes can be guided or constrained to seek out features in images with particular attributes. Perhaps their most common use is for finding edges and lines in images. Lines and edges have very distinct properties within images regarding their contrast with neighboring features (pixel gradient). Geometrically, a snake will attach itself to an edge location in an image and extend itself along the edge as a series of nodes and line segments until reaching a state of stability. The state of stability is defined by the minimizing energy function. The minimizing energy function defines both internal and external forces which constrain the snake to “slither” under “controlled continuity” (ibid.). Internal forces constraining a snake ensure a degree of smoothness and continuity in its shape. External forces attract or push the snake towards significant image features, i.e., edges. In addition, supplemental external approximations or constraints may be applied to initiate or guide the snake. These approximations may be a direction or a set of points the snake must reach. Most snake operations are semi-automatic, meaning some preliminary approximations must be provided to initiate the extraction procedure. However, these

approximations may also be derived automatically, moving the extraction process closer to a fully automated task. The snake is “active” or “deformable” because it will continue to seek or extend an edge until its constraints are met by a minimized energy function. This turns the object or edge extraction process into an optimization problem (Agouris, et al., 2001).

The snake’s position can be expressed parametrically by $v(s) = (x(s), y(s))$. Its total energy can be written in terms of its component energies:

$$E_{snake} = \int_0^l E_{int}(v(s)) + E_{image}(v(s)) + E_{con}(v(s)) ds \quad (\text{Kass et al., 1987})$$

where E_{int} is the internal energy (smoothness, continuity) of the snake, E_{image} are the image forces attracting the snake to an edge, and E_{con} are any external constraints or approximations supplied by the user.

Extensions of the original snake model include *differential snakes* (Agouris, et al., 2001), which further defines the total energy along a snake at each point as:

$$E_{snake} = \alpha \cdot E_{cont} + \beta \cdot E_{curv} + \gamma \cdot E_{edge}$$

where the three components are continuity, curvature, and edge. Finding edges in an image can be done using a simple calculation of gradients within an image. The larger the gradient is, the greater the snake’s attraction to the edge. The edge term, and all the terms, can be diminished or emphasized by adjusting their corresponding coefficients (a, b, g). The coefficients act as “energy costs” towards the total energy function. Since the snake is constrained by a minimizing function, it will iteratively search for the path that generates the least resistance, i.e., the least energy. The iterative behavior of the snake as it attempts to minimize the energy function holds significant implications for the errors associated with extracted lines and edges.

As the snake iteratively lengthens itself along an edge, it adds nodes to its shape in a continuous manner. A small error at an early iteration can therefore have an impact on the shape and error of the entire edge. For example, if the snake strays from the edge during its initial iterations, it may be inclined to continue its current course in order to minimize the energy function. The small error can be compounded iteration after iteration, and may eventually propagate throughout the entire contour line. The result is a line lying only partly on the edge with one end dangling in image space. It may seem that the simple solution would be to give the gradient a high emphasis. However, rarely are edges fully continuous and unobstructed by neighboring features or noise. Over-emphasizing the edge term can cause the snake to search for the *largest* gradient in the neighborhood, which may not be the current edge. The snake may otherwise search for *any* gradient, causing the snake to jump to different edges at edge junctions (e.g., road intersection, noisy areas, obstructed views). The challenge is coming up with suitable coefficients for the snake minimizing function.

Deformable contour models are a powerful feature extraction tool for extracting lines and edges as continuous objects. Section 4 will demonstrate how the continuous nature of deformable contour models can be used to extract uncertainty boundaries of multiple line segments. Building upon this approach, snakes will further be used to model the interaction of uncertainty boundaries of neighboring features.

Another semi-automated linear feature extraction method is based on sequential solutions derived by dynamic programming that requires seed points to provide a rough description of the line. Alternatively, a combination edge analysis follower and area-based correlation follower can employ an initial point and direction for linear extraction. Similar to snakes, these models are based on iterative processes that can result in positional error propagation. An analysis and

comparison of these methods with regard to road extraction is provided by Dal Poz and Gyftakis (2000).

3. ESTIMATING POSITIONAL UNCERTAINTY OF A LINE SEGMENT IN GIS

Developing methods to express the accuracy or uncertainty of spatial information has been the focus of much research within the spatial data community. With regards to positional uncertainty, these methods have been continually developed and extended over the last twenty years. Within our discussion, the terms 'error' and 'uncertainty' will be used almost interchangeably. The spatial data community, while recognizing the inherent differences between the terms, is often at odds when trying to define or separate them. This confusion is due, in part, to the similar concepts the terms are meant to convey. Error analysis is used to determine the discrepancy between the true and measured values of an object or location. However, a true value or location is a luxury not often available in spatial data. For example, determining a 'true' location for a wetlands boundary, or 'true' location of objects extracted from coarse imagery. In the absence of a true value, uncertainty is substituted for error. In order to achieve the goals of this paper, we must analyze and apply previous research on positional error and uncertainty. Any investigation of uncertainty measurement methods reveals extensive use of error analysis techniques. For the sake of simplicity we will assume that the terms 'uncertainty', and 'error' both indicate a deviation from an expected value. In addition, the term accuracy can be considered the complement to the two terms, i.e., the "closeness" to the true value.

The topics of this paper are concerned mainly with estimating spatial uncertainty boundaries and modeling their interactions with each other. The spatial uncertainty we address is that which arises from image-based measurement and data production methods, e.g., automated feature extraction. Furthermore, we wish to focus on interactions among data derived from different sources and techniques. As previously noted, spatial objects are comprised of points, lines, and polygons. As the most fundamental geometric element, points and their error models have long been studied in the fields of geodesy, surveying, and mapping (Shi 2000). Section 2.1.3 stated that all observations and measured values contain errors, and Section 2.3 indicated sources of

error or uncertainty within positional measurements. The uncertainty of digital spatial databases is typically expressed through point error measurements. Point errors can be quantified using standard deviations of points in the x, y, and z directions. Due to the two-dimensional nature of maps and imagery, error is typically quantified as either a single directionally independent measure (σ), or as standard deviation along two directions (σ_x, σ_y). Some common error measurement methods that utilize standard deviations are the root-mean-square positional error (RMSP), error ellipses, and the Circular Error Probable measure (CEP). Section 2.1 and Appendix B examine point error measurement methods more closely.

While point error models provide information regarding positional uncertainty, it is more useful to obtain uncertainty measures for lines and objects. Current techniques of spatial data measurement extract complex objects as separate entities made up of nodes and line segments. As the methods of data extraction advance, so too must the methods of estimating the associated uncertainty within the data. Despite solid point modeling theory, lines and polygons have proven more problematic for visualizing and modeling their associated errors. The complexity arises from the need to take independent error models of individual points and combine them to form a more complex, dependent model. Just as a line is composed of two endpoints, the line's error is derived from the error of its endpoints. In like manner, a polygon's error is derived from the error of its boundary line segments. By designing error models for spatial objects based on the error models of their more basic components, it is hoped that a building-block approach can be used to formulate uncertainty indices for complex objects. To this end, recent research has been devoted to develop error models for the positional uncertainty of a line segment. Appendix B includes an in-depth examination of four major efforts that have produced or advanced positional error models for line segments. The results will be reviewed here briefly.

3.1 Rigorous Error Models

Chrisman (1982), expanding on the work of Perkal (1966), investigates the idea of providing an uncertainty boundary surrounding a line segment. The uncertainty boundary, called an *epsilon band*, is based upon a constant radius (epsilon) around a line's true or most likely position. The quantity epsilon (ϵ) is derived from the radius of the line's endpoint error circles, assuming a digitization process that yields random coordinate error in a *circular normal distribution*. The circular normal distribution is two-dimensional (bivariate) and varies normally, meaning that it consists of errors in two directions that are equal and uncorrelated. As figure 9 demonstrates, the epsilon band's width is contingent on a single error quantity. The main drawback of this model is that it provides no interpretation of error distribution inside the band.

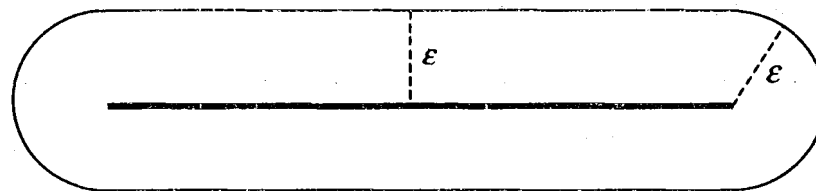


Figure 9. Chrisman's ϵ - band (Adapted from Chrisman, 1992)

Dutton (1992) tests the method Chrisman and Perkal use to derive vector representations of digitized map features. Similar to their work, Dutton assumes that digitized points produce error that follows a circular normal distribution. Likewise, his analysis characterizes feature uncertainty by constructing regions of "constant locational probability around the edges of polylines" (ibid.). However, Dutton's result describes concave curvilinear error bands along the most likely line segment position. An underlying basis for study of digital spatial feature uncertainty is that every feature is made up of points that are uncertain to some degree. Dutton assigns each point a circular "locus of uncertainty", within which "any location can be considered a reasonable alias" (ibid.). This uncertainty area is simply an error circle, with each error circle

possessing equal radii. Since any location within the circle can represent the actual point, Dutton postulates that a multitude of line segments can connect two uncertain points. In order to determine a most likely segment position, Dutton performs an experiment involving multiple realizations of possible segment positions.

Figure 10 illustrates Dutton's experiment and results. As a result of his experiments, Dutton finds that the displacement error from each segment to the median line it represents is greatest near the measured points and least halfway between them. Dutton finds the results "odd at first," because the midpoint error is at a minimum despite the lack of a coordinate measurement (ibid.). The conclusion is that despite the precision of a segment's endpoint positions, its centerpoint is the most reliable location. Based on the standard deviation at 11 evenly-spaced locations along the baseline, Dutton is further able to derive a probability contour one standard deviation (σ) in width. In the same year, the work of Caspary and Scheuring (1992) helps verify that Dutton's simulations are right on target.

Caspary and Scheuring refine Chrisman's idea to describe the accuracy of lines derived from positional errors of endpoints. Like Chrisman and Dutton, they assume equal endpoint coordinate errors following a circular normal distribution. However, the authors use error propagation and Monte Carlo simulation

Figure 10 illustrates Dutton's experiment and results. As a result of his experiments, Dutton finds that the displacement error from each segment to the median line it represents is greatest near the measured points and least halfway between them. Dutton finds the results "odd at first," because the midpoint error is at a minimum despite the lack of a coordinate measurement (ibid.). The conclusion is that despite the precision of a segment's endpoint positions, its centerpoint is the most reliable location. Based on the standard deviation at 11 evenly-spaced locations along the

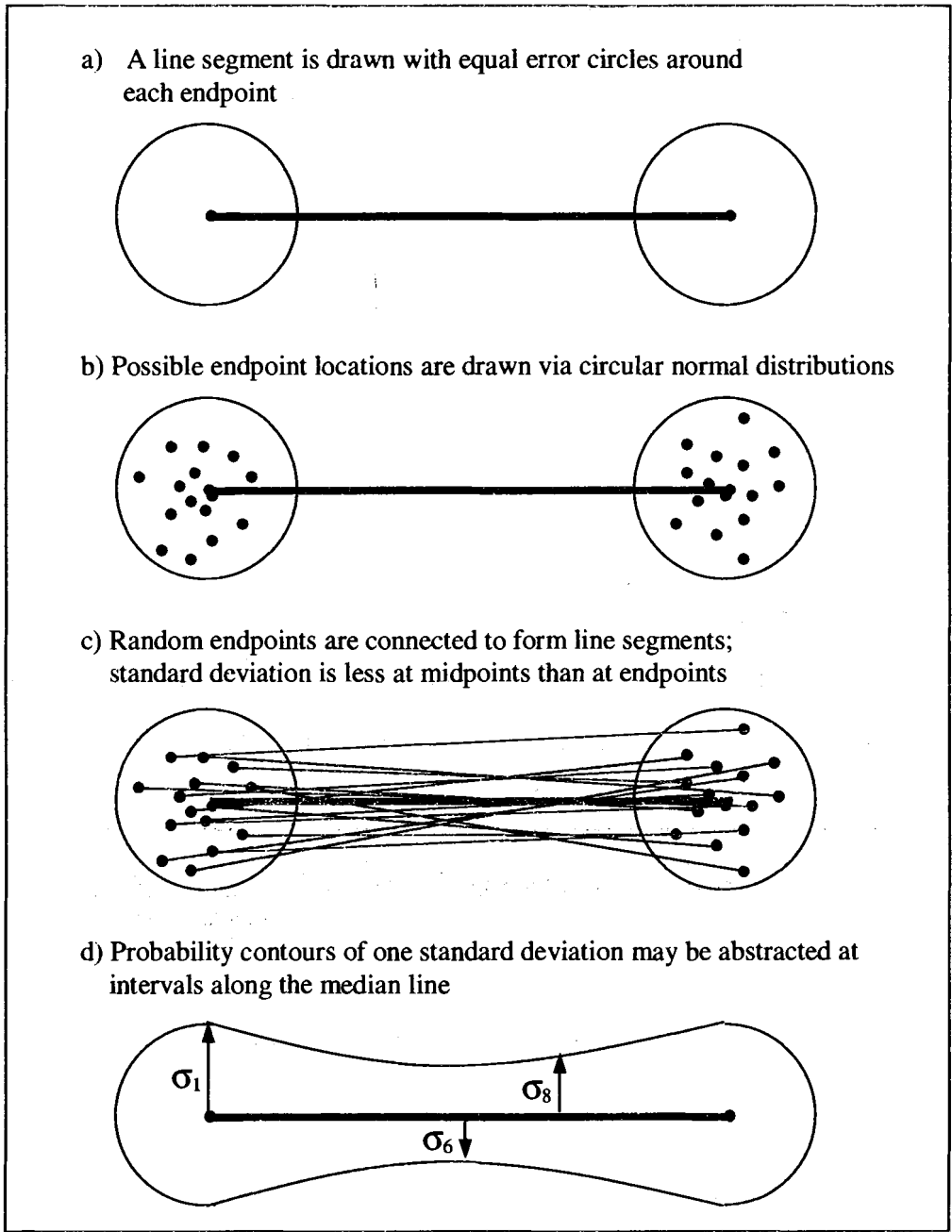


Figure 10. Dutton's experiment simulating line segments (Adapted from Dutton, 1992)

baseline, Dutton is further able to derive a probability contour one standard deviation (σ) in width. In the same year, the work of Caspary and Scheuring (1992) helps verify that Dutton's simulations are right on target.

Caspary and Scheuring refine Chrisman's idea to describe the accuracy of lines derived from positional errors of endpoints. Like Chrisman and Dutton, they assume equal endpoint coordinate errors following a circular normal distribution. However, the authors use error propagation and Monte Carlo simulation to derive their own *error-band* that sags at the midpoint of the line segment.

Caspary and Scheuring define the coordinates of an arbitrary point along a line as a function the line's endpoints and the point's position along the line. By applying error propagation law to this definition and assuming independent and equal endpoint errors, the authors are able to predict how the uncertainty varies along the length of the line. Using their derivations, Caspary and Scheuring show that points towards the middle of straight lines have smaller RMSP values than those at the endpoints. More precisely, the midpoint error proves to be a factor of $1/\sqrt{2}$ less than the endpoint error, while the error-band is 0.8 times smaller than the area of the epsilon-band. The authors propose that the more accurate error-band is an area determined by the error circle boundaries of all points along the line, rather than strictly the error of the endpoints. However, it should be noted that applying error propagation law still requires the inner error circles to be dependent on the endpoint error.

As a result of smaller error at a line's midpoint, Caspary and Scheuring's error-band curves towards the center, similar to Dutton's. Despite the admitted difficulties of analytically

expressing the shape of their error-band, the authors are able to approximate the shape and area of the region according to figure 11.

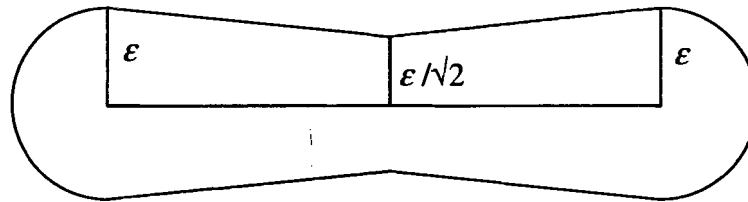


Figure 11. Approximation of the error-band
(Adapted from Caspary and Scheuring, 1992)

The authors wish to derive a region of constant probability around a straight line, which they represent as a four-dimensional random vector. In order to verify their work, they use Monte-Carlo simulation similar to that of Dutton's (1992), as illustrated in figure 12.

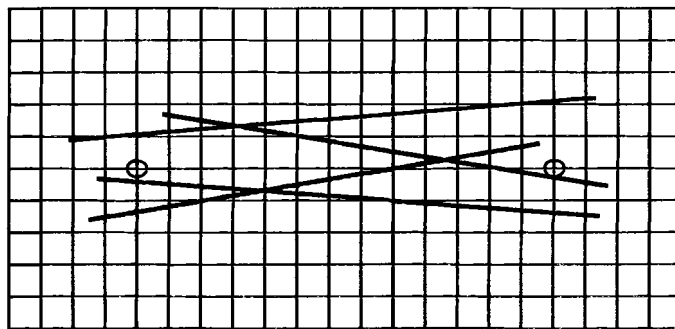


Figure 12. Cell array and random lines simulation
(Adapted from Caspary and Scheuring, 1992)

The work of Caspary and Scheuring (1992) is important for positional accuracy of objects within spatial databases because it:

1. Uses the error propagation law to derive positional errors along the line.
2. Concludes that an appropriate error-band is determined by the error circle boundaries of all points along the line, rather than strictly the error of the endpoints.
3. Views a straight line as a four-dimensional random vector.
4. Compares the marginal density of a line to the distribution function of an endpoint.

These observations are employed by Shi and colleagues (Shi and Tempfli, 1994; Shi and Liu, 2000) to expand on Caspary and Scheuring's work to model positional errors of line features in GIS. Once again, uncorrelated coordinate errors are assumed, following a normal distribution. In addition, the positional error and distribution of an arbitrary point on a line segment are dependent on the errors and distribution of the endpoints. Using these assumptions, Shi and Tempfli (1994) define the probability distribution of a line segment. Shi and Liu (2000), however, use the more general case of interrelation between two endpoints to generate a modified error-band.

Providing a more explicit characterization of Caspary and Scheuring's (1992) idea of a four-dimensional random vector, Shi and Tempfli (1994) define two endpoints as stochastic vectors following a normal distribution:

$$Z_1 = \begin{bmatrix} X_1 \\ Y_1 \end{bmatrix} \sim N_2 \left(\begin{bmatrix} \mu_1 \\ v_1 \end{bmatrix}, \begin{bmatrix} \sigma_{XX} & \sigma_{XY} \\ \sigma_{XY} & \sigma_{YY} \end{bmatrix} \right), \quad Z_2 = \begin{bmatrix} X_2 \\ Y_2 \end{bmatrix} \sim N_2 \left(\begin{bmatrix} \mu_2 \\ v_2 \end{bmatrix}, \begin{bmatrix} \sigma_{XX} & \sigma_{XY} \\ \sigma_{XY} & \sigma_{YY} \end{bmatrix} \right).$$

The equal variances and covariances indicate independent endpoint errors, which the authors admit, "may not be realistic in case of a multi-source GIS" (ibid.). The line connecting the two endpoints is expressed as a linear, normally distributed function of the endpoints. Drawing from Caspary and Scheuring's (1992) investigation of the marginal density of a line, Shi and Tempfli derive the probability distribution of a point in a direction perpendicular to the line. In this manner, a boundary can be formed indicating how the point's position can vary from its true or mean position. The probability distribution of the line segment can therefore be characterized by the perpendicular density of any point along the line and the density at the two endpoints. The line segment's probability distribution describes how the segment can deviate from its expected

or mean location (Shi and Tempfli, 1994). This concept is expanded upon in Shi's later work with Liu (2000).

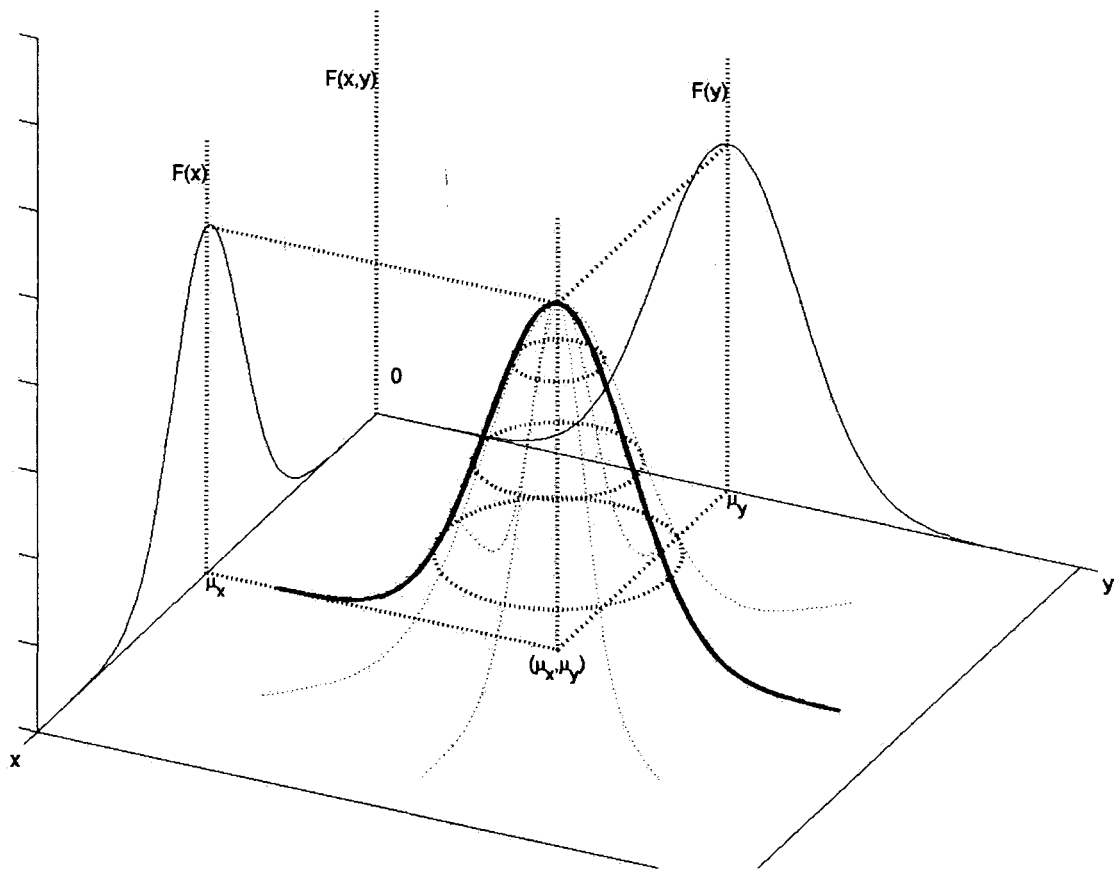


Figure 13. The probability density function (bivariate) of the point (x,y)
 (Adapted from Shi and Tempfli, 1994, and Shi and Liu, 2000)

Shi and Liu further develop these ideas by producing a more general model of the error band, called the G-band model. The main improvement of the G-band model is that it allows for correlation between two endpoints, a condition not handled by previous models. In addition, the authors specifically target cases with differing errors between the endpoints. Endpoint errors are still assumed to follow two-dimensional normal distributions. Based on Shi and Tempfli's work (1994), the authors statistically derive the distribution and density functions of a line segment to further define errors of arbitrary points on the line.

The representation of a line as a four-dimensional random vector indicates a four-dimensional normal distribution. The authors offer a parametrization similar to the one presented by Caspary and Scheuring (1992), and indicate that a line segment is a “composite of...infinite stochastic variables $X(t)$ and $Y(t)$ ”:

$$\begin{cases} X(t) = (1-t)X_0 + tX_1 \\ Y(t) = (1-t)Y_0 + tY_1 \end{cases} \quad (0 \leq t \leq 1) \quad (\text{Shi, 1994 and Shi and Liu, 2000})$$

The authors then derive an uncertainty information matrix which provides the linear correlation between segment points and their coordinates. The uncertainty matrix contains relationships between varying errors for two different points in two directions. The matrix is simplified when handling the condition of directional independence among the error components (i.e., for any point, $\sigma_x = \sigma_y$); error ellipses then become error circles with a radius of uncertainty equal to:

$$\Sigma_{zz} = [(1-t)^2 \sigma_0^2 + t^2 \sigma_1^2] \quad (\text{ibid.})$$

This is often the case within GIS vector data production operations, such as digitizing or automated feature extraction.

Based on work with distribution and density functions and their uncertainty information matrix, Shi and Liu derive a generic error band model. Named the G-band, its boundaries are defined by the error ellipses of arbitrary points on the line segment and the error ellipses of the endpoints. While based on conclusions previously drawn by Caspary and Scheuring, the G-band has distinct properties not before articulated. The G-band is directly linked to the distribution and density functions of a line segment, which completely describe a line’s statistical characteristics. As such, it is able to handle correlation between endpoint errors, as well as inequality between these errors. Figure 14 illustrates the definition of the generic error band according to Shi and Liu

(2000). By slicing the spatial density distribution surface *parallel to the X-Y plane*, an infinite number of two-dimensional bands can be obtained. Of these parallel slices through the density surface, the G-band is described by the plane passing through the error ellipse of the endpoints (ibid.).

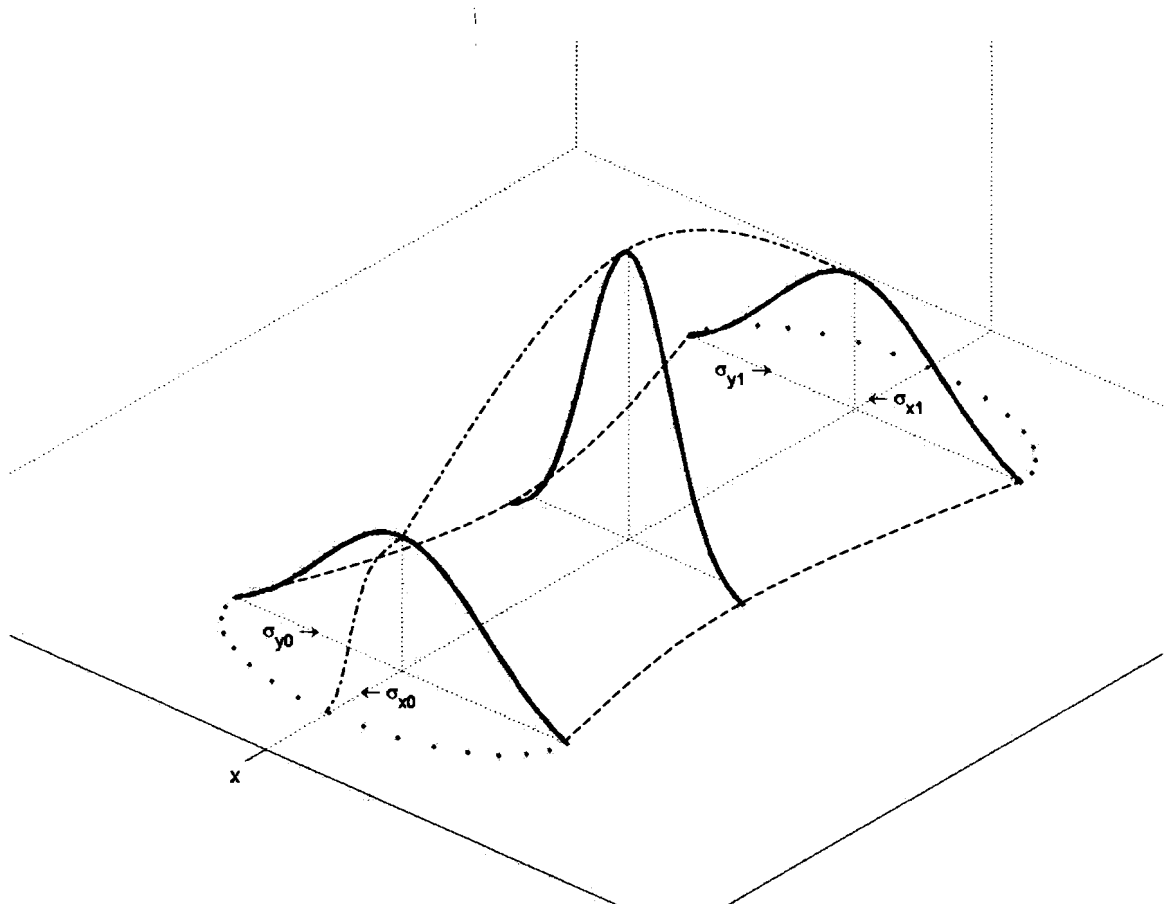


Figure 14. The probability density function of a line (Adapted from Shi and Liu, 2000)

Similar to previous band models, the G-band's shape is described by the error ellipses of all points along the line segment. While Caspary and Scheuring's (1992) error band relies on the assumption of directional independence, this condition is only a special instance of the G-band. Figure 15(a) illustrates this special case of the G-band, when endpoint errors are independent and equal. Under these conditions, the G-band reduces to the error band models of Caspary and

Scheuring (ibid.). Figure 15(b) illustrates the more general case of the G-band, which allows each endpoint to have varying errors in both dimensions.

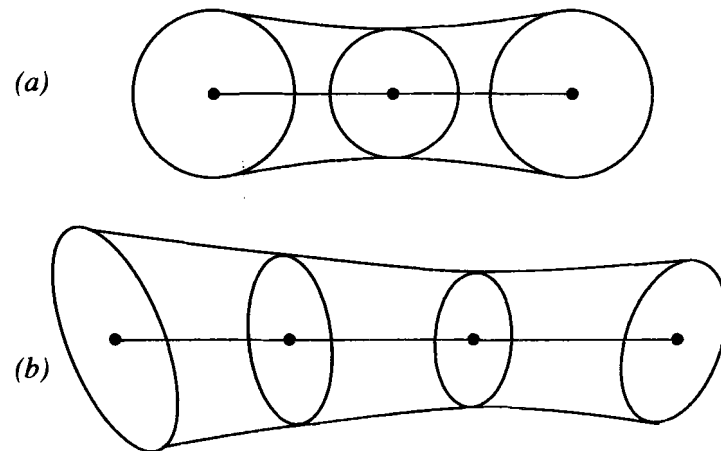


Figure 15. G-bands under varied conditions: (a) equal, uncorrelated errors; (b) unequal, correlated errors (Adapted from Shi and Liu, 2000)

Similar to previous error band models, the G-band sags as the error ellipses along the line decrease. However, due to the G-band's ability to handle unequal endpoint errors, the minimum error ellipse is not necessarily located at the center of the line segment. Figure 16 demonstrates this property with error circles.

Shi and Liu's G-band is the most advanced positional error model of linear GIS features to date. It is a flexible model that can handle unequal and correlated errors between endpoints. Appendix B offers a more comprehensive overview of the aforementioned error models and the statistical measures behind them.

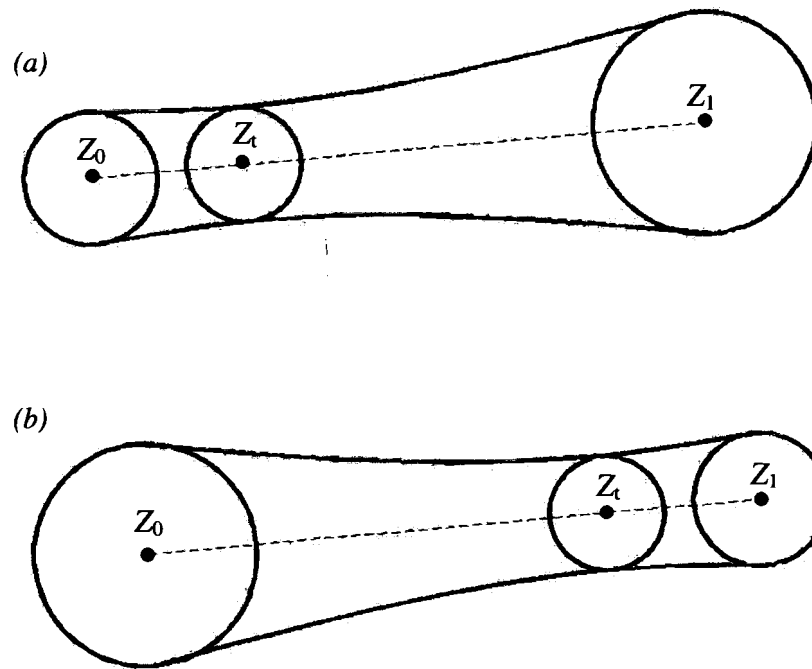


Figure 16. Location of minimum error circle: (a) $\sigma_0 < \sigma_1$, $t < 1/2$;
 (b) $\sigma_0 > \sigma_1$, $t > 1/2$;

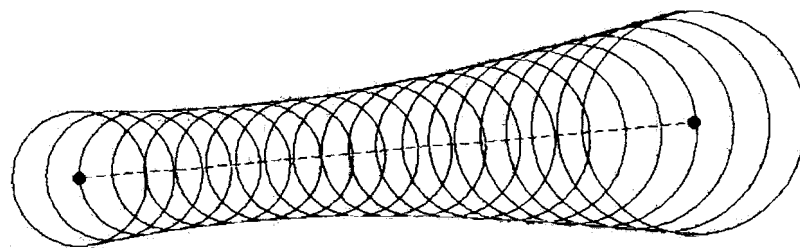


Figure 17. Visualization of G-band as composite of error ellipses (circles)

3.2 Improving Communication and Estimation of Positional Uncertainty Models

While research of positional uncertainty of line segments has been mathematically impressive, using these models as error measures may not be the best solution. The approaches have a sound foundation in mathematics and statistics, yet a few shortcomings are noticeable. One such pitfall involves effectively communicating the results of error measurement to the user. The G-band is a complex and dynamic modeling of the uncertainty of a line segment. Shi and Tempfli (1994) provide some complementary error indicators for a line segment, such as Segment Standard Error and Segment Probable Error. These indicators are less complicated for a user to understand, but offer only a narrow interpretation of the error. Visualization is perhaps the most useful method towards understanding error estimates. Tools such as error ellipses allow quick visual comparisons of relative precisions among points. A strength of the G-band is its unique shape, modeling complex relationships along a line in smooth sets of curves. However, the simple shape of the G-band itself, formed of multiple varying ellipses, is sophisticated. While visually intriguing, as in figure 17, the G-band may serve well in its most basic form: as a simple boundary of uncertainty on both sides of a line segment. In fact, Shi and Liu (2000) use the G-band in this manner to communicate the positional uncertainty of a simple GIS data set. However, the simple sagging towards the middle of recent error models is “odd at first”, and this alone requires a degree of understanding from the user (Dutton, 1992).

Which brings up a second difficulty: while communicating the results of error measures is one pitfall, understanding the foundation of these models is a more daunting task. The mathematical approaches used aren't always intuitive. The mathematical methods behind such error models can be rigorous and cumbersome for a single line segment alone. When deriving models for whole geometric features or scenes, the calculations can be overwhelming. Complicating matters is the application of such mathematical models by the user. An average user of spatial data will have little understanding of the basis of complex error models such as the G-band. As the state of

spatial information stands now, users are likely to take whatever error estimates are given to them by the data producers. Whether these error estimates are in the form of coordinate standard deviations or complex interpretations of error bands often matters little to the user. There is no doubt the error measures will enhance the quality indicators of a spatial database. Yet understanding these quality indicators will in turn require at least a moderate amount of expertise or proficiency in error analysis. However innovative an error model may be, the ultimate judgement of its value will be determined by the user. Hunter (1999) urges the GIS research community to prove that its algorithms and methodologies “are not simply esoteric exercises in higher mathematics and statistics.” Indeed, there is a need to demonstrate that these error models and concepts can be converted into useful tools.

A third complexity with recent error models is that even the most advanced (the G-band) is a measure of positional uncertainty of single line segments. The case of more complex geometric features, such as polygons or curves, is handled by simply overlaying each segment’s G-band endpoint to endpoint. This procedure ignores the complex interactions between the uncertainties of neighboring objects. The uncertainty distribution of one measured object is inherently affected by the uncertainty distribution of adjacent measured objects. The G-band is based on a stochastic process and indicates that a line segment can be represented as a four-dimensional random vector. This representation can take into account dependencies in two dimensions between the two endpoints of a line segment. Yet, the uncertainties of neighboring features, and the manner in which they affect the given feature, are ignored. This tends to examine a line segment as a stand-alone geometric feature, which is rarely the case in a GIS. Modeling uncertainty in the same manner that composite features are modeled (i.e., using a building block approach of point and line errors) ignores the influence of neighboring feature uncertainty. A more integrated approach to error modeling and analysis will account for the continuities and interactions that exist in and among spatial features due to differing automated production methods and sources.

Recent developments in modeling positional uncertainty of spatial elements have provided impressive statistical analysis. Yet there is a need for uncertainty measures that integrate a diverse composite of extracted features and the interactions of their uncertainties, while effectively communicating the results. There is little agreement on how spatial uncertainty information should be represented in order to be communicated reliably. Rather than restricting our examination of spatial uncertainty to individual objects, it may be beneficial to study feature uncertainty using a field model. Maps representing distributed uncertainty can be a preferable approach to estimate, model, and communicate data quality at a selected point or region. Accordingly, we will examine positional uncertainty by extending error-band modeling techniques to produce fields of uncertainty. A synthetic uncertainty map will enable us to outline the distribution of errors around a feature, and generate more accurate error boundaries. This uncertainty map is linked to the rigorous error models we have studied, but offers distinct advantages regarding communication and the manner in which uncertainty boundaries are generated.

An error band is a region of uncertainty around a geometric feature; in this case, a line segment. As we have explained, the G-band model of a line segment's errors is a closed crisp boundary defined by the standard deviations of endpoint coordinates (see figures 15, 16, 17).

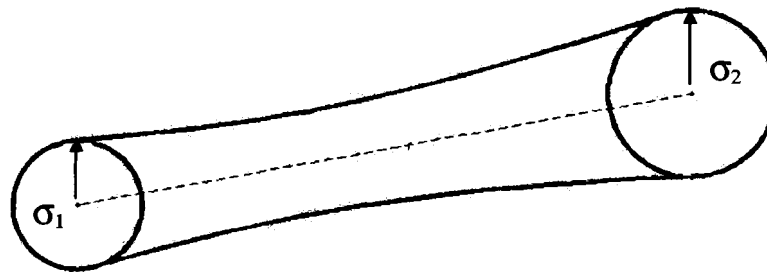


Figure 18. G-band of a line segment with unequal endpoint errors following a circular normal distribution

The use of a field to model the regions of uncertainty around a line segment may de-emphasize this crisp object model and re-focus on the uncertainty variation at points within the line's proximity. Using standard deviations and error band theory, it is possible to construct a field of uncertainty around a line segment. This field is consistent with uncertainty contours as they are derived from the G-band model, but extends their application from a single-level discrete curve to a multi-level uncertainty field. By assigning relative values to each contour based on its distance from the line segment, a field of error distribution can be created. The uncertainty field can visually indicate error distribution relative to the orthogonal distance from the line segment. Figure 19 illustrates such an uncertainty field associated with uncertainty contours derived from a segment's G-bands using 0.25σ , 0.5σ , 0.75σ , and 1σ for each endpoint. The contours are assigned a corresponding value (e.g., 1, 2, 3, or 4) and shaded to indicate relative errors. In figure 19, areas nearest the line receive the lightest shading, with uncertainty shading increasing at points further from the measured line.

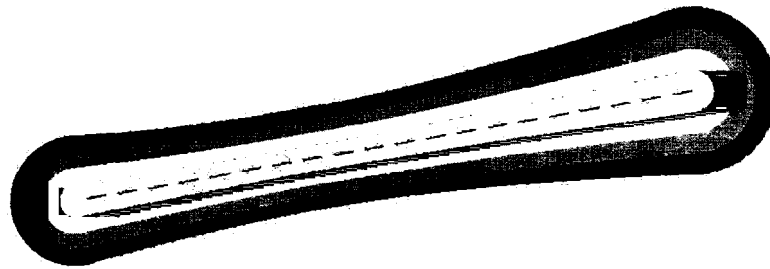


Figure 19. Uncertainty field of a line segment, with contours at $\sigma \cdot n$, where $n = 0.25, 0.5, 0.75, 1.0$

By using the relative values assigned to each contour line, a smooth uncertainty distribution can be obtained via interpolation, similar to constructing a digital elevation model. This permits the construction of a continuous error landscape for a spatial feature, as seen in figure 20.



Figure 20. Smoothed uncertainty field of a line segment, for $\sigma \cdot n, n \in [0,1]$

This continuous uncertainty field is produced by scaling the shading intensity (from black to white) to correspond with the contour values. In this case the intensity range is [0 (black), 10 (white)] corresponding to contour values for $\sigma \cdot n, n \in [0,1]$. However, the uncertainty field is not restricted by a standard deviation. Using G-band realizations for various target uncertainty boundaries, it is possible to map out any number of uncertainty field extents. For instance, figure 21 demonstrates an uncertainty field for $\sigma \cdot n, n \in [0, 3.2]$.

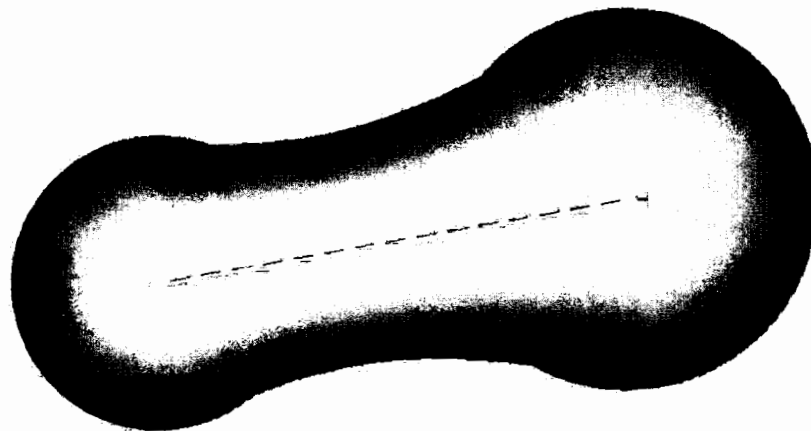


Figure 21. Uncertainty field of a line segment, for $\sigma \cdot n, n \in [0, 3.2]$

Representing the positional uncertainty of the line via an uncertainty field offers benefits over traditional error bands. While retaining the distinct G-band shape, the uncertainty field offers a noticeable improvement in communicating the band's results and meaning. The uncertainty map successfully conveys the notion of continuity among the line segment's errors. The smooth

uncertainty shading indicates that points farther from the measured line are less likely to be part of the true or expected line. The points nearest the line hold the most likely position of the true line; therefore they receive minimal uncertainty shading.

In the previous examples, the contour values serve as uncertainty intensity indicators increasing up to a given distance from the line segment, e.g., the σ value. However, it is also beneficial to model uncertainty up to *and beyond* a target error value. For instance, the visualization of an uncertainty boundary up to one standard deviation (σ) from a line (see figure 20) indicates an abrupt border where the uncertainty field ends. This may be misleading to users in that even the G-band's rigorous methods are still an approximation, as is any uncertainty field bounded by a value. Furthermore, such an abrupt boundary may be disadvantageous when attempting to approximate and extract continuous error boundaries. Therefore the uncertainty field may be enhanced by emphasizing the target uncertainty value σ while displaying uncertainty past this boundary. Doing so provides a more accurate and complete error model, communicating a boundary for the target uncertainty while providing a more extensive representation of the segment's uncertainty field. Figure 22 illustrates such an example of an uncertainty field designed to emphasize a target boundary of 1σ while displaying an uncertainty boundary up to 2.5σ .



Figure 22. Uncertainty field of a line segment emphasizing 1σ while displaying field up to 2.5σ

As figure 22 demonstrates, the continuous intensity values of the uncertainty field are altered to stress the target boundary distance, 1σ . This is accomplished by stretching the shading intensity along its full range (i.e., $[0,10]$) up to the target boundary of 1σ . An inverse stretch is then applied for distances between 1σ and 2.5σ in order to outline a more inclusive uncertainty field. A display of such intensity shading is given in figure 23. As a result, points lying farther from the measured line segment increase in uncertainty shading up to a distance of 1σ , at which point the uncertainty shading continuously decreases until 2.5σ . This extended uncertainty field allows a more comprehensive study of a line segment's error, isolating a target uncertainty boundary while still describing uncertainty beyond this boundary. In addition to the visual and communicative advantages, such a representation holds important benefits for continuity and contour extraction, as Section 4 will illustrate.

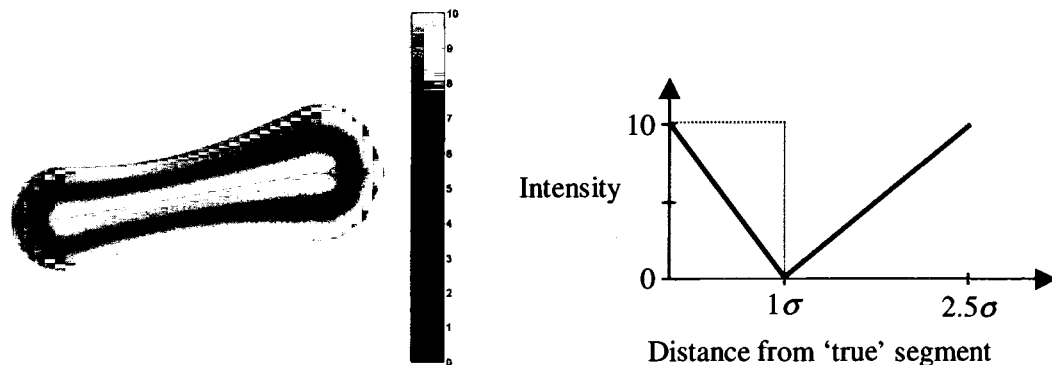


Figure 23. Stretching of uncertainty shading values over range $[0,10]$ as a function of distance from measured line segment. Note the valley shaped stretch of intensity values.

It should be noted that the obvious drawback of such a representation is the recurrence of equal intensity values. For instance, figure 23 illustrates a case where the same values represent distances both less than and greater than 1σ . A point at a distance of 0.5σ from the measured line segment has an uncertainty shading of approximately 5. Meanwhile, a point at 1.75σ will

have a similar intensity shading. Using a peak or valley approach for uncertainty shading prevents the field from representing a positive linear correlation between uncertainty and distance from segment. This particular representation therefore cannot be used as a stand-alone measure of positional uncertainty of a line segment. A user must first be aware that the uncertainty field has been altered to emphasize a target uncertainty value, and as a result, shading values do not always correspond to uncertainty.

The uncertainty field allows diverse visualization of error boundaries because of freedom when selecting tolerances and intensity stretching. Figures 24 through 26 illustrate some possible uncertainty fields based on varying combinations of intensity stretches. The three major examples are labeled based on the shapes of their intensity stretch graphs. These are: a “staircase” representation, a “peak-valley” stretch, and a “plateau” stretch. The staircase stretch is based on distinct contours within the uncertainty field; the “peak” or “valley” stretch is typified by the example in figure 23; the plateau stretch levels at a target value. In fact, the names should be self-explanatory with respect to their intensity stretch. The advantages and disadvantages of each representation are outlined in table 2.

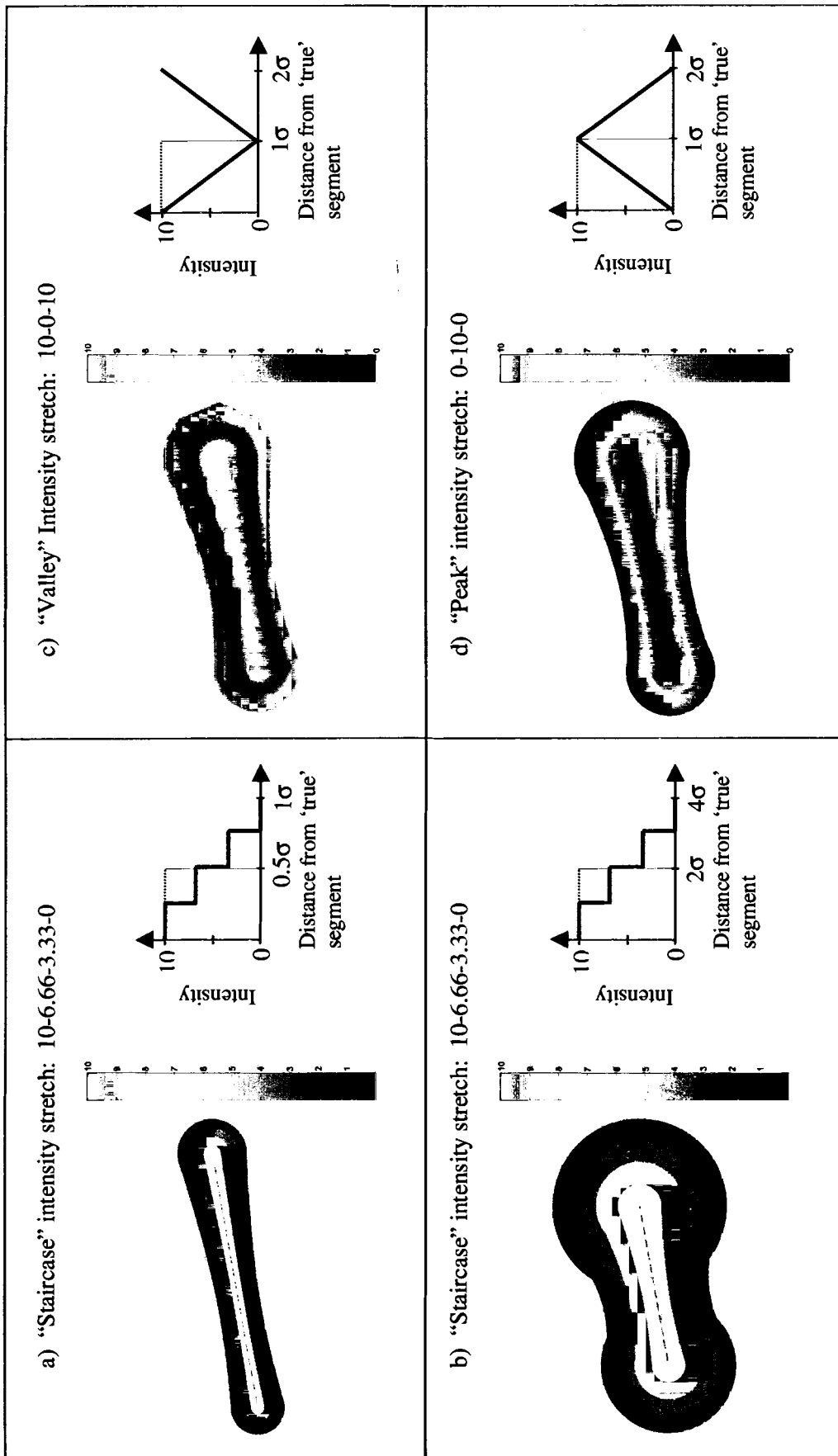


Figure 24. Some examples of "staircase" and "peak-valley" intensity stretching

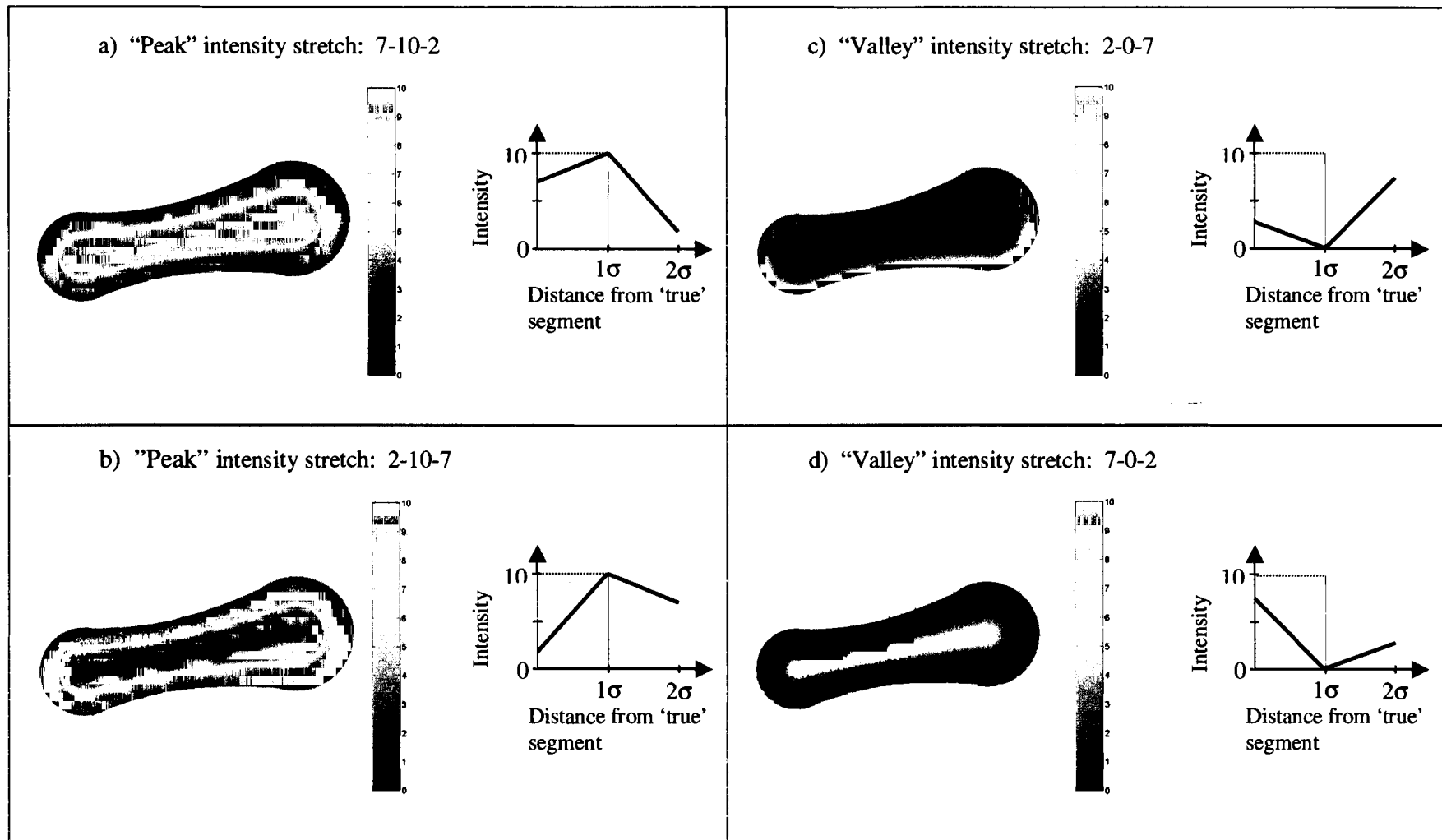


Figure 25. More examples of "peak-valley" intensity stretching

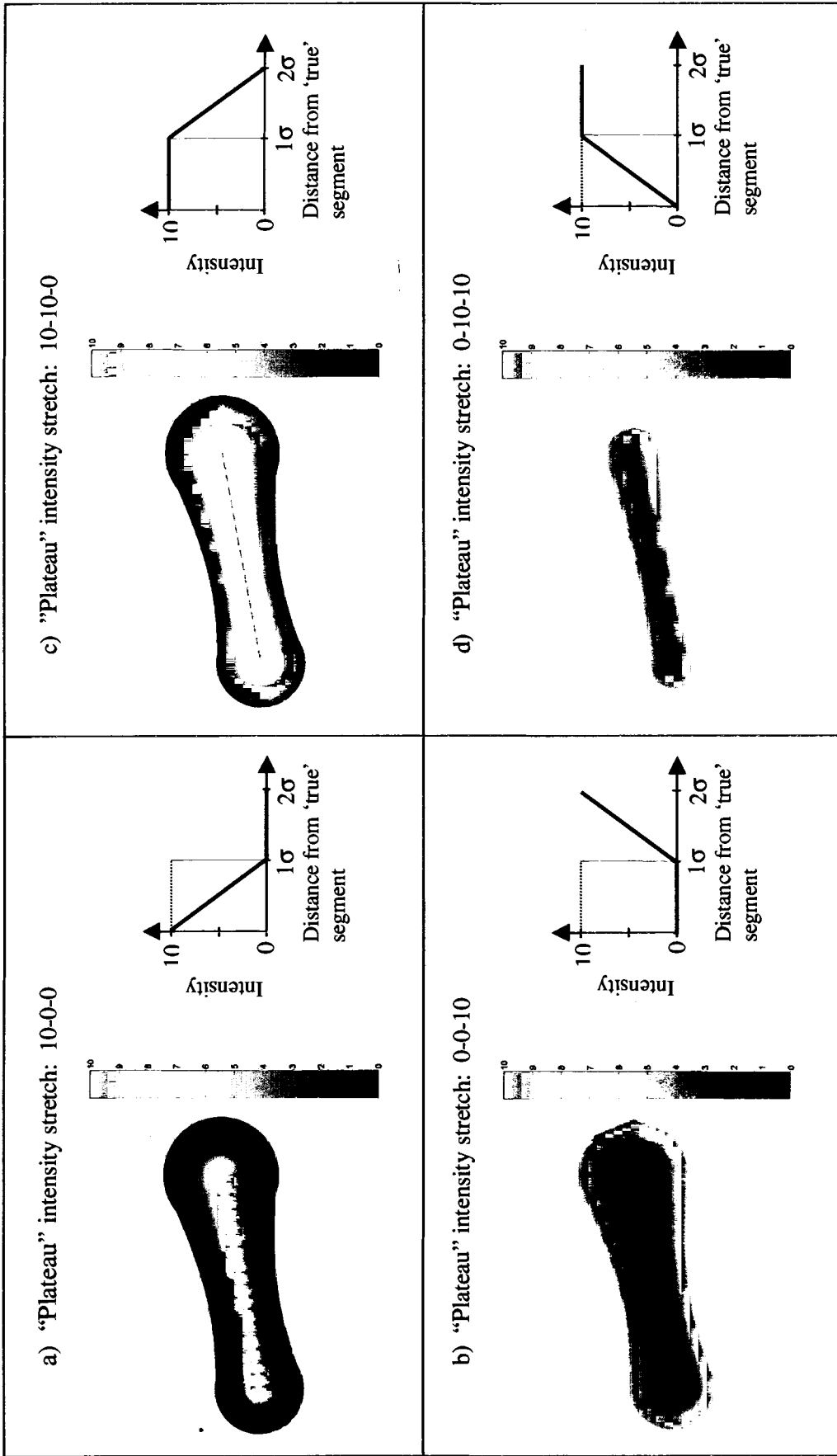


Figure 26. Some examples of "plateau" intensity stretching; note that d) is essentially a basic uncertainty field stretch over [0-10]

Representation	Advantages	Disadvantages
Staircase Field	<p>Approximate linear correlation between distance and uncertainty shading</p> <p>Intuitive – uncertainty contours easy to understand</p>	<p>Lack of continuous transition less appealing</p> <p>Abrupt edges not in accordance with <i>uncertainty</i> approximations – may be disadvantageous when extracting continuous uncertainty boundaries – see Section 4</p>
Basic Uncertainty Field	<p>Continuous, smooth transition - visually appealing</p> <p>Positive linear correlation between distance and uncertainty shading</p> <p>Basic, intuitive - needs less explanation</p>	<p>Abrupt edges not in accordance with <i>uncertainty</i> approximations – may be disadvantageous when extracting continuous uncertainty boundaries – see Section 4</p>
Peak or Valley Stretch	<p>Continuous, smooth transition is visually appealing</p> <p>Allows emphasis of target uncertainty while still displaying field to a larger extent</p>	<p>No positive correlation between distance and uncertainty shading</p> <p>Not intuitive - requires extra information</p>
Plateau Stretch	<p>Positive linear correlation between distance and uncertainty shading, up to a target uncertainty</p> <p>Capable of smooth transition to target distance, while providing larger extent</p>	<p>Lack of smooth transition less visually appealing – difficult to judge distance</p>

Table 2: Advantages and disadvantages of uncertainty field representations and intensity stretches

The benefits of improving an error band with an uncertainty field can be demonstrated through improved communication and content, as well as increased understanding by the user. Yet there are still two important issues that need to be addressed. The first, accessibility to the user, will be discussed here; the second, modeling the interactions of continuous uncertainty boundaries, is the topic of Section 4 and will be touched upon here.

Due to the diverse combinations of intensity shading capable with the uncertainty, it easily lends itself to be stored as an image. This format has many potential advantages for both user

interaction and estimation of continuous uncertainty boundaries. There are numerous image formats (TIFF, JPG, bitmap, etc...) available to store uncertainty fields. The simple grayscale shading of uncertainty fields combined with the efficient compression of popular image formats allows uncertainty fields to be stored in relatively small format size (10-40KB). The widespread use of the most popular image formats (compatible with virtually any image viewer) allow easy user access. In other words, uncertainty fields do not need to be restricted to an obscure accuracy file compatible only with a proprietary software. Small file sizes, universal compatibility, and ever-expanding network capabilities place no restriction on the accessibility of uncertainty fields in image format.

Additionally, representing uncertainty fields as images opens them up to the techniques and opportunities of the media and digital processing communities. Powerful digital processing algorithms exist to automatically alter and enhance virtually any attribute of an image. Automated processes can quickly and efficiently perform complex functions for acquisition, storage, processing, communication, and display. Images can be improved through transformations, enhancements, restoration, and compression. More importantly, images can be segmented, represented, recognized, and interpreted automatically. Section 2.3 discusses digital processing techniques used for spatial data. Among the most important are automated segmentation of images, classification of features, object recognition and extraction.

Image processing techniques can automatically identify spatial characteristics (which humans excel at) as well as spectral characteristics (where human perception is lacking). These methods allow complex problems to be solved and provide in-depth analysis in a fraction of the time it would take a human operator. Based on our representation of uncertainty through an uncertainty field stored as an image, and with the help of digital processing techniques, Section 4 will demonstrate a method to estimate the positional uncertainty of continuous line segments.

Furthermore, uncertainty fields will be used to model the interactions between uncertainty boundaries of adjacent features, and digital image processing techniques will be applied to extract a boundary of influence.

4.0 Modeling Uncertainty Field Interactions Among Adjacent Features

As discussed in Section 3, an error band is a region of uncertainty around a geometric feature; in this case, a line segment. The most advanced of the error band models, the G-band, is still only a measure of positional uncertainty for single line segments. Errors of multiple line segments are modeled by generating error regions for each line segment and overlaying them endpoint to endpoint. This process creates a composite of line models seemingly molded into a continuous entity with smooth error propagation.

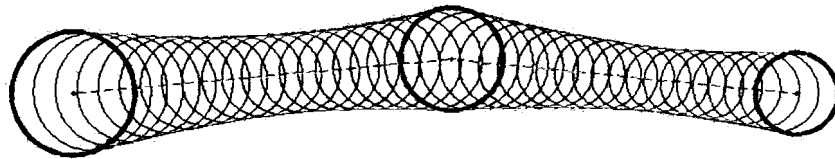


Figure 27. Overlaid G-bands (including error ellipses) of two adjacent line segments

Simply overlaying the G-band creates a visually smooth and successful model. However, the statistical assumptions for a G-band are based on a stochastic process and indicates that a line segment be represented as a four-dimensional random vector. Essentially, this representation can effectively model dependencies between two endpoints of a line. However, since the line segment is viewed as a random object, its uncertainty cannot be examined with relation to neighboring objects. For instance, while the G-band smoothly models a field of uncertainty from endpoint to endpoint of a feature, it is useful to know how this field is affected by a neighboring G-band overlapping its area. Yet as a result of the G-band's stochastic nature, a measured line segment is viewed as an independent entity, which is rarely the case for GIS data, especially that derived from image-based applications. For example, current techniques of spatial data measurement extract complex objects as separate entities made up of nodes and line segments. As the methods of data extraction advance, so too must the methods of estimating the associated uncertainty within the data. Not only will objects' uncertainties be modeled, but the connections

between these uncertainties will also be estimated. This precludes limiting features (and their uncertainties) to a model of independent units. Such a representation ignores the complex interrelationships between the uncertainties of neighboring features that arise through a feature extraction process. A more integrated approach will account for the connections that exist between spatial features due to automated production methods. As a result of modeling interactions between object uncertainties, propagation of error through an entire scene can be better represented.

This section will examine uncertainty boundary interactions between neighboring features using uncertainty fields to model and snakes to estimate. We will first examine uncertainty fields representing the error of continuous line segments, and extracting their boundaries with deformable contour models. Section 4.2 will then model the interaction between neighboring uncertainty fields, and apply deformable contour models to extract a boundary of influence between the two fields. These results will then be applied to a more complex scene of uncertainty in Section 4.3.

4.1 Extracting Continuous Uncertainty Boundaries Using Snakes

As we have noted, an uncertainty field can be used to effectively communicate and model the continuity of a line segment's errors. The uncertainty field is derived from the G-band, a rigorous statistical approximation of a line segment's positional uncertainty. However, modeling single line segments is of limited use within a GIS; of more value is an estimation of composite line features. A G-band represents continuous line segments by overlaying the adjacent G-bands of independent line segments. Figure 28 provides an illustration of the G-band's modeling of an extracted line feature. Each pair of points connects a line segment, and the boundary of uncertainty around each segment is modeled independently. Each line segment shares a node

with an adjacent line segment, and the G-bands cumulatively link to form a boundary of uncertainty around the composite line feature.

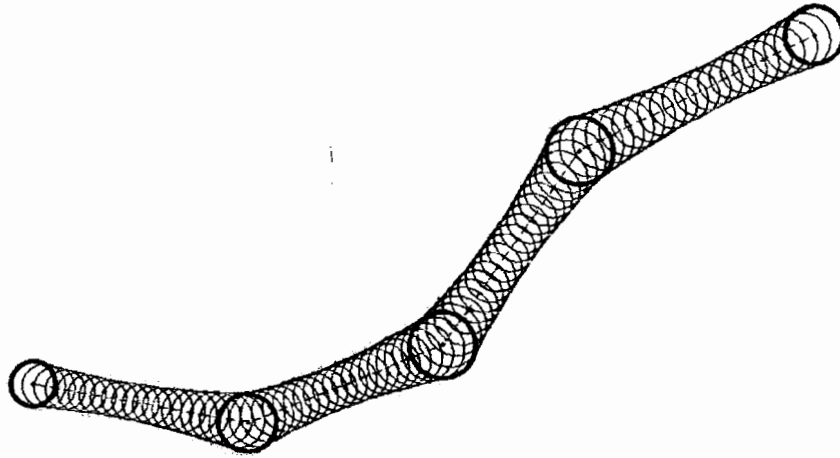


Figure 28. G-band overlays of five connected line segments.

We will examine the use of deformable contour models to estimate the continuous boundary represented by G-band (and subsequent uncertainty field) overlays. More important to our purposes, however, is the snake's ability to model interactions between uncertainty boundaries of adjacent features. Just as an uncertainty field can model an individual G-band, multiple uncertainty fields can be connected to model a composite of G-bands. These multiple uncertainty fields combine to represent a map of an object's continuous uncertainty boundaries. Uncertainty maps for a linear object are given in figures 29 and 30.

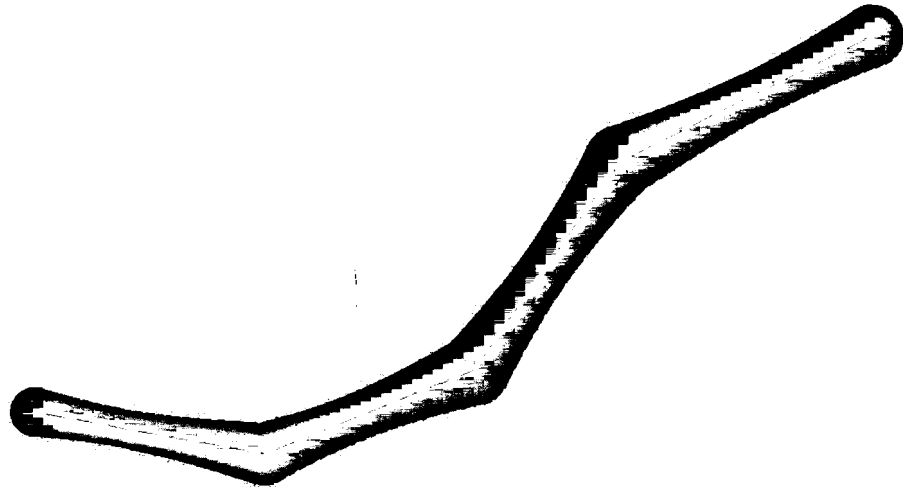


Figure 29. Uncertainty map overlay, consisting of five connected line segments' individual uncertainty fields

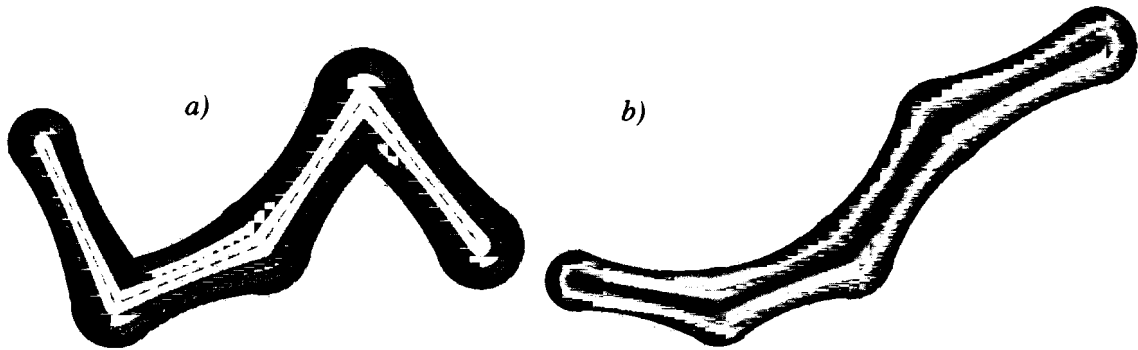


Figure 30. Uncertainty maps; a) staircase representation, b) peak-valley representation

These figures illustrate a few of the uncertainty field representation options outlined in table 2. The selection of uncertainty field representation may vary depending on the uncertainty being communicated and the method of extracting the uncertainty boundary. Section 3.2 discussed the advantages of storing uncertainty fields as digital images. Expanding upon this notion, the edges present in these uncertainty maps allow deformable contour models to be a useful digital processing tool for extracting uncertainty boundaries. As detailed in Section 2.3.4, the snake model employs an external edge constraint along with internal continuity and curvature

constraints. A gradient measure is used to push or attract the snake to an edge. The larger the gradient, the more likely the snake will attach to the edge. It is sometimes advantageous to increase the likeness between the initial (feature) and secondary (uncertainty) extraction procedures; this can be done using various uncertainty field representations. The choice of uncertainty field can reflect the nature of the image clarity, or that of particular features within an image. For instance, if an image has little noise and there exists sharp contrast between road edges and surrounding features (forest, field, etc.), the snake process will have little difficulty finding the road edge. In such an example, it may be more appropriate to use the staircase or plateau representation of uncertainty fields, which exhibit distinct edges between bands of uncertainty (see table 2). On the other hand, an image degraded by noise or possessing indefinite feature edges would be better to use the peak-valley representation, which is characterized by a constant gradient peaking at a target uncertainty value. The lack of an extreme gradient allows the snake more flexibility in its extraction process.

In addition, a peak-valley representation can communicate a target uncertainty boundary while providing a larger extent of uncertainty. A staircase representation is useful for displaying varying contours of uncertainty, while the basic uncertainty field provides a linear correlation between distance from segment and degree of uncertainty. Such characteristics of the various representations are compiled in table 2 of Section 3. Figure 31 offers examples of gradient images of the four uncertainty field representations for a target uncertainty distance of 1σ . The basic uncertainty field is shown in 31(a); the gradient is constant until reaching its target value of 1σ , hence its uniform interior and sharp edge. Figure 31(b) displays a staircase representation with uncertainty contours at 0.5σ , 1σ , 1.5σ , and 2σ . The staircase creates steps of constant uncertainty shading, meaning a gradient exists only at contour edges. The gradient of a plateau stretch can be viewed in 31(c); there is a constant gradient until the target distance is reached,

followed by no gradient until the 2σ boundary, where there is a large gradient. As figure 31(d) illustrates, the peak-valley uncertainty field has a symmetric gradient throughout the range $\sigma \in [0,2]$. As discussed in Section 3.2, the intensity shading increases to a maximum (or falls to a minimum) as it reaches a target uncertainty level. In this case, the target uncertainty level is 1σ . After reaching the target level, the shading reverses its trend back to its initial intensity. In this manner, a continually changing field, and therefore constant gradient, represents the uncertainty values. The target uncertainty is still distinguished from its surroundings because it is at this value that the gradient reverses its trend, i.e., from increasing to decreasing, or vice versa. On the other hand, the basic uncertainty field, staircase field, and plateau-stretch representations all possess well-defined edges at the target value of 1σ .

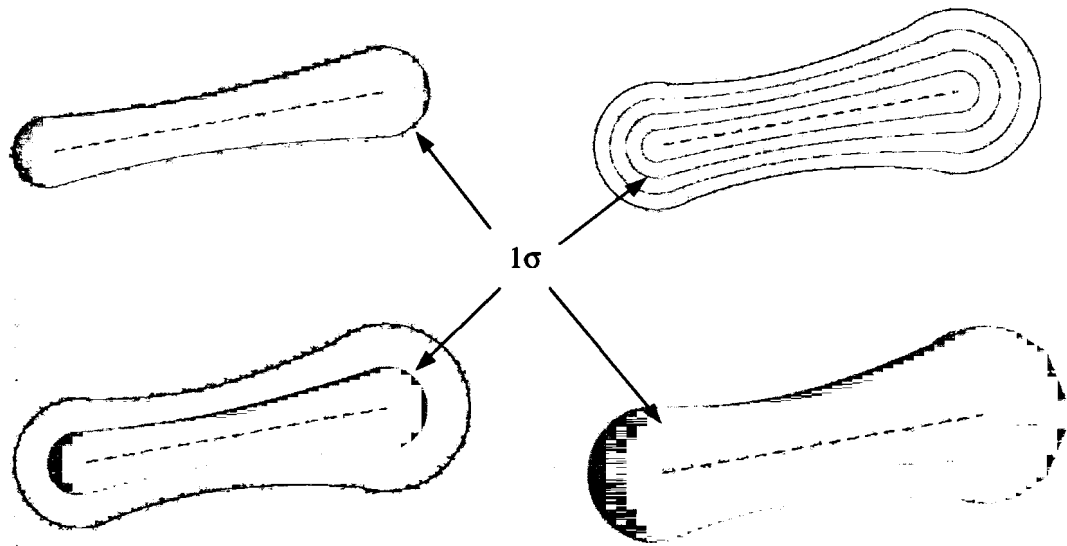


Figure 31. Example gradient images; a) basic uncertainty field, b) staircase field, c) plateau stretch, d) peak-valley stretch

This results in a large gradient value, which will most certainly cause a marked bias in the snake's edge-seeking trends. The slowly changing intensity values of the peak-valley representation allow the snake to find a continuous path along a defined edge while maintaining flexibility not

available with the other uncertainty field representations. However, it will be seen that the other representations have value for sharply angled linear features.

A sample snake extraction from a continuous uncertainty map is presented here. A linear feature of five connected line segments was given an uncertainty map with a peak-valley representation. The snake was then given approximation points to extract the 1σ boundary from the continuous uncertainty map; these approximations are viewed in figure 32.

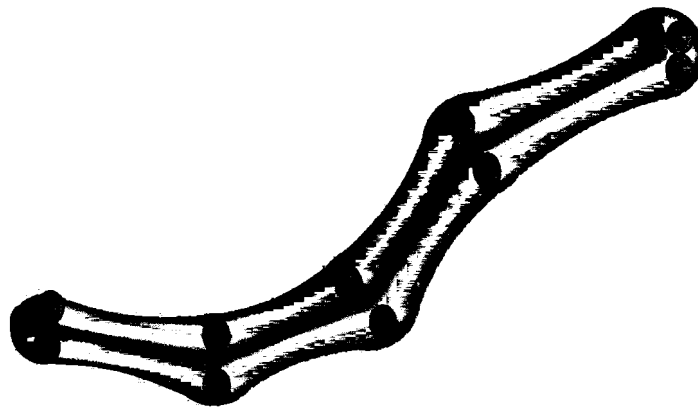


Figure 32. Sample point approximations for figure 33

These initial seed point approximations are supplied by the calculations of the G-Band. In the case of figure 32, a minimum number of points are taken in order to minimize the approximation stage and force the snake to find its way based on its internal and external constraints. The resulting linear snake extraction can be seen in figure 33. An adequate representation, this snake is based on minimal point approximation, a high gradient weight, and a medium curvature term. The snake proceeds from the first point, extrapolating segment by segment according to the edge it is following and the constraints on its shape. An arrow in figure 33 points out an edge anomaly caused by the large spacing between approximation points.

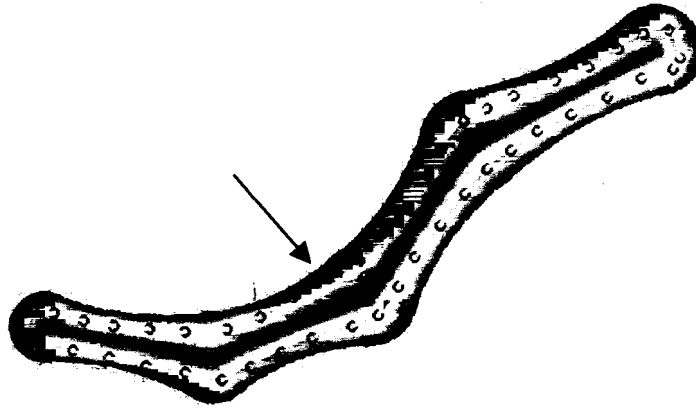


Figure 33. Snakes extraction using only endpoint approximations, as seen in figure 32; high weight on gradient, minimal weight on continuity

Figure 34 employs a slightly different approach; only one uncertainty boundary is extracted, and it is done so after providing many initial approximation points, with the weighting reduced to a minimum. As such, the approximations and gradient component guide the snake very accurately. There are no obvious irregularities, and it appears that the snake performed well in extracting a continuous uncertainty boundary. However, these results are to be expected with many seed points; an ideal case minimizes the number of constraining points used, in order to allow the snake freedom to minimize itself based on its energy functions.

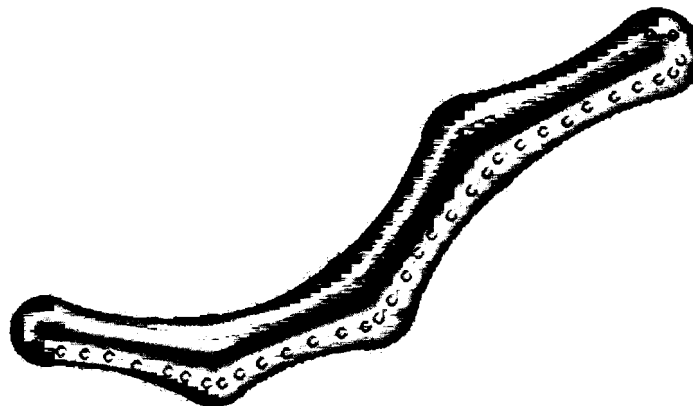


Figure 34. Many G-band approximation points used, minimal weighting

The snake approach and use of the “peak-valley” stretch of uncertainty fields works very well for extracting smooth, continuous linear features. However, when encountering sharp angles and sudden shifts in direction, the snake struggles to adjust. Decreasing the curvature weight and increasing the gradient coefficient helps to this end, but often the integrity of the snake’s shape is compromised to account for isolated cases such as extreme angles. The peak-valley representation handles sharp angles rather poorly, but other uncertainty field representations can improve the snake’s extraction performance. For instance, the snake failed to accurately extract a 1σ uncertainty boundary based on the peak-valley stretch for the segment geometry in figure 35. By substituting a staircase representation into the extraction process, the snake was able to make use of the sharper gradients exhibited by that uncertainty field representation. The sharp edges defined by the uncertainty contour bands of the staircase representation create a large gradient for the snake to be attracted to. With such strong gradients, it is not necessary to heavily weight the component in the energy minimizing functions. The accuracy of the extraction process is largely dependent on initial approximations and the continuity weighting. Figure 36 illustrates an extraction using sparse initial approximations located at segment endpoints and midpoints. The continuity weight is high, while the gradient is medium and curvature is minimally weighted. Having a heavily weighted curvature term will tend to straighten the shape of the snake; with such sharp angles present in the uncertainty map, the straightening is not a trait that should be emphasized.

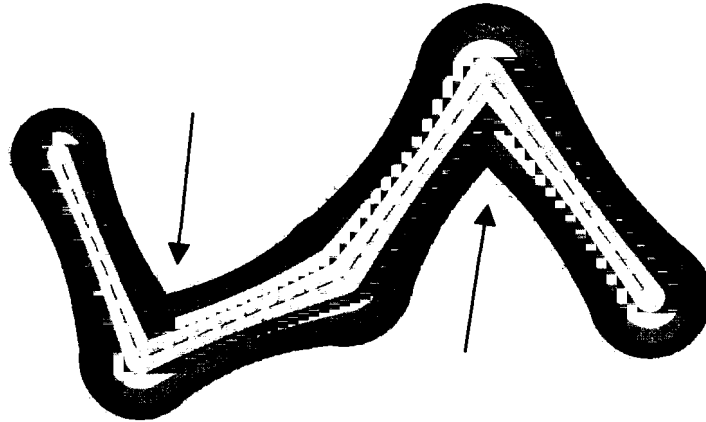


Figure 35. Sample overlaid uncertainty fields, staircase representation

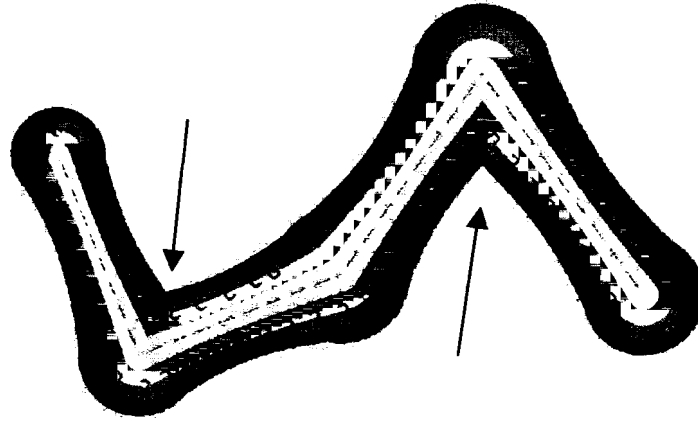


Figure 36. Segment endpoint and midpoint G-Band approximations used, snake interpolates points based on weighted continuity, medium gradient and curvature

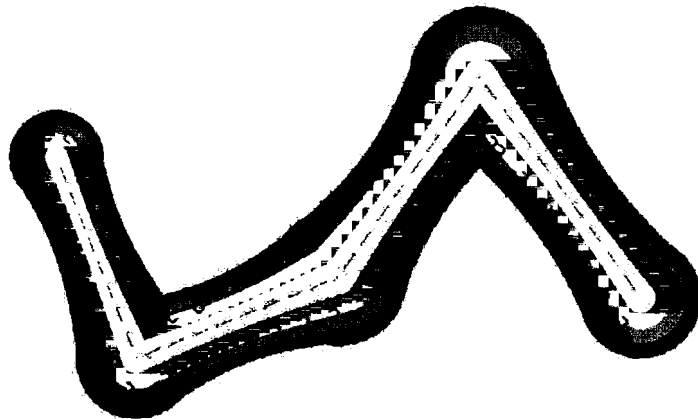


Figure 37. Many G-band approximation points used, heavy weighting on continuity, minimal weighting on curvature and gradient

The arrows in figure 36 make it apparent that the sharp angles are a source of conflict for the snake. The snake attempts to smooth the angle despite the minimally weighted curvature term. The same geometry is run through the snake process again, this time with ample approximation points as guides. The resulting extraction is highly accurate, which can be attributed to the sharp edge contrast and the initial approximations. The approximation points anchor the snake's position close to the appropriate edge, and the strong gradient (due to lack of a continuous boundary) keeps the snake attached tightly. However, the use of such a dense set of approximation points detracts from the snake's freedom and flexibility. If too many points constrain the snake, it is unable to extract a border in a manner that minimizes its energy function to produce a continuous boundary. It becomes apparent that choosing the weights and constraints of the snake is a process that rarely has a flawless solution.

A distinct advantage of using uncertainty fields connected via snakes is that it can be a fully automated process. Deformable contour models are often referred to as a semi-automated approach because they require initial approximations (points and/or direction) to proceed. The extraction of uncertainty fields can therefore be fully automated by supplying these initial approximations. The G-band of Shi and Liu (2000) is the basis of the uncertainty fields that have been developed for individual line segments. The G-band is a rigorous statistical error model to determine the positional uncertainty of individual line segments. By sampling points from segment G-band boundaries, the snake can be supplied with the initial approximations necessary to commence the process. Subsequently, error analysis can commence immediately after the feature extraction process is complete, with no need for human input.

The deformable contour model provides a diverse tool that can be tailored to extract many varying line feature types. The dynamic nature of snakes is based on adjustable components that can help format the snake to behave in a variety of ways. The coefficients weighting continuity,

curvature, and the edge gradient can be modified to navigate a snake through smooth, loping uncertainty fields or a sequence of sharp angles. It has been demonstrated that deformable contour models can be used to extract a continuous uncertainty boundary for a feature from a composite of its uncertainty fields. It is now worthwhile to examine how neighboring fields of uncertainty interact and whether a similar uncertainty boundary can still be obtained.

4.2 Modeling and Estimating Interactions Between Uncertainty Fields

We have shown that uncertainty fields of individual segments can be combined to form a continuous uncertainty field of a composite line feature. Furthermore, we have demonstrated that deformable contour models can successfully extract the boundaries of uncertainty from these fields. While the correct shape and extent of ‘zones’ to model positional uncertainty is subject to varying opinions, less work has been dedicated to studying the interactions between neighboring zones of uncertainty. Rather than view object uncertainty fields as stand-alone objects, it is more useful to handle them as individual objects interacting within a scene or framework. This allows a more realistic and comprehensive view of spatial data, as uncertainties can be analyzed within the context of their given framework, rather than as independent values. As a result, we achieve a better understanding of the relationships that exist between members of differing datasets. The G-band’s independent boundaries do not take into account connections between areas of uncertainty. Therefore, we will use the continuous nature of uncertainty fields to model complex interactions between boundaries of uncertainty between objects.

The uncertainty fields of a line segment and a composite line feature are shown in figure 38. Such representations allow one to ask, for instance: “At a confidence of 1σ , where could the measured line be?” An uncertainty field acts as an isolated object whose uncertainty distribution extends outward ad infinitum; such an object is usually constrained to a target uncertainty boundary (e.g., 2σ). Uncertainty field representation works well to convey the extent of such a

boundary and how it varies along the length of the line feature. However, since this representation is based on an independent error model, it does not provide any indication of the influence of neighboring objects within a scene. Suppose the two linear features of figure 38 are located in close proximity within the same scene (see sample geometry in figure 39).

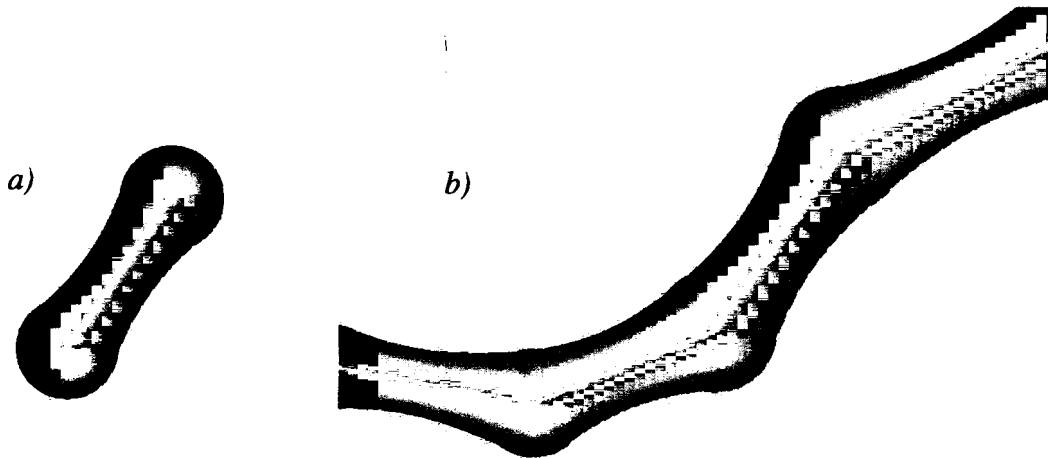


Figure 38. Uncertainty fields of (a) an individual line segment and (b) a composite line feature

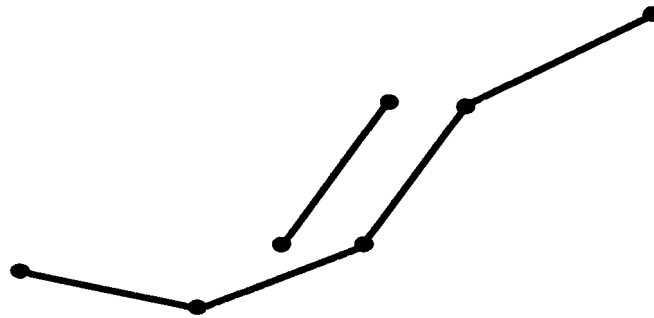


Figure 39. Sample geometry of two adjacent line features

At a particular uncertainty boundary, the extent of one feature's uncertainty band will coincide with the adjacent feature's uncertainty band. Such a situation can be viewed in figure 40, which shows two probability distributions for the positional uncertainty of two spatial features. These

two features are in close proximity in space, and both show a distribution extent past their 1σ uncertainty boundary. If uncertainty fields for the two features were to be displayed for a target uncertainty of 1σ , their nearness would result in an intersection between the two fields. Using the uncertainty fields to derive an area of confidence around a feature therefore results in a region of conflict. The question of where a line segment can be located with a given confidence in turn becomes an observation of where the line segment cannot be at that confidence, despite what an independent error model may indicate. Consequently, it is useful to derive the intersection of the distribution of two uncertainty fields. If the uncertainties in a scene are normalized (with respect to varying data sources, production, resolution, etc.) then the intersection of distribution curves can be determined by examining the confidence region of overlap. The resulting model is a more complete definition of a feature's uncertainty, and is the first step towards modeling interactions between object uncertainties. Ultimately, an interactive scene of uncertainty can develop from the estimation of uncertainty field intersection.

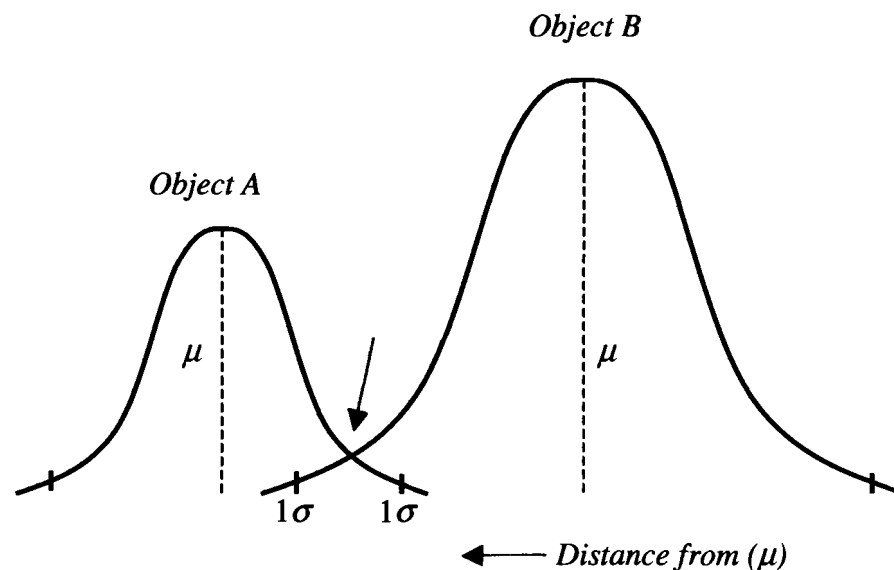


Figure 40. Intersection of uncertainty distributions for neighboring features

An example situation can be visualized in figure 41, which illustrates two overlapping uncertainty bands of adjacent features. Uncertainty fields, based on the independent G-band model, do not recognize such areas of interaction between uncertainty regions of objects and provide no method of analyzing their connections. As evidenced by figures 40 and 41, one would expect the encroachment of an adjacent uncertainty field to narrow the extent to which the afflicted uncertainty field can be determined. This is not to imply that an adjacent uncertainty field will lower the uncertainty of a given line feature. Rather, the confidence width with which we can extract an uncertainty boundary for a given feature is narrowed. This concept will be clarified by the following example.

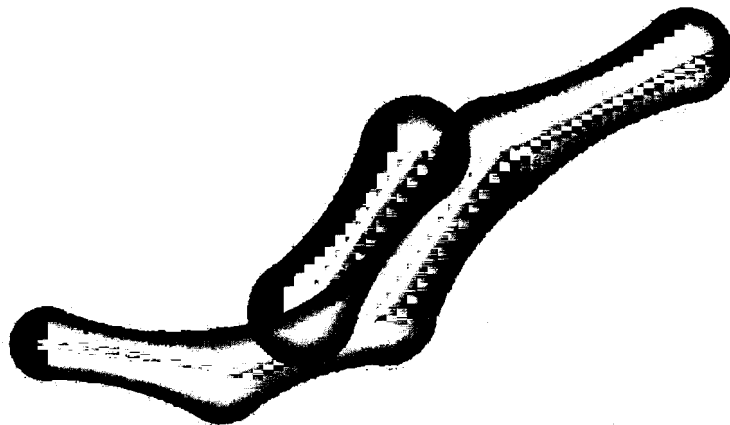


Figure 41. Overlapping uncertainty bands of neighboring line features

While overlapping G-bands or uncertainty fields do not provide a study of field interaction, uncertainty fields stored as images possess attributes that are conducive to combination and interpolation techniques. Digital image processing techniques can use the continuous nature of uncertainty bands to derive a boundary of interaction between the two fields. One simple image processing technique for combining two images is designed to display the minimum pixel value

within the union of both images. Such a minimum operation will compare each pixel location within the two images and store whichever location has the lower gray value. A typical gray value scale increases in intensity from 0 to 255; hence black pixels values are close to 0, and white pixel values are close to 255. In the instance of overlapping images, the minimum operation stores the lowest value (i.e., darkest pixels) within the area of intersection. In the representation of figure 38, the darker pixels indicate higher uncertainty, while the lighter pixels indicate lower uncertainty. The minimum operation is therefore a detection of the darkest pixels, i.e., highest uncertainty. In areas where the images do not overlap, the pixels are preserved. Figures 41 and 42 display the result of such a minimum operation applied to the overlapping uncertainty fields of figure 38. Note that the result of the operation is a darker band of intersection between the two fields. This section is where the minimum operation sought the lowest pixel values, resulting in the area of highest uncertainty that the two fields share. The result of the minimum operation allows the extent of interference between two uncertainty fields to be viewed. Figure 42 also indicates a residual line approximately down the center of the area of interference that is relatively brighter to its surroundings. This line indicates the positions of lowest uncertainty within the area of intersection, and will be very useful in extracting a boundary of interaction. However, a separate operation is needed to emphasize this boundary.

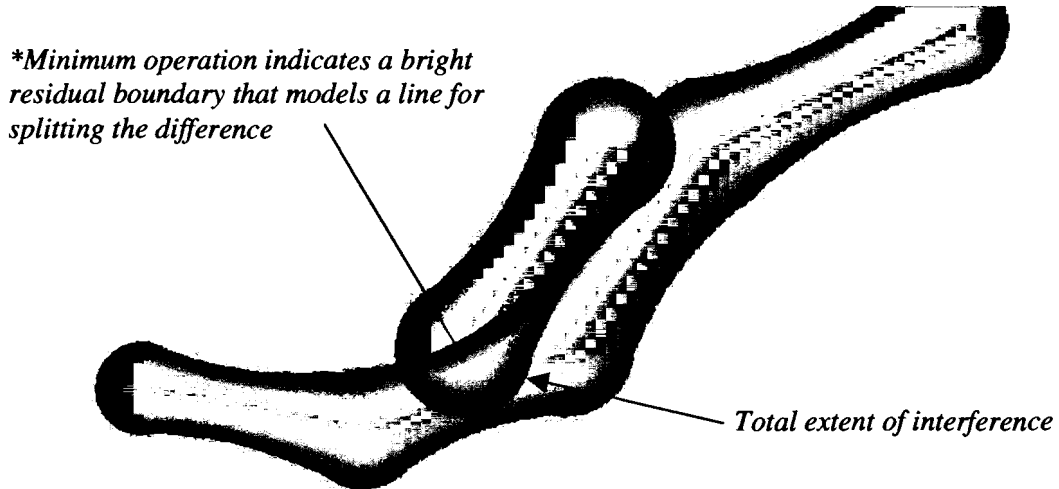


Figure 42. Result of minimum operation between two uncertainty field images

While a minimum operation can be used to denote areas of highest uncertainty, in the same manner a maximum operation can highlight areas of lowest uncertainty. Figure 43 illustrates the result of applying the maximum operation to the two uncertainty fields. It shows only the area of intersection denoted by the minimum operation. The maximum operation favors high gray values; since neither image occupies the same pixel location *outside* of their area of intersection, any pixel location not within this area will be replaced with white.

Maximum operation produces a dark boundary near the center of the area of intersection...this boundary is the inverse of that seen in the minimum operation



Figure 43. Result of maximum operation between two uncertainty field images

The advantage of the maximum operation is that it displays those locations within the area of intersection which possess the lowest uncertainty. For a measured feature, the uncertainty increases in a direction away from the feature (a higher σ value). Referring back to the model of intersecting probability distributions in figure 40, there exist two uncertainty values, high and low, at each position within the area of intersection. However, it is obvious that at one point the decreasing distribution curves meet. It is at this point that the uncertainty field of one feature gains emphasis over another uncertainty field; instead of traveling outward within an uncertainty field, the direction is now inward within the adjacent uncertainty field. Using the minimum operation, this point will remain the brightest feature within the intersection, because there is only one value existing as the minimum and the maximum. All other locations within the area of intersection have two uncertainty values; the higher uncertainty is stored, and the position appears darker. Within the maximum operation, the opposite occurs. The point with a single uncertainty

value has no maximum gray value (lowest uncertainty) to choose from, therefore this point of intersection is the darkest feature within the area of intersection. If a line is drawn approximately parallel to the two uncertainty field boundaries, this point would become the bright line viewed in the resulting minimum operation. The line marks the boundary of influence, where one uncertainty field ends and another begins.

By utilizing the maximum operator, we can replace the area of intersection between the two features with the least uncertain pixel value at each location. This serves to highlight a continuous distribution that models the errors from one uncertainty field to another. Figure 44 illustrates such an operation, which is essentially an overlay of the result of the maximum operation on the two uncertainty fields. Since the lowest uncertainty is stored, each location is represented with the uncertainty of the feature it most likely represents. Additionally, the maximum operator denotes the border of interaction between the two fields as the darkest line within the area of intersection. It is obvious that this border of interaction encroaches on the position of either uncertainty field. With respect to the larger line feature, the uncertainty field of the smaller feature alters the extent of its own uncertainty field. As a result, the sag of the uncertainty field around the segment midpoints appears to slump even more towards the measured line feature. It is therefore worthwhile to extract a more precise position of this boundary of influence. Once again, we will use snakes to extract an uncertainty boundary, this time from a composite of interacting uncertainty fields.

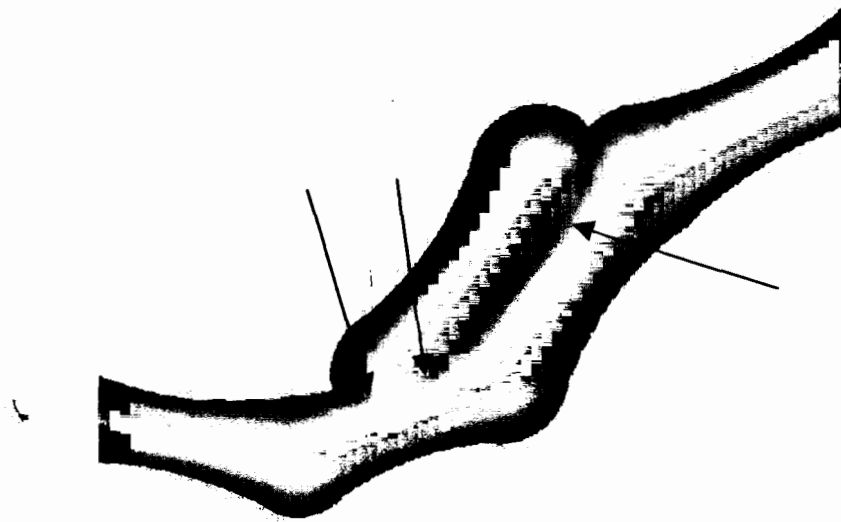


Figure 44. Overlaying the result of the maximum operation (figure 41) on the two uncertainty fields...note the dark boundary produced within the area of intersection

The result of a snake extraction of the original line feature can be seen in figure 45. The uncertainty field's upper 1σ boundary is approximated by the underlying G-band calculations. The sharpness of this representation's boundary edge requires only sporadic sampling at the endpoints and midpoint of each segment to be adequate. Therefore, the approximations are automatically supplied to the snake by the G-band, and an excellent estimation of the uncertainty band's boundary is derived.

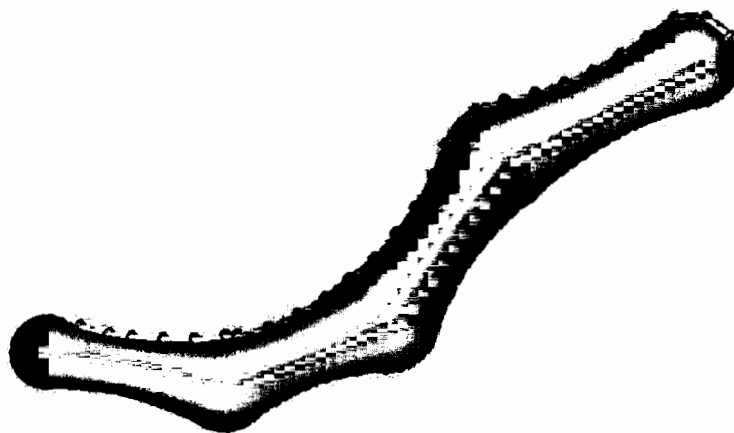


Figure 45. Snake extraction of original line feature

Before performing the snake extraction on the composite uncertainty field image, we will first perform an image enhancement technique to further emphasize the boundary of intersection. Since the area of intersection decreases in gray value towards a dark boundary in its center, scaling the pixels within the area can augment the darkness of the feature. Figure 46 displays the enhanced composite image of the two uncertainty fields, with the area of intersection emboldened. Enhancing the area of interest allows the snake to perform a more accurate extraction within the nebulous area.

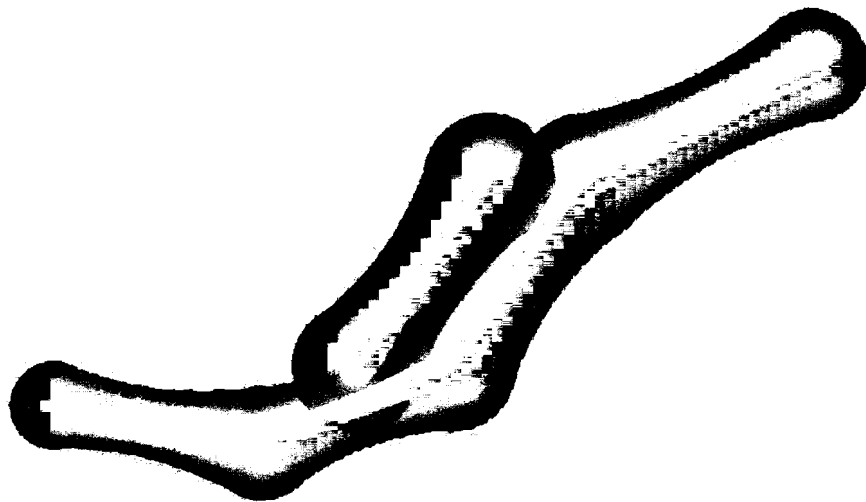


Figure 46. Enhancement of area of intersection

The result of the subsequent snake operation can be seen in figure 47. The snake is given the same point approximation pattern that it received when extracting the original uncertainty field of figure 45. The line feature's original 1σ uncertainty field boundaries (based on the G-band calculations) supply the points that drive the extraction process. The main difference for this case is that the point approximation sampling is denser. This is to account for the 'tangled' area of interaction which features multiple boundaries at varying angles. The snake does an excellent job of modeling the boundary of influence between the two uncertainty fields, as represented in figure 44. Furthermore, the original uncertainty field is preserved in those areas where the single

segment had no influence. The snake essentially splits the difference of the field of intersection, accurately modeling the boundary that was accentuated by the maximum operation. As a result, the inherent shape of both objects' uncertainty fields is pushed inward toward each measured line segment. However, this should not be interpreted as decreasing the uncertainty of a given line feature. The boundary of interaction is simply updating the current independent uncertainty model with outside information, a form of contrary evidence to the existing statistical measure. The statistical measures still hold up until reaching the boundary of influence. The amended model then indicates that at this point, the field of uncertainty for a given confidence can no longer be calculated at that particular location, as an adjacent uncertainty field now is just as likely to hold the given point.

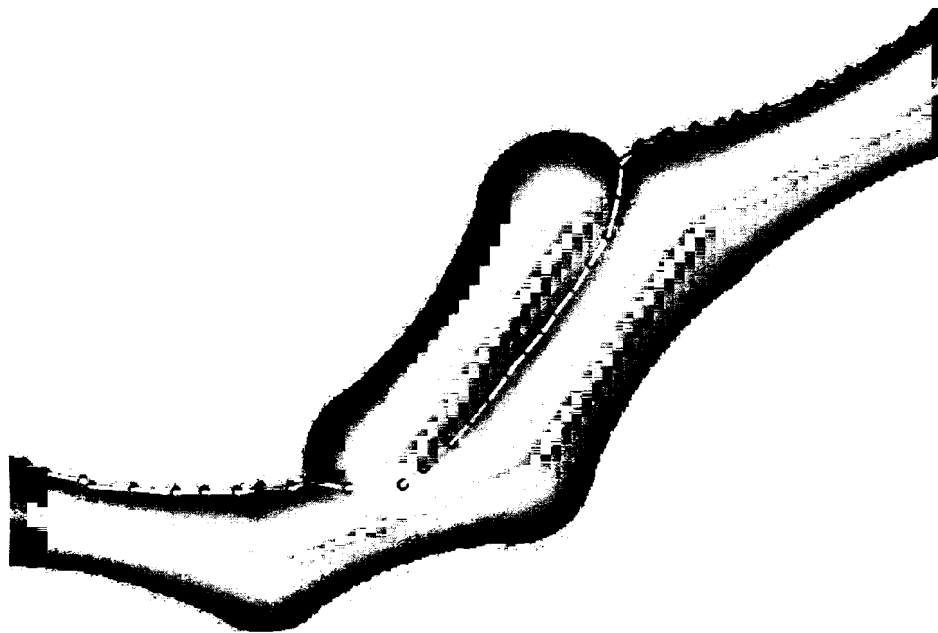


Figure 47. Snake extraction of the boundary of influence between two uncertainty fields

Having shown that snakes can model the interaction between two line features' uncertainty fields, we will now examine the suitability of applying this process to a more complex scene.

4.3 Modeling Interactions of Uncertainty Boundaries Within Complex Scenes

We have shown that deformable contour models can be used to extract continuous uncertainty boundaries from uncertainty fields. It has been demonstrated that uncertainty fields are capable of modeling the interactions between their regions for neighboring features, and snakes were further used to extract the boundary of interaction. It is worthwhile to examine the use of snakes to extract boundaries of influence within complex scenes. Based on advancing techniques for deriving geospatial data as objects, the methods used to model uncertainty must also advance and adapt in order to be relevant. Complex scenes of uncertainty may result, depicting uncertainty in terms of the objects themselves. Such scenes of uncertainty should also convey the interactions between object uncertainties. One way to represent such behavior is through regions of influence for each object within a scene. As such, we are concerned with modeling how an object's uncertainty field is influenced by those uncertainty fields around it.

Figures 48 and 49 display the uncertainty fields of a line feature and three adjacent building outlines. Using the same maximum operation overlay techniques from Section 4.2, a complex scene of uncertainty can be produced, as viewed in figure 50. Notice that within the regions of overlap, the boundary of influence is accentuated by darker pixels (lower gray values). The previous image enhancement techniques can heighten the disparity between these pixels and their surroundings, as seen in figure 51; the snake extraction can then be applied. The goal of the snake extraction is to produce the line feature's updated uncertainty field, one which now depicts the influences on it from neighboring uncertainty fields.

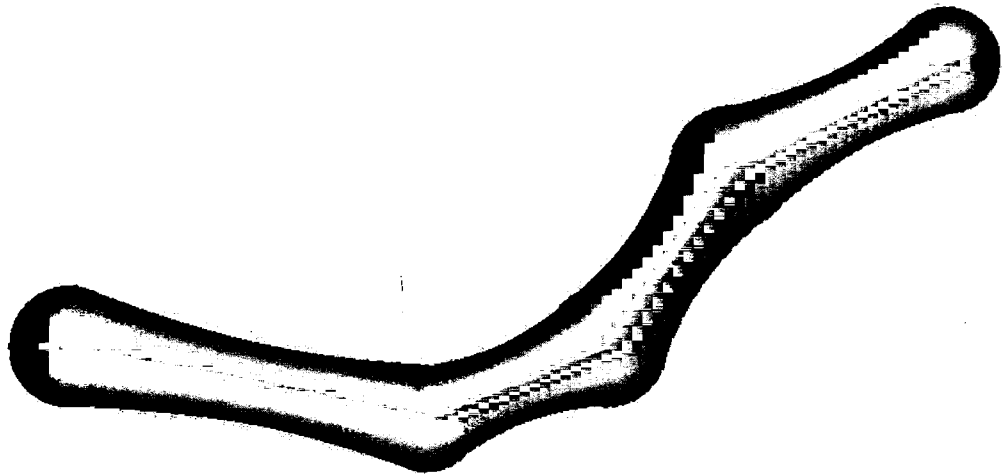


Figure 48. Uncertainty field of a line feature

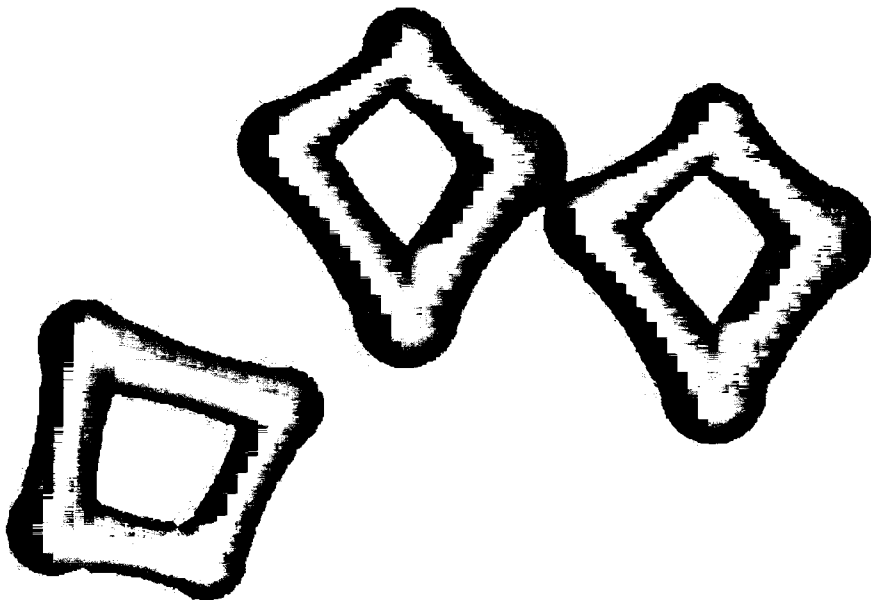


Figure 49. Uncertainty fields of 3 adjacent building outlines

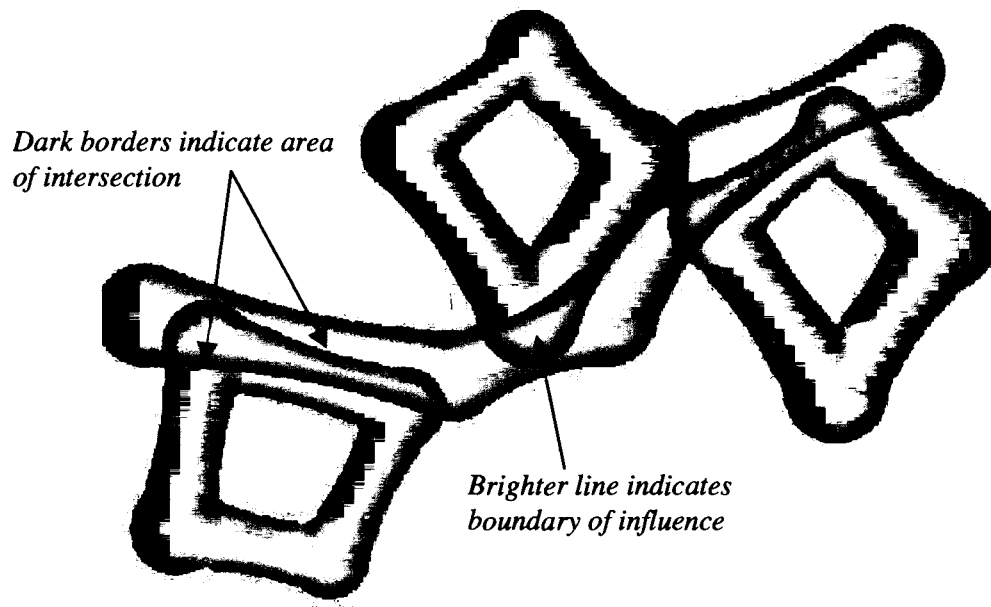


Figure 50. Result of minimum operation showing extent of interactions between uncertainty fields

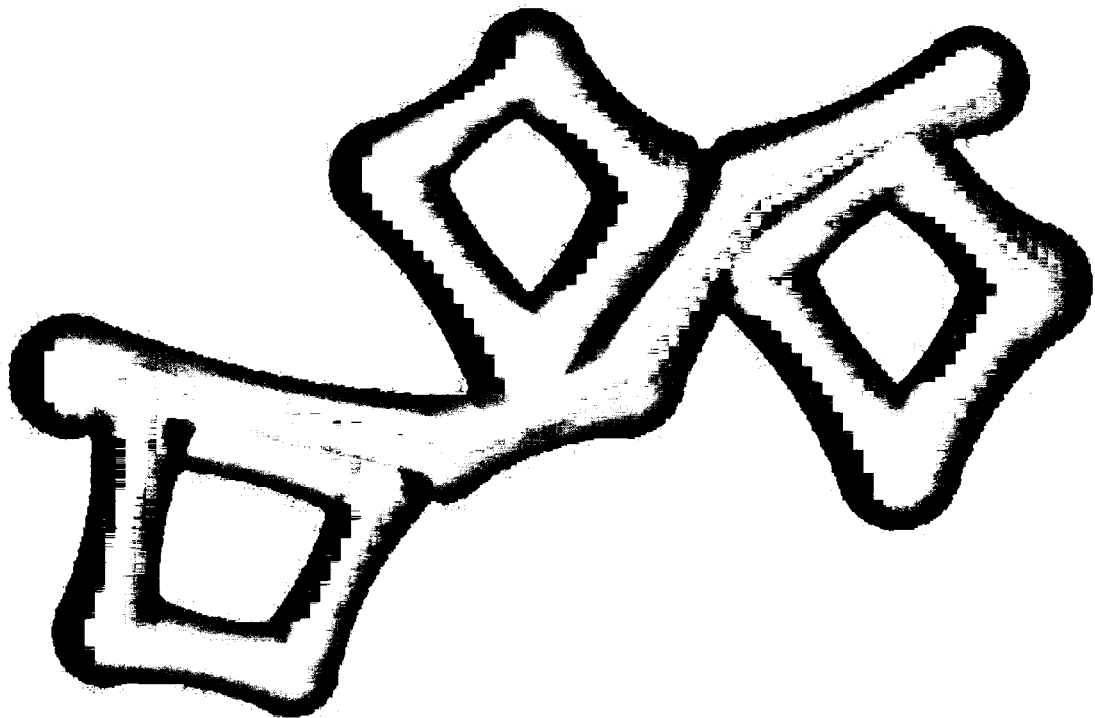


Figure 51. Following maximum operation, complex scene of uncertainty combining building uncertainty boundaries with that of the line feature's

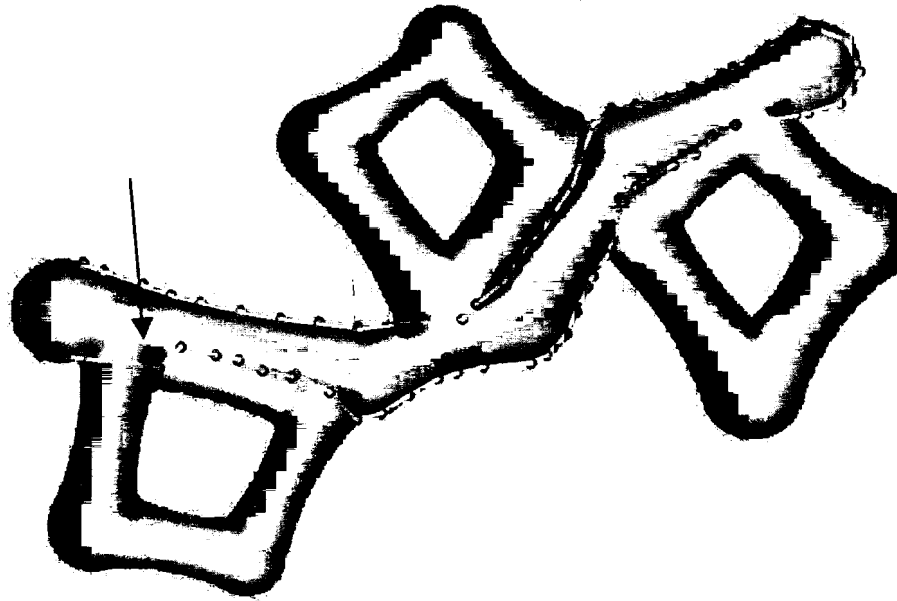


Figure 52. Snake extraction of boundary of influence of original line feature's uncertainty field within complex scene. Arrow denotes section where snake poorly extracts the influenced boundary.

Based on the complexity of the tangled scene, the snake procedure was given a dense sampling of initial approximations, generated from the boundaries of the original line feature's uncertainty field. The snake does a suitable job of extracting the boundaries of influence within the composite of line features. The arrow in figure 52 indicates a section where the snake does not accurately model the boundary of influence between two uncertainty fields. This particular anomaly is due more to the snake behavior than the unsuitability of the representation. Adjusting components of the snake's energy terms or including a denser sampling of initial approximations may produce a more smooth and accurate boundary extraction. Otherwise, the line feature's uncertainty field is correctly modeled in areas where there is no interference from neighboring uncertainty fields. Where uncertainty fields meet, the snake properly deforms to accommodate the introduction of outside uncertainty. The shape of the line feature's uncertainty field is therefore no longer a smooth curve constantly sagging towards its middle. Rather, the uncertainty field reflects the outside influences that its neighboring uncertainty fields impose upon it.

Applying uncertainty fields to model and deformable contours to estimate proves a suitable combination of procedures to extract these relationships. It allows the user to see not just how well a feature is defined by its measurement, but also to what degree the feature is defined by its neighbors.

5. CONCLUDING REMARKS

5.1 Summary

Within a GIS environment, the proper use of information requires the identification of the uncertainty associated with it. As such, there has been a substantial amount of research dedicated to describing and quantifying spatial data uncertainty.

Recent advances in sensor technology and image analysis techniques are making image-derived geospatial data increasingly popular. Along with development in sensor and image analysis technologies have come departures from conventional point-by-point measurements. Current advancements support the transition from traditional point measures to novel techniques that allow the extraction of complex objects as single entities (e.g., road outlines, buildings). As the methods of data extraction advance, so too must the methods of estimating the uncertainty associated with the data. Not only will object uncertainties be modeled, but the connections between these uncertainties will also be estimated.

The current methods for determining spatial accuracy for lines and areas typically involve defining a zone of uncertainty around the measured line, within which the "actual" line exists with some probability. The latest positional error models, such as the epsilon band, error band, and G-band, are rigorous statistical models for estimating independent linear features. However, there remain problems in the effectiveness with which these models communicate uncertainty and model interactions among neighboring uncertainties. Uncertainty fields, based on G-band calculations, may be more appropriate for communicating the distribution of uncertainty around a feature. An uncertainty field allows diverse visualization of error boundaries based on tolerances and intensity stretching, which consequently allows easy storage in image format. Like the G-band, uncertainty fields can be linked node-by-node to form a continuous boundary of uncertainty around a feature. Storing uncertainty fields as images makes them accessible to image processing

techniques, such as deformable contour models, which can be used to estimate these continuous uncertainty boundaries. In addition, image processing algorithms can be used to model interactions between the fields. Such interactions occur as uncertainty field distributions of neighboring features intersect and overlap. Applying image filtering techniques can extract high or low pixel values at each point, producing an image boundary between the two uncertainty fields. This boundary of influence denotes the transition where one feature's uncertainty field claims higher precedence than a neighboring uncertainty field. Again making use of deformable contours, these boundaries can be extracted to produce an accurate estimation of the fields' boundary of influence. Modeling such interactions between object uncertainties shifts the focus from independent objects within a dataset to the more useful view of single objects interacting within a scene or framework. This allows a more realistic and comprehensive view of spatial data, as uncertainties can be analyzed within the context of their given framework, rather than as independent, absolute values.

5.2 Future Research Issues

Further examination of uncertainty boundary interaction should cover comparisons of separability and accuracy among uncertainty fields. By analyzing snake energy through intersection areas, some qualitative measures can be produced which indicate the degree of interaction among uncertainty fields. Different object extraction techniques should be applied, such as template matching, snake variations, and splines. Due to the evident connection between uncertainty fields and fuzzy regions, fuzzy set theory can be employed to explore whether its techniques and methods can be used to enhance the modeling of interaction boundaries. Ultimately, research should be directed towards the goal of advancing in stride with data production methods, which currently indicate the need for uncertainty estimates on the object level.

REFERENCES

- Agouris, P., S. Gyftakis, and A. Stefanidis. "Dynamic Node Distribution in Adaptive Snakes for Road Extraction." *Vision Interface 2001*. Ottawa, Canada, 2001. 134-40.
- Agouris, P., A. Stefanidis, and S. Gyftakis. "Differential Snakes for Change Detection in Road Segments." *Photogrammetric Engineering & Remote Sensing* 67.12 (2001): 1391-99.
- Alesheikh, A., and R. Li. "Rigorous Uncertainty Models of Line and Polygon Objects in GIS." *Proceedings of GIS/LIS '96*. Denver, Colorado, 1996. 906-20.
- Azouzi, M. "Introducing the Concept of Reliability in Spatial Data." *Spatial Accuracy Assessment: Land Information Uncertainty in Natural Resources*. Eds. Kim Lowell and Annick Jatou. Quebec City, Canada: Ann Arbor Press, 1999. 139-44.
- Bandemer, H. Modelling Uncertain Data. Ed. H. Bandemer. Berlin: Akademie Verlag, 1992.
- Bastin, L., J. Wood, and P.F. Fisher. "Visualization of Fuzzy Spatial Information in Spatial Decision-Making." *Spatial Accuracy Assessment: Land Information Uncertainty in Natural Resources*. Eds. Kim Lowell and Annick Jatou. Quebec City, Canada: Ann Arbor Press, 1999. 151-56.
- Bertziss, A. Uncertainty Management. 2002. HTML. *Handbook of Software Engineering and Knowledge Engineering*. Available: <ftp://cs.pitt.edu/chang/handbook/01UNb.pdf>. March 2002.
- Blakemore, M. "Generalisation and Error in Spatial Data Bases." *Sixth International Symposium on Computer-Assisted Cartography*, 1983. 313-22. Vol. 1.
- Bonin, O. "Attribute Uncertainty Propagation in Vector Geographic Information Systems: Sensitivity Analysis." *Proceedings of the 10th International Conference on Scientific and Statistical Database Management*, 1998. 254-59.
- Carosio, A., and I.H. Kutterer. First International Symposium on Robust Statistics and Fuzzy Techniques in Geodesy and GIS. 2001. HTML. International Association of Geodesy. Available: <http://www.gis.ethz.ch/IAG/default.htm>. Jan 2002.
- Caspary, W., and R. Scheuring. "Error-Bands as Measures of Geometrical Accuracy." *EGIS 1992*. Eds. Janjaap Harts, Henk F.L. Ottens and Henk J. Scholten. Munich, Germany: EGIS Foundation, 1992. 226-33. Vol. 1. 2 vols.
- Cheng, T. "Fuzzy Objects: Their Changes and Uncertainties." *Photogrammetric Engineering & Remote Sensing* 68.1 (2002): 41-49.
- Chrisman, N. Exploring Geographic Information Systems. New York: John Wiley & Sons, Inc., 1997.
- . "A Theory of Cartographic Error and Its Measurement in Digital Data Base." *Fifth International Symposium on Computer-Assisted Cartography*. Bethesda, Maryland: American Congress on Surveying and Mapping, 1982. 159-68.

Committee, United States Federal Geographic Data. Geospatial Positioning Accuracy, Part 3: National Standard for Spatial Data Accuracy. Washington, D.C., 1998.

Duda, R.O. Covariance. 1997. HTML. San Jose State University. Available: http://www.engr.sjsu.edu/~knapp/HCIRODPR/PR_Mahal/cov.htm. June 2002.

Dutton, G. "Handling Positional Uncertainty in Spatial Databases." Proceedings Spatial Data Handling Symposium 5. Charleston, South Carolina, 1992. 460-69. Vol. 2.

Easa, S.M. "Estimating Line Segment Reliability Using Monte Carlo Simulation." Surveying and Land Information 55.3 (1995): 136-41.

Ehlschlaeger, C.R. and M.F. Goodchild. "Uncertainty in Spatial Data: Defining, Visualizing, and Managing Data Errors." GIS/LIS Proceedings. Phoenix, Arizona, 1994. 246-52.

Elia, P.B., and S.C. Bandis. "Neurofuzzy Systems in Landslide Hazard Assessment." Proceedings of the 4th International Symposium on Spatial Accuracy Assessment in Natural Resources and Environmental Sciences. Eds. G.B.M. Heuvelink and M.J.P.M. Lemmens. Amsterdam: Delft University Press, 2000. 199-202.

Fahsi, A. Air Photo Interpretation and Photogrammetry. 1996. HTML. Remote Sensing Core Curriculum. Available: <http://umbc7.umbc.edu/~tbenja1/santabar/vol1/lec6/6lecture.html>. March 2002.

Fauerbach, E.D., et al. Visualization of Uncertainty in Meteorological Forecast Models. 1996. HTML. International Cartographic Association: Commission on Visualization. Available: http://www.geovista.psu.edu/sites/icavis/icavis/feb/rep_issues.html. January 2002.

Fegeas, R.G., J.L. Cascio, and R.A. Lazar. "An Overview of Fips 173, the Spatial Data Transfer Standard." Cartography and Geographic Information Systems 19.5 (1992): 278-93.

Fisher, P.F. "Models of Uncertainty in Spatial Data." Geographic Information Systems: Principles and Technical Issues. Eds. M.F. Goodchild, P.A. Longley, D.J. Maguire, and D.W. Rhind. Second ed. Vol. 1. New York: John Wiley & Sons, Inc., 1999. 191-203.

Flack, J. On the Interpretation of Remotely Sensed Data Using Guided Techniques for Land Cover Analysis. Feb. 1996 1996. HTML. School of Computer Science, Curtin University of Technology, Western Australia. Available: <http://www.per.dem.csiro.au/staff/FlackJulien/thesis/node56.html>. Jan 2002.

Goodchild, M.F. "Keynote Address." Symposium on Spatial Database Accuracy. Melbourne, Australia, 1991.

---. "Generalization, Uncertainty, and Error Modeling." GIS/LIS Proceedings. Denver, Colorado, 1996. 765-74.

---. "Uncertainty: The Achilles Heel of GIS?" Geo Information Systems (1998).

Goodchild, M.F., and G.J. Hunter. "A Simple Positional Accuracy Measure for Linear Features." International Journal of Geographical Information Science 11.3 (1997): 299-306.

Goodchild, M.F., and W. Min-hua. "Modeling Errors for Remotely Sensed Data Input to GIS." Ninth International Symposium on Computer-Assisted Cartography. Baltimore, Maryland: ASPRS, ACSM, 1989. 530-36.

Gordon, J., and E.H. Shortliffe. "A Method for Managing Evidential Reasoning in a Hierarchical Hypothesis Space." *Artificial Intelligence* 26 (1985): 323-57.

Gottsegen, J., D. Montello, and M. Goodchild. "A Comprehensive Model of Uncertainty in Spatial Data." *Spatial Accuracy Assessment: Land Information Uncertainty in Natural Resources*. Eds. K. Lowell and A. Jaton. Quebec City, Canada: Ann Arbor Press, 1999. 175-81.

Guptill, S.C., and J.L. Morrison. Elements of Spatial Data Quality. New York: Elsevier, 1995.

Henrion, M., H.J. Suermondt, and D.E. Heckerman. "Probabilistic and Bayesian Representations of Uncertainty in Information Systems: A Pragmatic Approach." *Uncertainty Management in Information Systems: From Needs to Solutions*. Boston: Kluwer Academic Publishers, 1997.

Heuvelink, G.B.M. Error Propagation in Environmental Modelling with GIS. London: Taylor & Francis Ltd., 1998.

---. Geographic Information Technologies in Society. February 05, 1998 1998. HTML. NCGIA Core Curriculum GIScience. Available: http://www.ncgia.ucsb.edu/giscc/units/u098/u098_f.html. January 2002.

Heuvelink, G.B.M., P.A. Burrough, and A. Stein. "Propagation of Errors in Spatial Modelling with GIS." *International Journal of Geographical Information Science* 3.4 (1989): 303-22.

Hunter, G.J. "New Tools for Handling Spatial Data Quality: Moving from Academic Concepts to Practical Reality." *Journal of the Urban and Regional Information Systems Association* 11.2 (1999): 25-34.

Hunter, G.J., and M.F. Goodchild. "Managing Uncertainty in Spatial Databases: Putting Theory into Practice." *Journal of the Urban and Regional Information Systems Association* 5.2 (1993): 55-61.

---. "A New Model for Handling Vector Data Uncertainty in Geographic Information Systems." *Journal of the Urban and Regional Information Systems Association* 8.1 (1996): 51-57.

---. "Communicating Uncertainty in Spatial Databases." *Transactions in GIS* 1.1 (1996): 13-22.

Jackson, M.J., and P.A. Woodsford. "GIS Data Capture Hardware and Software." *Geographical Information Systems: Overview, Principles, and Applications*. Eds. D.J. Maguire, M.F. Goodchild and D.W. Rhind. Harlow, Essex: Longmans, 1991. 239-49.

Kass, M., A. Witkin, and D. Terzopoulos. "Snakes: Active Contour Models." *International Journal of Computer Vision* (1988): 321-31.

Kiiveri, H.T. "Assessing, Representing and Transmitting Positional Uncertainty in Maps." *International Journal of Geographical Information Science* 11.1 (1997): 33-52.

- Klir, G.J., and B. Yuan. Fuzzy Sets and Fuzzy Logic: Theory and Applications. Englewood Cliffs: Prentice-Hall, 1995.
- Leick, A. GPS Satellite Surveying. New York: John Wiley & Sons, Inc., 1995.
- Lillesand, T.M., and R.W. Kiefer. Remote Sensing and Image Interpretation. 3rd ed. New York: John Wiley & Sons, Inc., 1994.
- Mikhail, E. M., and F. Ackermann. Observations and Least Squares. New York: IEP-A Dun-Donnelley Publisher, 1976.
- Motulsky, H.J. Analyzing Data with Graphpad Prism. San Diego: GraphPad Software, Inc., 1999.
- Narasimhan, B. The Normal Distribution. 1996. HTML. Stanford University. Available: <http://www-stat.stanford.edu/~naras/jsm/NormalDensity/NormalDensity.html>. June 2002.
- Parsons, S. "Current Approaches to Handling Imperfect Information in Data and Knowledge Bases." *IEEE Transactions on Knowledge and Data Engineering* 8.3 (1996): 353-72.
- Perkal, J. "On the Length of Empirical Curves." Discussion Paper 10. Ann Arbor, Michigan: Michigan Inter-University Community of Mathematical Cartographers, 1966.
- Project, Computational Science Education. Gaussian (Normal) Distribution. 1996. HTML. U.S. Department of Energy. Available: http://csep1.phy.ornl.gov/gif_figures/mcf7.gif. June 2002.
- Rogge, D.M., and N.M. Halden. Mineralization Potential Modeling: An Aid to Exploration and Land Use Management. 2000. HTML. University of Manitoba, Winnipeg, Manitoba, Canada. Available: http://home.cc.umanitoba.ca/~umrogge/msc_project.html. Feb. 2002.
- Shi, W. Modelling Positional and Thematic Uncertainty in Integration of GIS and Remote Sensing. Enschede: International Institute for Geo-Information Science and Earth Observation, 1994.
- . "Statistical Modeling Uncertainties of Three-Dimensional GIS Features." *Cartography and Geographic Information Systems* 24.1 (1997): 21-26.
- . "A Generic Statistical Approach for Modeling Error of Geometric Features in GIS." *International Journal of Geographical Information Science* 12.2 (1998): 131-43.
- Shi, W., M. Ehlers, and K. Tempfli. "Modelling and Visualizing Uncertainties in Multi-Data-Based Spatial Analysis." *EGIS 1994*. Eds. J.J. Harts, H.F.L. Ottens and H.J. Scholten. Paris, France: EGIS Foundation, 1994. 454-64. Vol. 1.
- Shi, W., and W. Liu. "A Stochastic-Based Model for the Positional Error of Line Segments in GIS." *International Journal of Geographical Information Science* 14.1 (2000): 51-66.
- Shi, W., and K. Tempfli. "Modelling Positional Uncertainty of Line Features in GIS." *ASPRS/ACSM Annual Convention: ASPRS, 1994*. Vol. 1.

Shi, W.Z., and C.K. Cheung. "A Reliability of Spatial Objects in a 3d GIS." Journal of the Urban and Regional Information Systems Association. Chicago, Illinois: Urban and Regional Information Systems Association, 1999. 314-19.

Sorensen, R. Vagueness. 2002. HTML. Stanford Encyclopedia of Philosophy. Available: <http://plato.stanford.edu/entries/vagueness/>. March 2002.

Stanfel, L.E., and C. Stanfel. "A Generalization on Line Segment Reliability Measures." Surveying and Land Information Systems 54.1 (1994): 41-44.

---. "A Model for the Reliability of a Line Connecting Uncertain Points." Surveying and Land Information Systems 53.1 (1993): 49-52.

Stanislawski, L.V. "Mapping Positional Accuracy of Geographic Information System Data Layers through Error Propagation." Proceedings of the 4th International Symposium on Spatial Accuracy Assessment in Natural Resources and Environmental Sciences. Eds. G.B.M. Heuvelink and M.J.P.M. Lemmens. Amsterdam: Delft University Press, 2000. 597-600.

Stassopoulou, A., and T. Caelli. "Building Detection Using Bayesian Networks." International Journal of Pattern Recognition and Artificial Intelligence 14.6 (2000): 715-33.

Stassopoulou, A., M. Petrou, and J.V. Kittler. "Bayesian and Neural Networks for Geographic Information-Processing." Pattern Recognition Letters 17.13 (1996): 1325-30.

Strahler, A.H. "The Use of Prior Probabilities in Maximum Likelihood Classification of Remotely Sensed Data." Remote Sensing of Environment 10 (1980): 135-63.

Technology, US National Institute of Standards and. US Spatial Data Transfer Standard: Federal Information Processing Standard 173, 1992.

Tsoukalas, L.H., and R.E. Uhrig. Fuzzy and Neural Approaches in Engineering. New York: John Wiley & Sons, Inc., 1997.

National Consortia on Remote Sensing in Transportation. Automatic Feature Recognition and Extraction from Remote Sensing Imagery. 2001. HTML. University of New Mexico. Available: http://riker.unm.edu/DASH_new/pdf/Application%20Briefs/Automatic%20Feature%20Extraction.PDF. June 2002.

Veregin, H. Data Quality Measurement and Assessment. March 23, 1998 1998. HTML. NCGIA Core Curriculum in GIScience. Available: http://www.ncgia.ucsb.edu/education/curricula/giscc/units/u100/u100_f.html. January 2002.

Wel, F.J.M. Van der, and R.M. Hootsman. "Visualization of Quality Information as an Indispensable Part of Optimal Information Extraction from a GIS." Proceedings of the 16th International Cartographic Conference. Cologne, 1993. 881-97. Vol. 2.

Wolf, P.R., and C.D. Ghilani. Adjustment Computations: Statistics and Least Squares in Surveying and GIS. Wiley Series in Surveying and Boundary Control. Ed. Roy Minnick. New York: John Wiley & Sons, Inc., 1997.

Yu, Z. C., and L. C. Lu. *Fundamentals of Surveying Adjustment*. Beijing: China Surveying and Mapping, 1983.

Zeng, T.Q., and P. Cowell. "Assessing Uncertainty in Modeling Coastal Recession Due to Sea Level Rise." *Spatial Accuracy Assessment: Land Information Uncertainty in Natural Resources*. Eds. K. Lowell and A. Jatou. Quebec City, Canada: Ann Arbor Press, 1999. 79-88.

APPENDICES

APPENDIX A. MODELS FOR ESTIMATING AND ASSESSING POSITIONAL UNCERTAINTY

As mentioned in Section 2.2.1, there are numerous methods and models for determining the positional uncertainty of spatial features, be they points, lines, or polygons. An in-depth examination of all methods is beyond the scope of this paper, but a table outlining some recent and noteworthy positional accuracy models is provided. This table is an introductory piece to the more detailed review of statistical methods found in Section 3.1 and Appendix B.

The table is designed to outline significant models for estimating and assessing positional uncertainty. The first column provides the sources or authors of the model. This column also includes a description of if the model has been developed and tested through rigorous mathematics and statistics, or whether it is a conceptual method. The second column gives a brief description of the model, while the third column addresses the suitability of the model for visual representation. The fourth column indicates whether the model is based on a Normal distribution. The fifth column details how accuracy point indicators are provided, and whether correlation between the errors of feature points is assumed. Finally, any other noteworthy details or other assumptions the model makes are included.

<ul style="list-style-type: none"> • Sources • Model Type [Rigorous] [Conceptual] 	Description	Assume a Gaussian (Normal) Distribution?	Compute or provide accuracy indicators? Correlation between points?	Notes and/or assumptions made
<p>Epsilon Band Perkal, 1966 Chrisman, 1982 Blakemore, 1984 Alai, 1993 Alesheikh and Li, 1996</p> <p>[Conceptual]</p>	<p>Approach for modeling positional error of linear features. A line feature connecting two points is surrounded on each side by an area of constant width, epsilon. Result represents a buffer zone of error around the measured line feature. Model was designed to provide users with a measure of error associated with digitizing cartographic lines.</p>	<p>Assumes circular normal distributions of error at endpoints, but provides no error distribution inside band.</p>	<p>Assumes point accuracy measures are provided.</p>	<p>Epsilon band is a popular model for positional uncertainty of lines, and many interpretations exist. Probabilistic interpretation proven inconsistent.</p>
<p>Error Band Dutton, 1992 Caspary and Scheuring, 1992 Shi, 1994 Alesheikh and Li, 1996</p> <p>[Conceptual]</p>	<p>An extension of the epsilon band model; rather than a band of constant width, the error band model proposes a band that becomes narrower in the middle of the line segment.</p>	<p>Assumes circular normal distributions of error at the endpoints (no directional bias).</p>	<p>Assumes point accuracy measures are provided.</p> <p>Assumes errors of the two endpoints are independent of each other.</p>	<p>Introduced the notion that a segment's centerpoint, though fictional, is more reliable location than its known endpoints.</p>
<p>G-Band Shi, 2000 Shi, 1998</p> <p>[Rigorous]</p>	<p>More generic description of the error band model, allowing for interrelation between two endpoints. 2-D normal distributions of endpoint errors allow for varying shape and size of G-Band, determined by error ellipses of endpoints and its spatial density distribution surface.</p>	<p>Assumes errors of line segment endpoints follow two-dimensional normal distributions.</p>	<p>Assumes point accuracy measures are provided.</p> <p>Takes into account correlation between two endpoints.</p>	<p>Based on stochastic process theory.</p> <p>G-Band is not symmetrical, error ellipses possess varying axes and rotations.</p>

APPENDIX B. METHODS FOR DERIVING POSITIONAL UNCERTAINTY OF DIGITAL SPATIAL FEATURES

Developing methods to express the accuracy or uncertainty of spatial information has been the focus of much research within the spatial data community. With regards to positional uncertainty, these methods have been continually developed and extended over the last twenty years. Within our discussion, the terms ‘error’ and ‘uncertainty’ will be used almost interchangeably. The spatial data community, while recognizing the inherent differences between the terms, is often at odds when trying to define or separate them. This confusion is due, in part, to the similar concepts the terms are meant to convey. In order to achieve the goals of this paper, we must analyze and apply previous research on positional error (and uncertainty). For the sake of simplicity we will assume that the terms ‘uncertainty’, and ‘error’ both indicate a deviation from the true value. In addition, the term accuracy can be considered the complement to the two terms, i.e., the “closeness” to the true value.

As previously noted, spatial objects are comprised of points, lines, and polygons. As the most fundamental geometric element, points and their error models have long been studied in the fields of geodesy, surveying, and mapping (Shi 2000). Section 2.1.3 stated that all observations and measured values contain errors, and Section 2.3 indicated sources of error or uncertainty within positional measurements. The uncertainty of digital spatial databases is typically expressed through point error measurements. Point errors can be quantified using standard deviations of points in the x, y, and z directions. Due to the two-dimensional nature of maps and imagery, error is typically quantified as either a single directionally independent measure (σ), or as a standard deviation in two directions (σ_x, σ_y). One important measure of error that utilizes standard deviations is the root-mean-square positional error, or RMSP. The RMSP for a point can be calculated accordingly:

$$RMSP = \sqrt{\sigma_x^2 + \sigma_y^2} \quad (\text{Caspary and Scheuring, 1992})$$

A visual indicator of error or uncertainty of points is an error ellipse. An error ellipse uses standard deviations in two directions (e.g., x and y) to define its semi-major and semi-minor axes and rotation. The ellipse's axes are defined in the following manner:

$$\text{Semi-major axis} = \frac{\sigma_x^2 \sigma_y^2}{2} + \sqrt{\frac{\sigma_x^2 \sigma_y^2}{4} + \sigma_{xy}^2}$$

$$\text{Semi-minor axis} = \frac{\sigma_x^2 \sigma_y^2}{2} - \sqrt{\frac{\sigma_x^2 \sigma_y^2}{4} + \sigma_{xy}^2}$$

Along with the rotation of the ellipse (angle t in figure B.1), these axes provide useful visual information regarding a point's positional uncertainty. The shape and orientation of error ellipses can provide information on the precision of points and allows visual comparisons among multiple points. The semi-major axis defines the weakest direction in which a point's position is known (i.e., the direction of maximum uncertainty). Consequently, the semi-minor axis defines the point's direction of least uncertainty, or the strongest direction in which the point's position is known (Wolf and Ghilani, 1997).

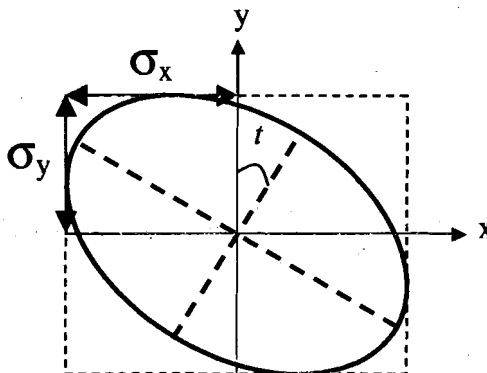


Figure B.1: Error ellipse and its components

If the uncertainties in both directions are equal (i.e., $\sigma_x = \sigma_y$) and independent, the ellipse's shape is an error circle. Yet another measure of positional uncertainty is Circular Error Probable (CEP). The CEP is defined to be $CEP = 0.589(\sigma_x\sigma_y)$, where the probability of the point's true position lying inside a circle with radius CEP is 50 percent. The RMSP, error ellipse, and CEP are common methods of quantifying point positional error.

While point error models provide information regarding positional uncertainty, it is more useful to obtain uncertainty measures for lines and objects. Despite solid point modeling theory, lines and polygons have proven more problematic for visualizing and modeling their associated errors. The complexity arises from the need to take independent error models of individual points and combine them to form a more complex, dependent model. Just as a line is composed of two endpoints, the line's error is derived from the error of its endpoints. In like manner, a polygon's error is derived from the error of its boundary line segments. By designing error models for spatial objects based on the error models of their more basic components, it is hoped that a building-block approach can be used to formulate uncertainty indices for complex objects.

B.1 Chrisman and Perkal's Epsilon Band

Chrisman (1982), expanding on the work of Perkal (1966), investigates the idea of providing an uncertainty boundary surrounding a line segment. The uncertainty boundary, called an *epsilon band*, is based upon a constant radius (epsilon) around the line's true or most likely position. The quantity epsilon (ϵ) is derived from the radius of the line's endpoint error circles, assuming a digitization process that yields random coordinate error in a *circular normal distribution*. The circular normal distribution is two-dimensional (bivariate) and varies normally, meaning that it consists of errors in two directions that are equal and uncorrelated. As figure B.2 demonstrates,

the epsilon band's width is contingent on a single error quantity. The main drawback of this model is that it provides no interpretation of error distribution inside the band.

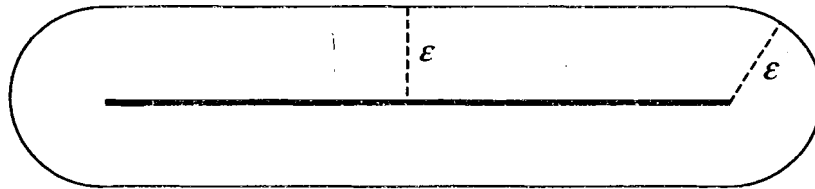


Figure B.2: Chrisman's ϵ - band (Adapted from Chrisman, 1992)

B.2 Dutton's Error Band Simulations

Dutton (1992) tested the method Chrisman and Perkal used to derive vector representations of digitized map features. Similar to their work, Dutton assumes that digitizing points produces error that follows a circular normal distribution. Likewise, his analysis characterizes feature uncertainty by constructing regions of "constant locational probability around the edges of polylines" (ibid.). However, Dutton's result describes concave curvilinear error bands along the most likely line segment position. An underlying basis for study of digital spatial feature uncertainty is that every feature is made up of points that are uncertain to some degree. Dutton assigns each point a circular "locus of uncertainty", within which "any location can be considered a reasonable alias" (ibid.). This uncertainty area is simply an error circle, with each error circle possessing equal radii. Since any location within the circle can represent the actual point, Dutton postulates that a multitude of line segments can connect two uncertain points. In order to determine a most likely segment position, Dutton performs an experiment involving multiple realizations of possible segment positions.

Figure B.3 illustrates Dutton's experiment and results. A line (representing a median) is drawn and equal error circles are assigned around each endpoint, within which the true endpoints may

lie. Endpoints are then generated from a circular normal distribution within each error circle, representing possible endpoint positions.

Random endpoints are connected to form line segments that fall left, right, or across the median line. The distance from each segment to the median line it represents is calculated at regular intervals along the line. The standard deviation for these distance residuals are then calculated at each interval along the median line. As a result, Dutton finds that the displacement error from each segment to the median line it represents is greatest near the measured points and least halfway between them. Dutton finds the results “odd at first” because the midpoint error is at a minimum despite the lack of a coordinate measurement (ibid.). The conclusion is that despite the precision of a segment’s endpoint positions, its centerpoint is the most reliable location.

Based on the standard deviation at eleven evenly-spaced locations along the baseline, Dutton is further able to derive a probability contour one standard deviation (σ) in width. In the same year, the work of Caspary and Scheuring (1992) helps verify that Dutton’s simulations are right on target.

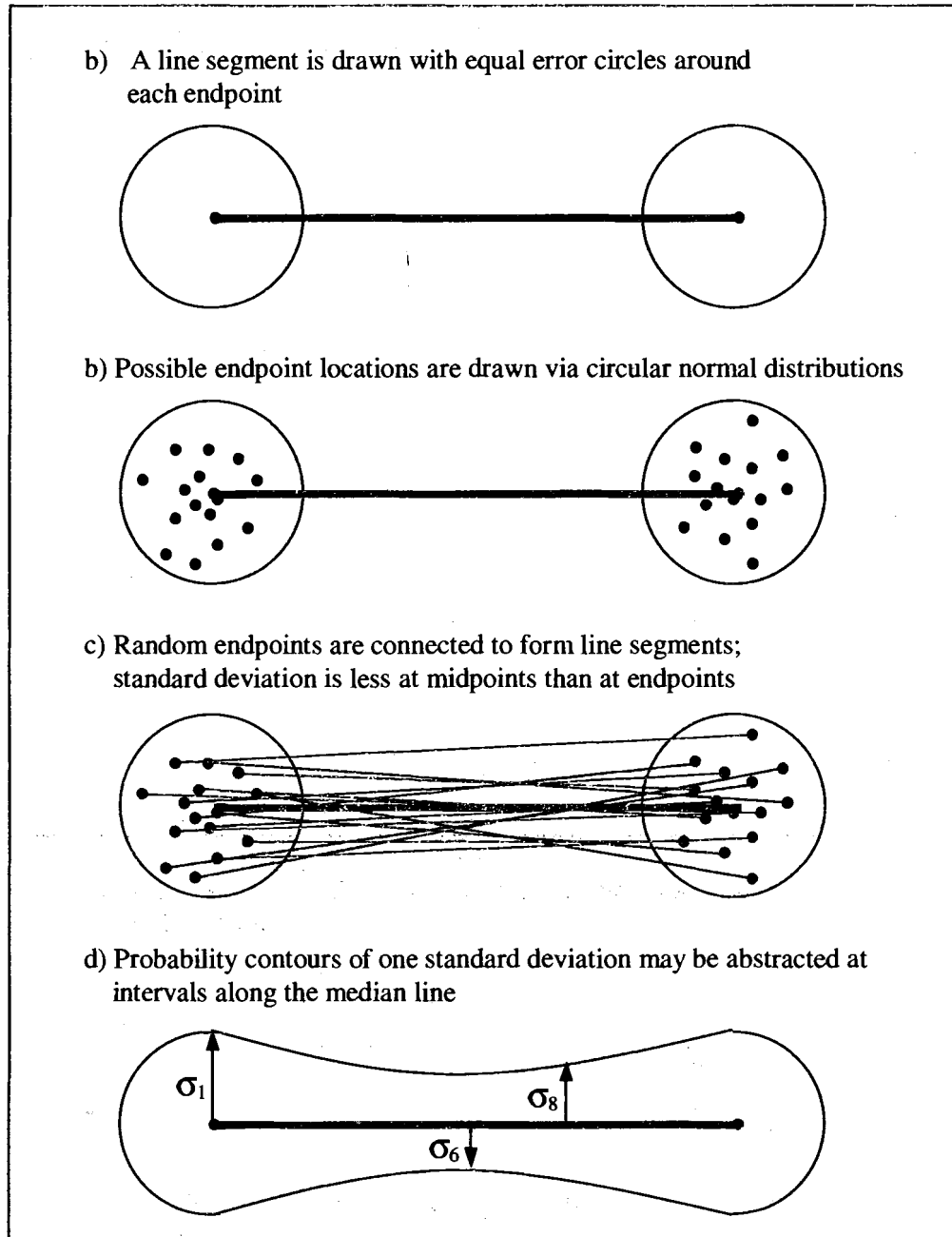


Figure B.3: Dutton's experiment simulating line segments (Adapted from Dutton, 1992)

B.3 Caspary and Scheuring's Error-Band

Caspary and Scheuring (1992) refine Chrisman's idea to describe the accuracy of lines derived from positional errors of endpoints. Like Chrisman and Dutton, they assume equal endpoint coordinate errors following a circular normal distribution. However, the authors use error propagation and Monte Carlo simulation to derive their own *error-band* that sags at the midpoint of the line segment.

Caspary and Scheuring define the coordinates of an arbitrary point along a line as a function of its endpoints and a parameter. The parametrization is expressed as a function of the point's position along the line (L_i) and the length of the line (L):

$$x_i = x_1 + (x_2 - x_1) \frac{L_i}{L}, \quad y_i = y_1 + (y_2 - y_1) \frac{L_i}{L}, \quad 0 \leq L_i \leq L \quad (\text{ibid.})$$

The parametrizations still follow a normal distribution because they are linear transformations of normally distributed variables (Mikhail and Ackermann, 1976; Shi and Liu, 2000). By applying error propagation law and the independent-and-equal error assumption, the authors are able to predict how the uncertainty varies along the length of the line.

$$\sigma_{x_i}^2 = \sigma_{y_i}^2 = \left(1 - \frac{2L_i}{L} + \frac{2L_i^2}{L^2} \right) \sigma^2, \quad RMSP_i = \sqrt{2} \sigma_{x_i}$$

Using this formula, Caspary and Scheuring show that points towards the middle of straight lines have smaller RMSP values than those at the endpoints. More precisely, the midpoint error proves to be a factor of $1/\sqrt{2}$ less than the endpoint error, while the error-band is 0.8 times smaller than the area of the epsilon-band. The authors propose that the more accurate error-band is an area determined by the error circle boundaries of all points along the line, rather than strictly the error

of the endpoints. However, it should be noted that applying error propagation law still requires the inner error circles to be dependent on the endpoint error.

As a result of smaller error at a line's midpoint, Caspary and Scheuring's error-band curves towards the center, similar to Dutton's. Despite the admitted difficulties of analytically expressing the shape of their error-band, the authors are able to approximate the shape and area of the region according to figure B.4.

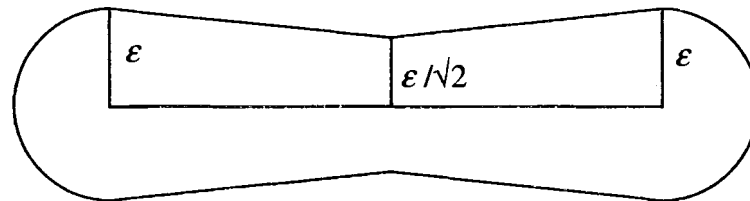


Figure B.4: Approximation of the error-band
(Adapted from Caspary and Scheuring, 1992)

Caspary and Scheuring further observe that a straight line can be viewed as a random object defined by four random variables (four coordinates of two endpoints), forming a four-dimensional random vector. The authors wish to describe a region of constant probability around this four-dimensional random vector, while avoiding a rigorous derivation of two-dimensional probability contours. Instead, they verify their work using Monte-Carlo simulation similar to that of Dutton's (1992).

By generating random coordinates for two endpoints based on a circular normal distribution, the authors derive random positions of a median straight line. By placing the random lines within a cell array, each line's intersection with a cell can be tabulated (see figure B.5). The cells and the frequencies with which they are intersected are used to produce lines of constant probability density. An area with a fixed probability of containing the true line segment can be found by calculating the frequencies of cells along profiles perpendicular to the expected line. The

resulting area is the representation of the correct error-band (ibid.). The authors briefly relate the one-directional probability density of the line to the probability distribution functions of the endpoints. The same Monte Carlo method is also used to analyze the error-band around the vertices, where the bands overlap.

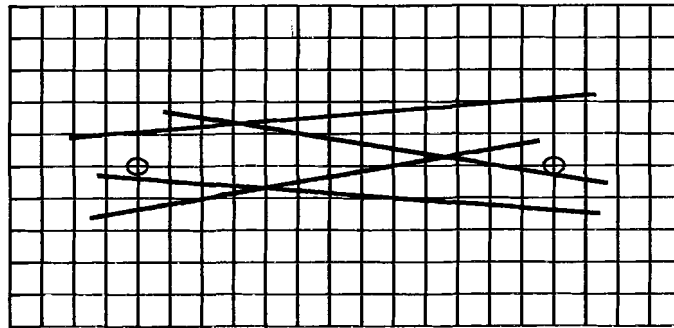


Figure B.5: Cell array and random lines (schematic)
(Adapted from Caspary and Scheuring, 1992)

The authors conclude that the error band's area can be used as a measure of accuracy of the digital representation of a line. In addition, they make the distinction between the standard deviation of area computed from error propagation and the area of a polygon boundary's error-band. The error-band is said to contain "the uncertainty of the area of the polygon and of its position", while standard deviation of area "expresses the accuracy of the (polygon's) area only" (ibid.).

Caspary and Scheuring's work is important for positional accuracy of objects within spatial databases because it:

5. Uses the error propagation law to derive positional errors along the line.
6. Concludes that an appropriate error-band is determined by the error circle boundaries of all points along the line, rather than strictly the error of the endpoints.
7. Views a straight line as a four-dimensional random vector.
8. Compares the marginal density of a line to the distribution function of an endpoint.

B.4 Shi and Tempfli's Error Model

These observations are employed by Shi and colleagues (Shi and Tempfli, 1994; Shi and Liu, 2000) to expand on Caspary and Scheuring's work to model positional errors of line features in GIS. Again, it is assumed that coordinate errors follow a normal distribution and are uncorrelated. In addition, the positional error and distribution of an arbitrary point on a line segment are dependent on the errors and distribution of the endpoints. Using these assumptions, Shi and Tempfli (1994) define the probability distribution and confidence region of a line segment. Shi and Liu (2000), however, use the more general case of interrelation between two endpoints to generate a modified error-band. It should be noted that within the context of this paper the probability distribution of a line is more relevant than a confidence region. A probability distribution describes how a measured segment composed of four random variables can deviate from a true location. Confidence regions are used more for generating a region of certainty around a measured segment within which the true location lies. The difference is subtle, but a probability distribution for a line is better suited when the true location of a line is unknown.

Shi and Tempfli (1994) define two endpoints as stochastic vectors following a normal distribution, a more explicit characterization of Caspary and Scheuring's (1992) idea of a four-dimensional random vector:

$$Z_1 = \begin{bmatrix} X_1 \\ Y_1 \end{bmatrix} \sim N_2 \left(\begin{bmatrix} \mu_1 \\ \nu_1 \end{bmatrix}, \begin{bmatrix} \sigma_{XX} & \sigma_{XY} \\ \sigma_{XY} & \sigma_{YY} \end{bmatrix} \right), \quad Z_2 = \begin{bmatrix} X_2 \\ Y_2 \end{bmatrix} \sim N_2 \left(\begin{bmatrix} \mu_2 \\ \nu_2 \end{bmatrix}, \begin{bmatrix} \sigma_{XX} & \sigma_{XY} \\ \sigma_{XY} & \sigma_{YY} \end{bmatrix} \right)$$

The equal variances and covariances indicate independent endpoint errors, which the authors admit, "may not be realistic in case of a multi-source GIS" (Shi and Tempfli, 1994). The line Z_1Z_2 connecting the two endpoints is expressed as a linear, normally distributed function of Z_1 and Z_2 through parametrization. Drawing from Caspary and Scheuring's (1992) investigation of

the marginal density of a line, Shi and Tempfli derive the probability distribution of a point in a direction perpendicular to the line. A marginal density allows a study of the distribution of a single variable within a multi-variable distribution. In this case, the marginal density allows a study of a point's distribution in a single direction within a two-dimensional distribution. Consequently, the marginal distribution of X or Y can be derived from the joint distribution of (X, Y) .

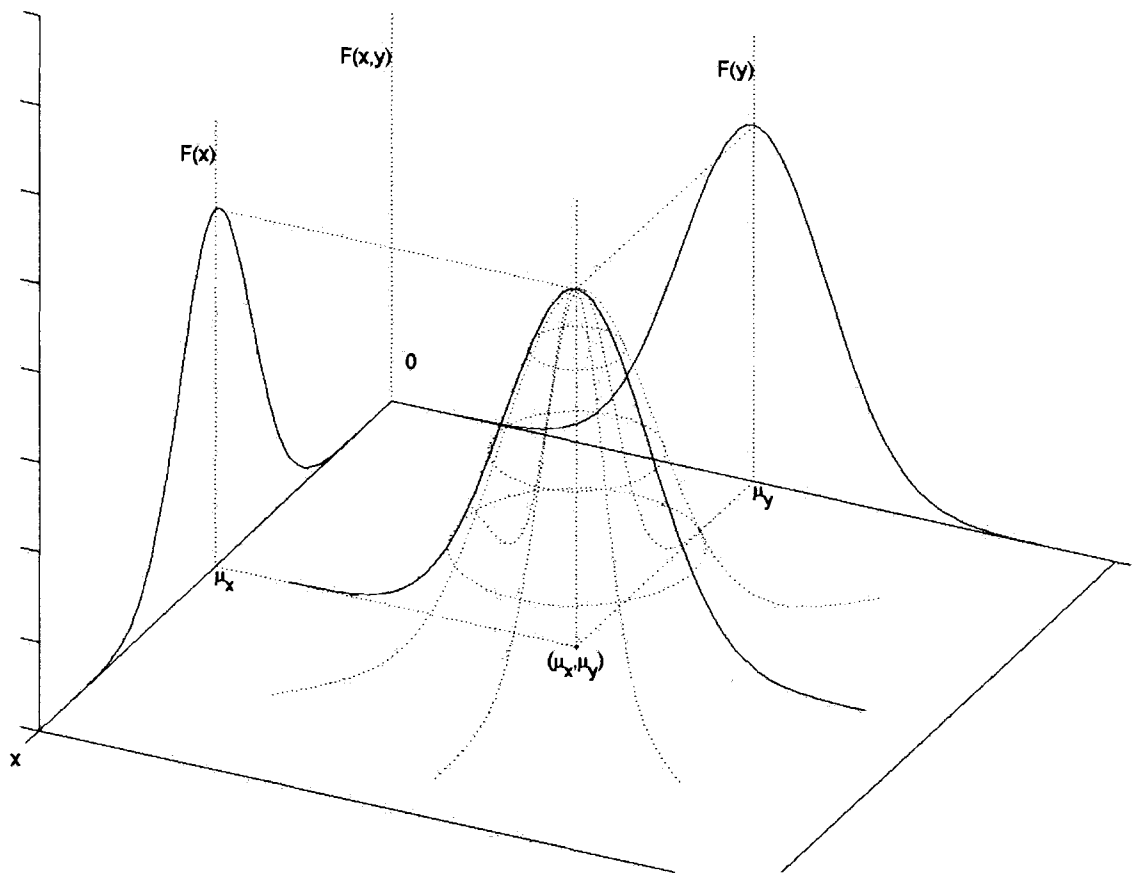


Figure B.6: The probability density function (bivariate) of the point (x,y)
(Adapted from Shi and Liu, 2000)

By calculating the probability distribution of a point in a direction perpendicular to the line, a boundary can be formed indicating how the point's position can vary from its true or mean position. The probability distribution of the line segment can therefore be characterized by the

perpendicular density of any point along the line and the density at the two endpoints. The line segment's probability distribution describes how the segment can deviate from its expected or mean location (Shi and Tempfli, 1994). This concept is expanded upon in Shi's later work with Liu (2000) and will be examined shortly.

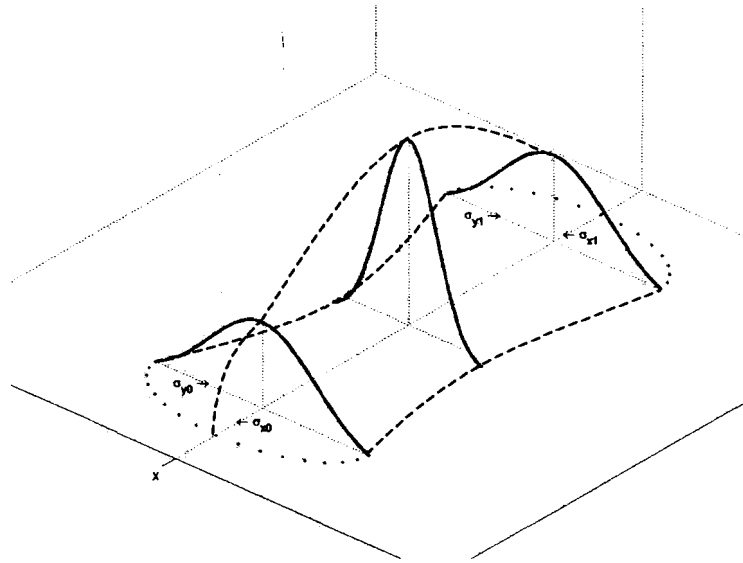


Figure B.7: The probability density function of a line
(Adapted from Shi and Tempfli, 1994; Shi and Liu, 2000)

Shi and Tempfli (1994) also develop a set of indicators for segment errors based upon the probability density of a line segment. Among the suggested indicators are segment standard error, segment near certainty error, segment map accuracy standard, and probable segment error. In addition, the authors briefly investigate features made up of multiple line segments where the segment probability distributions overlapped. The probability distributions of both segments can determine the probability that a point belongs to the feature using fuzzy theory.

B.5 Shi and Liu's G-Band Model

Shi and Liu (2000) further develop the ideas of Caspary and Scheuring (1992) and Shi and Tempfli (1994) by producing a more general model of the error band, called the G-band model. The main improvement of the G-band model being that it allows for correlation between two

endpoints, a condition not handled by previous models. In addition, the authors specifically target cases with differing errors between the endpoints. Endpoint errors are once again assumed to follow two-dimensional normal distributions. Many of the same procedures of Shi and Tempfli (1994) are employed with modifications to allow for the more general case of endpoint error variation and dependency. That is, the authors statistically derive the distribution and density functions of a line segment to further define errors of arbitrary points on the line.

A line segment Z_0Z_1 , being the composite of two endpoints (Z_0 and Z_1), can be represented as a four-dimensional random vector Z_{01} . Consequently, Z_{01} follows a four-dimensional normal distribution (Yu and Lu, 1983; Shi and Liu, 2000):

$$Z_{01} \sim N_4(\mu_{Z_{01}}, \Sigma_{Z_{01}Z_{01}})$$

with mean and variance-covariance matrix:

$$\mu_{Z_{01}} = (\mu_{X_0}, \mu_{Y_0}, \mu_{X_1}, \mu_{Y_1}), \quad \Sigma_{Z_{01}Z_{01}} = \begin{bmatrix} \sigma_{X_0}^2 & \sigma_{X_0Y_0} & \sigma_{X_0X_1} & \sigma_{X_0Y_1} \\ \sigma_{Y_0X_0} & \sigma_{Y_0}^2 & \sigma_{Y_0X_1} & \sigma_{Y_0Y_1} \\ \sigma_{X_1X_0} & \sigma_{X_1Y_0} & \sigma_{X_1}^2 & \sigma_{X_1Y_1} \\ \sigma_{Y_1X_0} & \sigma_{Y_1Y_0} & \sigma_{Y_1X_1} & \sigma_{Y_1}^2 \end{bmatrix}.$$

The authors offer a parametrization similar to the one presented by Caspary and Scheuring (1992), and indicate that a line segment is a “composite of...infinite stochastic variables $X(t)$ and $Y(t)$ ”:

$$\begin{cases} X(t) = (1-t)X_0 + tX_1 \\ Y(t) = (1-t)Y_0 + tY_1 \end{cases} \quad (0 \leq t \leq 1) \quad (\text{Shi, 1994 and Shi and Liu, 2000})$$

The authors prove that the two-dimensional vector $Z(t)$ composed of $\{X(t), Y(t)\}^T$ can fully described the statistical characteristics of line segment Z_0Z_1 . This is accomplished by expanding Shi and Tempfli’s (1994) work with a line’s distribution and density functions. These functions

can describe the stochastic variables $X(t)$ and $Y(t)$ as well as the correlation between them. Again, $X(t)$ and $Y(t)$ follow a normal distribution because they are linear transformations of normally distributed variables (Mikhail and Ackermann, 1976; Shi and Liu, 2000). Accordingly, an arbitrary point $Z_t(X(t), Y(t))$ on the line segment will follow the line segment's two-dimensional normal distribution:

$$Z(t) = (X(t)Y(t))^T \sim N_2(\mu_Z(t), \Sigma_{ZZ}(t)) \quad (\text{Shi and Liu, 2000})$$

The point's positional variation can thus be predicted, yet the model still lacks estimates of $\mu_Z(t)$ and $\Sigma_{ZZ}(t)$. While the distribution and density functions provide complete statistical characteristics of a line segment, due to practical complexity it cannot be used to describe the positional uncertainty of the segment (Shi and Liu, 2000). Therefore, the authors derive an uncertainty information matrix Σ_{ZZ} of a line as an extension of the covariance matrix of a point.

$$\Sigma_{ZZ}(t_1, t_2) = \begin{bmatrix} \sigma_X^2(t_1, t_2) & \sigma_{XY}(t_1, t_2) \\ \sigma_{YX}(t_1, t_2) & \sigma_Y^2(t_1, t_2) \end{bmatrix}$$

The matrix is a non-stochastic function of t_1 and t_2 used to describe the linear correlation of the points on a line segment and their coordinates. By combining the parametrization of $X(t)$ and $Y(t)$ with t_1 and t_2 of Σ_{ZZ} , an explicit uncertainty information matrix can be derived. In a similar manner, the line's mean value vector $\mu_Z(t)$ can be estimated:

$$\mu_Z(t) = \begin{bmatrix} \mu_X(t) \\ \mu_Y(t) \end{bmatrix} = \begin{bmatrix} (1-t)\mu_{X_0} + t\mu_{X_1} \\ (1-t)\mu_{Y_0} + t\mu_{Y_1} \end{bmatrix} \quad (\text{ibid.})$$

A single evaluation of the uncertainty matrix for two points can provide the linear correlation between those two points and their coordinates. The uncertainty information matrix explains relationships between varying errors for two different points in two directions, resulting in a

rather complex 2-by-2 array. However, the matrix is simplified when handling the condition of directional independence among the error components (i.e., for any point, $\sigma_x = \sigma_y$). This is often the case within GIS vector data production operations, such as digitizing or automated feature extraction.

Based on work with distribution and density functions and their uncertainty information matrix, Shi and Liu derive a generic error band model. Named the G-band, its boundaries are defined by the error ellipses of arbitrary points on the line segment and the error ellipses of the endpoints. While based on conclusions previously drawn by Caspary and Scheuring, the G-band has distinct properties not before articulated. The G-band is directly linked to the distribution and density functions of a line segment, which completely describe a line's statistical characteristics. As such, it is able to handle correlation between endpoint errors, as well as inequality between these errors. Figure B.8 illustrates the definition of the generic error band according to Shi and Liu (2000). By slicing the spatial density distribution surface *parallel to the X-Y plane*, an infinite number of two-dimensional bands can be obtained. Of these parallel slices through the density surface, the G-band is described by the plane passing through the error ellipse of the endpoints (ibid.).

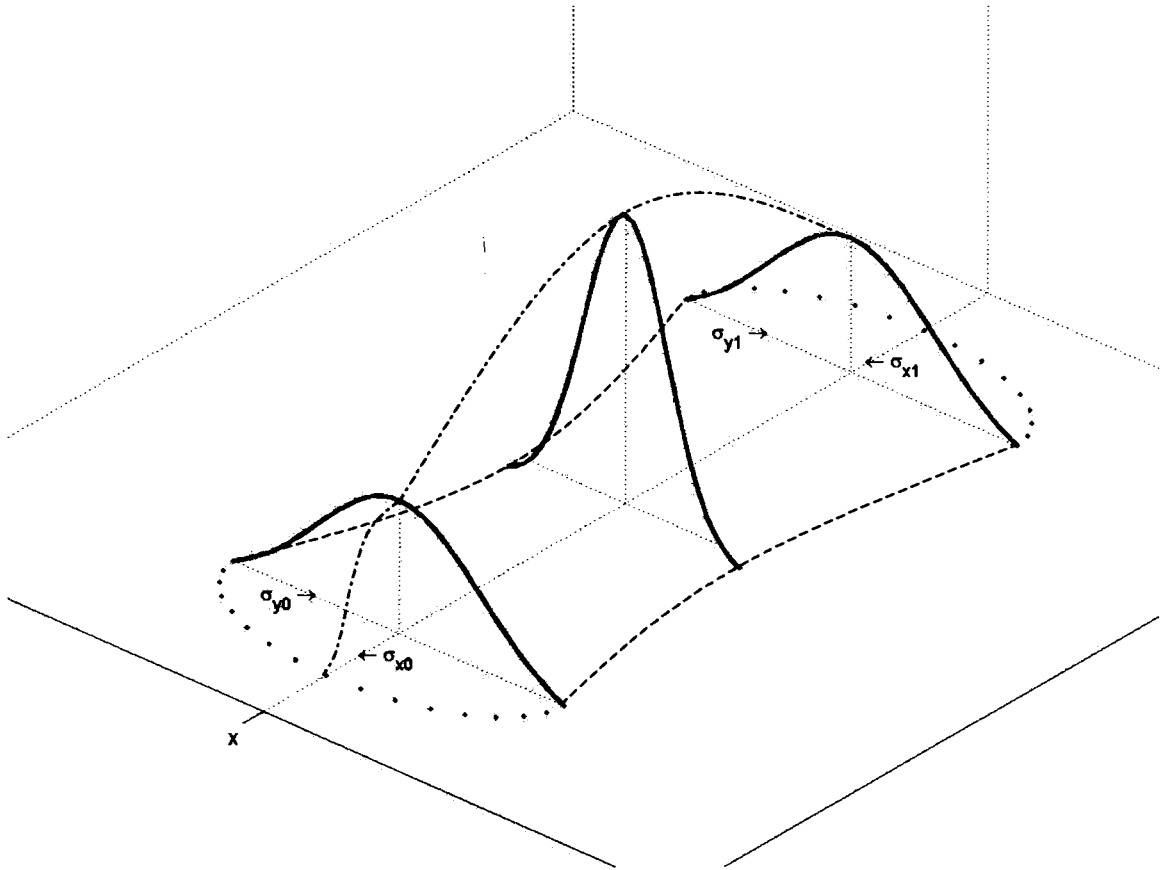


Figure B.8: The probability density function of a line [enlarged]
 (Adapted from Shi and Templi, 1994; Shi and Liu, 2000)

Similar to previous band models, the G-band's shape is described by the error ellipses of all points along the line segment. The error ellipses at the endpoints describe the extreme ends of the the band, while the error ellipses of the inner points construct the boundary lines of the band. The error ellipses are described by their semi-major axis, semi-minor axis, and direction to the semi-major axis, defined by Shi and Liu (ibid.) to be:

$$\left. \begin{aligned}
 A^2(t) &= \sigma_0^2 \lambda(t)_1 = \frac{1}{2} \{ \sigma_X^2(t) + \sigma_Y^2(t) + \omega \} \\
 B^2(t) &= \sigma_0^2 \lambda(t)_2 = \frac{1}{2} \{ \sigma_X^2(t) + \sigma_Y^2(t) - \omega \} \\
 \operatorname{tg} 2\phi(t) &= \frac{2\sigma_{XY}(t)}{\sigma_X^2(t) - \sigma_Y^2(t)}
 \end{aligned} \right\} \text{ where } \omega = \sqrt{(\sigma_X^2(t) - \sigma_Y^2(t))^2 + 4\sigma_{XY}^2(t)}.$$

As mentioned previously, if the errors in the coordinate components are independent and equal to each other (i.e., for any point, $\sigma_x = \sigma_y$), the uncertainty information matrix is greatly simplified. Under this condition of directional independence, the error ellipses become error circles with a radius of uncertainty equal to:

$$\Sigma_{zz} = [(1-t)^2 \sigma_0^2 + t^2 \sigma_1^2] \quad (\text{ibid.})$$

While Caspary and Scheuring's (1992) error band relies on the assumption of directional independence, this condition is only a special instance of the G-band. Figure B.9(a) illustrates this special case of the G-band, when endpoint errors are independent and equal. Under these conditions, the G-band reduces to the error band models of Caspary and Scheuring (ibid.). Figure B.9(b) illustrates the more general case of the G-band, which allows each endpoint to have varying errors in both dimensions. In this case, the endpoint errors in the two directions are correlated and of varying magnitudes.

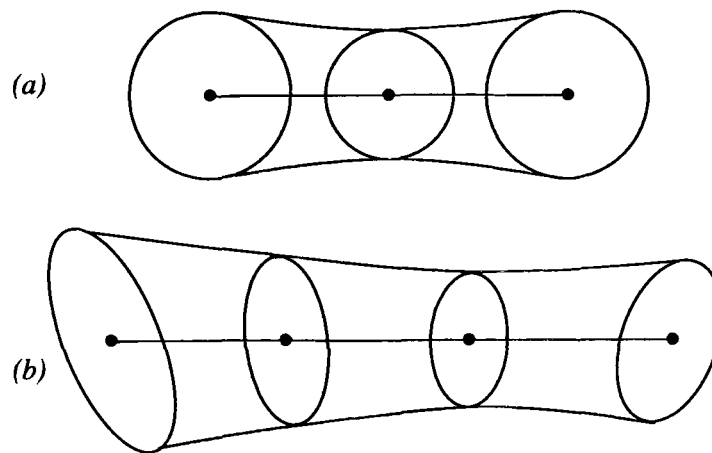


Figure B.9: G-bands under varied conditions: (a) equal, uncorrelated errors; (b) unequal, correlated errors (Adapted from Shi and Liu, 2000)

Similar to previous error band models, the G-band sags as the error ellipses along the line decrease. However, due to the G-band's ability to handle unequal endpoint errors, the minimum error ellipse is not necessarily located at the center of the line segment. The minimum error ellipse location is dependent on the relative endpoint error magnitudes; its position will be closer to the endpoint with less error. Figure B.10 demonstrates this property with error circles, where point Z_0 has error σ_0 , point Z_1 has error σ_1 , and the minimum error circle is centered on Z_t . Note the minimum error circle is located nearest the endpoint with least error.

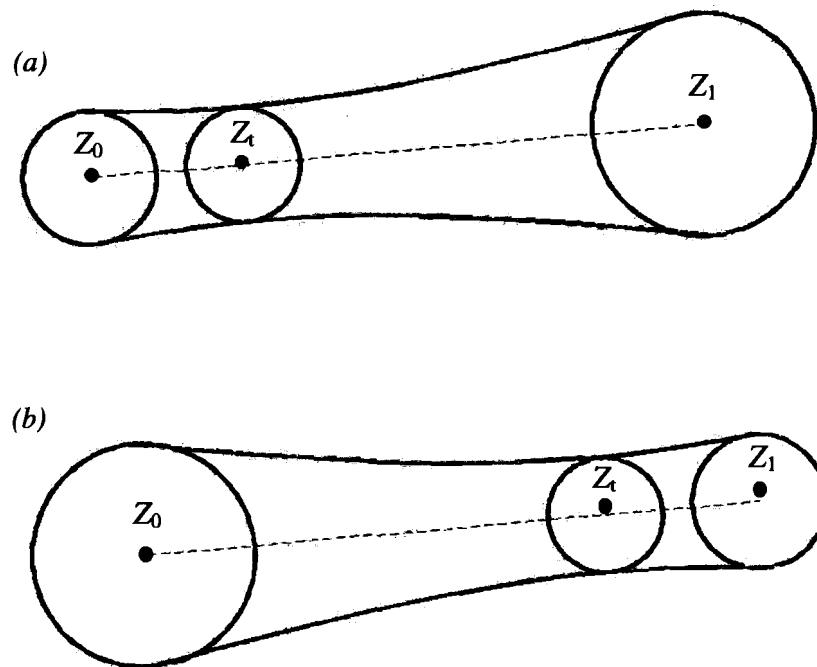


Figure B.10: Location of minimum error circle: (a) $\sigma_0 < \sigma_1$, $t < 1/2$;
 (b) $\sigma_0 > \sigma_1$, $t > 1/2$;

Shi and Liu's G-band is the most advanced positional error model of linear GIS features to date. It is a flexible model that can handle unequal and uncorrelated errors between endpoints.

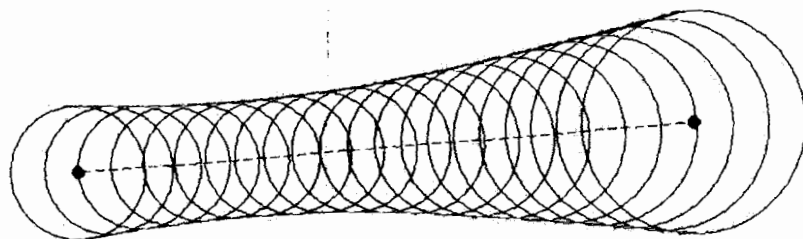


Figure B.11: Visualization of G-band as composite of error ellipses (circles)

BIOGRAPHY OF THE AUTHOR

Joshua Paul King was born in Anchorage, Alaska on January 9th, 1978. His family moved to Hollis, Maine in 1986, where Joshua attended secondary school and made the ill-advised conversion to a fan of the Boston Red Sox. He graduated as a scholar athlete with highest honors from Bonny Eagle High School in 1996.

Joshua enrolled at the University of Maine in the fall of 1996. He graduated *summa cum laude* with a B.S. in Spatial Information Science and Engineering in the spring of 2000. While an undergraduate, he was employed by the GIS department of a local civil engineering firm and subsequently by a local mapping company. In the fall of 2000, Joshua entered the University of Maine graduate school as a research assistant investigating positional uncertainty within spatial information. Joshua is a candidate for the Master of Science degree in Spatial Information Science and Engineering from the The University of Maine in December, 2002.